

**THIN LAYERS: PHYSICAL AND CHEMICAL CUES CONTRIBUTING TO
OBSERVED COPEPOD AGGREGATIONS**

A Dissertation
Presented to
The Academic Faculty

By

Clifton Brock Woodson

In Partial Fulfillment
of the Requirements for the Degree
Doctor of Philosophy in Civil Engineering

School of Civil and Environmental Engineering
Georgia Institute of Technology, Atlanta, GA

December 2005

**THIN LAYERS: PHYSICAL AND CHEMICAL CUES CONTRIBUTING TO
OBSERVED COPEPOD AGGREGATIONS**

Approved by:

Dr. Donald R. Webster, Advisor
School of Civil and Environmental
Engineering
Georgia Institute of Technology

Dr. Marc J. Weissburg
School of Biology
Georgia Institute of Technology

Dr. Phillip J. W. Roberts
School of Civil and Environmental
Engineering
Georgia Institute of Technology

Dr. Jeannette Yen
School of Biology
Georgia Institute of Technology

Dr. Terry W. Sturm
School of Civil and Environmental
Engineering
Georgia Institute of Technology

Date Approved: 15 November 2005

Acknowledgements

The author would like to express deep gratitude to his advisor and friend, Dr. Donald R. Webster for advice, supervision, and motivation.

The author would also like to thank committee members, Dr. Mark E. Hay (examining committee), Dr. Phillip J.W. Roberts, Dr. Terry W. Sturm, Dr. Marc J. Weissburg, Dr. Jeannette Yen for guidance, criticisms, harassments, and suggestions during the entire research process.

This work would not have been possible without the dynamic environment provided by the NSF-IGERT program at Georgia Tech, Signals in the Sea, or the support of the Office of Naval Research (ONR Grant #N000140310366).

A thank you goes out to my parents, Charles M. and Carol W. Smith, my deceased father, H. Clifton Woodson, my brothers and sister, Clint H. Woodson, C. Michael Smith, and Melissa C. Woodson, and the in-laws, Ashley W. Woodson, and Sara H. Smith, and the rest of my family for their understanding and support.

Thanks also go to Deron Burkepile, Alexander D. Chequer, Anne C. Prusak, John D. Parker, Jeremy D. Long, Matt J. Ferner, Jen Mitchell, the Webster lab folks, and the rest of the IGERTers for help collecting animals, reviewing manuscripts, and good old fashion camaraderie.

The author also thanks Flora Moir for review, critique, and motivation during the conclusion of this work.

Finally, the author expresses special gratitude to the Superfools, you know who you are.

TABLE OF CONTENTS

ACKNOWLEDGEMENTS	iii
LIST OF TABLES	vi
LIST OF FIGURES	viii
SUMMARY	xvii
Chapter 1 Introduction and Motivation	1
Chapter 2 Literature Review	4
2.1 Observations of thin layers	4
2.1.1 Properties of thin layers	5
2.1.2 Field studies	9
2.1.3 Laboratory studies	11
2.1.4 Thin layer formation	14
2.2 Properties of free shear flows	16
2.2.1 General analysis of laminar free shear flows	18
2.2.2 Laminar plane jet properties	20
2.2.3 Characteristics of mixing	25
2.2.4 Effects of density differences	26
2.2.5 Limitations of past studies	28
2.3 Zooplankton behavior	28
2.3.1 Natural history	29
2.3.2 Mechanical signals and responses	35
2.3.3 Chemical signals and responses	42
2.3.4 Cue hierarchy and associations	45
2.3.5 Aggregations and patchiness	48
2.4 Conclusions	51
Chapter 3 Methods	54
3.1 Flow system	54

3.2 Experimental parameters	59
3.3 Physical measurement techniques	65
3.3.1 Particle image velocimetry	65
3.3.2 Planar laser induced fluorescence	67
3.4 Biological observation techniques	69
3.4.1 Organisms and cultures	69
3.4.2 Behavioral assays	72
3.4.3 Statistical analyses	76
Chapter 4 Results	82
4.1 Model thin layer characterization	82
4.1.1 Velocity gradient layer	82
4.1.2 Density gradient layer	87
4.1.3 Chemical and biological layers	89
4.1.4 Thickness of the gradient layer	89
4.1.5 Combined layers	92
4.1.6 Synthesis	96
4.2 <i>Acartia tonsa</i> and environmental structure	100
4.2.1 Responses to the velocity gradient layer	100
4.2.2 Responses to the density gradient layer	108
4.2.3 Responses to the chemical/biological gradient layer	112
4.2.4 Responses to combined layers	115
4.3 <i>Temora longicornis</i> and environmental structure	118
4.3.1 Responses to the velocity gradient layer	118
4.3.2 Responses to the density gradient layer	130
4.3.3 Responses to the chemical/biological gradient layer	133
4.3.4 Responses to combined layers	135
4.3.5 Significance of responses and variability	138
4.4 <i>Calanus</i> spp., biogeographic and stage comparisons	140
4.4.1 Responses to the velocity gradient layer	140
4.4.2 Responses to the density gradient layer	144
4.4.3 Responses to the chemical/biological layers	147
4.4.5 Nauplii of <i>Calanus finmarchicus</i>	151

4.5 Survey of species responses	151
4.5.1 Responses to the velocity gradient layer	151
4.5.2 Responses to the density gradient layer	159
4.4.3 Responses to the chemical layer	162
4.4.3 Responses to food layers	164
Chapter 5 Discussion	166
5.1 Scales, interactions, aggregations	167
5.2 Cue hierarchy and associations	170
5.3 Variability and the ecological niche	176
5.4 Modeling and simulation	178
5.4.1 Model description and assumptions	179
5.4.2 Model calibration	182
5.4.3 Model results	184
Chapter 6 Conclusions and future directions	188
6.1 Summary	188
6.2 Conclusions	189
6.3 Unique contributions and applications	189
6.4 Implications	190
6.5 Future directions	195
REFERENCES	196

LIST OF TABLES

TABLE		PAGE
Table 2.1	Physical and biological characteristics of observed thin layers.	7
Table 2.3	Escape response thresholds among copepods and nauplii.	41
Table 3.1	Sample experimental parameters.	60
Table 3.2	Copepod species, average sizes, ambient temperatures, and collection locations.	71
Table 3.3	Matrix of experimental parameters for the behavioral trials. Copepod species were either subjected to isolated cues (Trials 1-5), or to all isolated and combined experiments (<i>A. tonsa</i> and <i>T. longicornis</i> , Trials 1-9). Two replicates were performed for each treatment.	73
Table 3.4	Summary of calculations for a single-factor ANOVA (adapted from Zar, 1999).	79
Table 4.1	Results of general linear model (ANOVA) on proportional residence time with four factors (replicate, velocity, density, and chemical) and interactive effects for <i>A. tonsa</i> . * indicates significance at $p < 0.05$, and ** indicates significance at $p < 0.001$. Significance shows that the factor or the interaction of the listed factors has an effect on the behavior of the organism with respect to proportional residence time.	101
Table 4.2	Swimming speeds for <i>A. tonsa</i> pre-contact and post-contact with the model thin layer. * denotes significant differences ($p < 0.05$) between pre-contact and post-contact values by single-factor ANOVA; control values are shown for comparison.	105
Table 4.3	Turn frequency for <i>A. tonsa</i> pre-contact and post-contact with the model thin layer. * denotes significant differences ($p < 0.05$) between pre-contact and post-contact values by single-factor ANOVA; control values are shown for comparison.	106

Table 4.4	Results of balanced ANOVA on proportional residence time with four factors (replicate, velocity, density, and chemical) and interactive effects for <i>T. longicornis</i> . * indicates significance at $p < 0.05$, and ** indicates significance at $p < 0.001$. Significance shows that the factor or the interaction of the listed factors has an effect on the behavior of the organism with respect to proportional residence time.	119
Table 4.5	Swimming speeds for <i>T. longicornis</i> pre-contact and post-contact with the model thin layer. * denotes significant differences ($p < 0.05$) between pre-contact and post-contact values by single-factor ANOVA; control values are shown for comparison.	123
Table 4.6	Turn frequency for <i>T. longicornis</i> in all gradients pre-contact and post-contact with the model thin layer. * denotes significant differences ($p < 0.05$) between pre-contact and post-contact values by single-factor ANOVA; control values are shown for comparison.	124
Table 4.7	Species comparison of behavioral responses (swimming speed and turn frequency) to the velocity gradient layer treatment. * denotes significant differences ($p < 0.05$) between pre-contact and post-contact values by single-factor ANOVA.	141
Table 4.8	Species comparison of behavioral responses (swimming speed and turn frequency) to the density gradient layer treatment. * denotes significant differences ($p < 0.05$) between pre-contact and post-contact values by single-factor ANOVA.	145
Table 4.9	Species comparison of behavioral responses (individuals crossing the gradient layer) to the density gradient layer treatment. * denotes significant differences ($p < 0.05$; two-tailed) between pre-contact and post-contact values by Fisher's exact test.	148
Table 4.10	Species comparison of behavioral responses (swimming speed and turn frequency) to the chemical exudate layer treatment. * denotes significant differences ($p < 0.05$) between pre-contact and post-contact values by single-factor ANOVA.	149
Table 4.11	Species comparison of behavioral responses (swimming speed and turn frequency) to food layer treatment (e.g. phytoplankton, <i>Tetraselmis</i> spp.). * denotes significant differences ($p < 0.05$) between pre-contact and post-contact values by single-factor ANOVA.	150

LIST OF FIGURES

FIGURE		PAGE
Figure 2.1	Sample profile showing a thin layer. This example is for particle absorption measured by Deksheniaks et al. (2001).	6
Figure 2.2	Common oceanic free shear flows. a) a plane mixing layer and b) a plane jet.	17
Figure 2.3	Velocity profiles of a Bickley jet (adapted from Andrade, 1939).	22
Figure 2.4	Self-similar velocity profiles of a Bickley jet (adapted from Andrade, 1939).	23
Figure 2.5	Sketch of the omnivorous calanoid copepod, <i>Temora longicornis</i> .	31
Figure 2.6	Swimming patterns of calanoid copepods: a) cruise style, b) cruise-sink style, c) hop-sink style.	32
Figure 2.7	Decomposition of simple shear flow. Any flow can be decomposed in rotational (r_{ij}) and deformation (e_{ij}) components. These sketches show a) a simple shear flow with its corresponding b) rotational component, and c) deformation component.	38
Figure 2.8	Schematic of bending patterns in response to fluid disturbances for an idealized creature with setae (adapted from Kiørboe et al., 1999).	39
Figure 3.1	Plane jet flow system. a) PIV/LIF arrangement and b) behavioral assay arrangement.	55
Figure 3.2	Plane jet flow system. Hydraulic schematic and flow chart.	56
Figure 3.3	Photo of experimental apparatus showing plane jet nozzle, test section, main tank, and flow meters.	57
Figure 3.4	Experimental representation of a stratified plane jet layer where $\rho_u < \rho_l$.	61

Figure 3.5	Individual paths of living and dead <i>Candacia ethiopica</i> in response to model thin layer with flow velocity gradient.	77
Figure 4.1	Velocity and shear strain rate fields for the velocity gradient layer treatment with $U_j = 6.7$ mm/s. Contours show the magnitude of the strain rate.	83
Figure 4.2	Comparison of measured velocity and shear strain rate ($S = \frac{1}{2} \left(\frac{\partial u}{\partial y} + \frac{\partial v}{\partial x} \right)$) profiles (shown with data points) at $x = 100$ mm to the analytical solution of Bickley (1937) indicated by a solid line.	84
Figure 4.3	The position of the boundary of the layer, δ_s , is indicated by the squares and the solid lines, and is defined by a threshold level of shear strain rate (0.025 s^{-1}). The location of the maximum shear strain rate is indicated by the triangles and dashed lines.	86
Figure 4.4	Density profile for the $\Delta\sigma_t = 1.8$ density gradient layer treatment (upper layer $S = 30.0$ ppt, lower layer $S = 32.0$ ppt).	88
Figure 4.5	Concentration field for the chemical layer treatment.	90
Figure 4.6	Vertical concentration profiles at various x -locations (60, 100, 140 mm) for the chemical layer treatment.	91
Figure 4.7	Definition of the model thin layer thickness for behavioral experiments with isolated cues. The edge of the layer is defined by the location of a threshold value of the shear strain rate in each case (0.025 s^{-1}) indicated by the arrows.	93
Figure 4.8	Combined velocity-density layer. (a) Vector field, (b) flow velocity and density profile at $x = 100$ mm, and (c) strain rate and density profile at $x = 100$ mm. Arrows indicate edge of layer defined by the 0.025 s^{-1} threshold.	94
Figure 4.9	Combined velocity-chemical layer. (a) Vector field and concentration contours, and (b) flow velocity, shear strain rate, and concentration profiles at $x = 100$ mm. Arrows indicate edge of layer defined by the 0.025 s^{-1} threshold.	96
Figure 4.10	Combined density-chemical layer. Density and concentration profiles at $x = 100$ mm. Arrows indicate edge of layer defined by the 0.025 s^{-1} threshold.	97

Figure 4.11	Combined velocity-density-chemical layer. (a) Velocity vector field and concentration contours, (b) flow velocity, density, and concentration profiles at $x = 100$ mm, and (c) strain rate, density, and concentration profiles at $x = 100$ mm. Arrows indicate edge of layer defined by the 0.025 s^{-1} threshold.	98
Figure 4.12	Sample paths for <i>A. tonsa</i> for the (a) velocity gradient layer, (b) density gradient layer, (c) chemical layer, and (d) control. The dashed lines indicate the edge of the layer corresponding to δ_s .	102
Figure 4.13	Proportional residence time of <i>Acartia tonsa</i> in presence of individual and combined cue layers. Layer constituents are velocity (V), density (D), and chemical exudates (C). * indicates a significant effect of single treatments relative to the control as determined with a balanced, nested ANOVA ($p < 0.05$). For combined layers, + indicates significant interactive effects between the isolated layer constituents.	103
Figure 4.14	Instantaneous swimming speeds for four <i>A. tonsa</i> paths plotted against shear strain rate for the velocity gradient layer treatment. The solid line shows the threshold of 0.025 s^{-1} . The dashed lines show the average swimming speed above and below threshold. Open symbols correspond to pre-contact with the layer, and solid symbols correspond to post-contact.	107
Figure 4.15	Threshold shear strain rate values for <i>A. tonsa</i> in the velocity gradient layer treatment. Data from four sample paths are shown in each figure. $\Delta\mu$ is the difference between the mean swim speed values calculated for data above and below a threshold. $\Delta\sigma$ is the difference between the standard deviation values for swim speed data above and below a threshold value. An abrupt change in $\Delta\mu$ or $\Delta\sigma$ indicates a behavior transition, and hence suggests the threshold value for behavioral response.	109
Figure 4.16	Proportional residence time of <i>A. tonsa</i> in response to the density gradient layer with varying density jump magnitude. Density gradients are a result of a change in salinity (0, 0.25, 0.5, 1, 2, 4 ppt) corresponding to change in $\Delta\sigma_t$ (0, 0.2, 0.4, 0.8, 1.8, 3.1 respectively).	111
Figure 4.17	Behavioral response of <i>A. tonsa</i> to density gradient layer treatment is represented by the number of individuals that cross the gradient layer (sigmoidal curve fit; $R^2 = 0.972$, $p = 0.094$). Sample sizes are the same for all gradient levels ($n = 40$).	113

- Figure 4.18 Proportional residence time for *A. tonsa* in the presence of a chemical exudate layer of *Tetraselmis* spp. Exudate concentration is calculated as equivalent biomass concentration ($\mu\text{g C L}^{-1}$). * indicates significant difference ($p < 0.05$) of treatment value versus preceding value via S-N-K post-hoc test. 114
- Figure 4.19 Threshold shear strain rate values for *A. tonsa* in combined layers with a velocity gradient: (a,b) velocity-density, (c,d) velocity-chemical, and (e,f) velocity-chemical-density. Data from four sample paths are shown in each figure. (a,c,e) $\Delta\mu$ is the difference between the mean swim speed values calculated for data above and below a threshold. (b,d,f) $\Delta\sigma$ is the difference between the standard deviations for swim speed data above and below a threshold value. An abrupt change in $\Delta\mu$ or $\Delta\sigma$ indicates a behavior transition, and hence suggests the threshold value for behavioral response. 117
- Figure 4.20 Sample paths for *T. longicornis* for the (a) velocity gradient layer, (b) density gradient layer, (c) the chemical exudate layer, and (d) control. The dashed lines indicate the edge of the layer corresponding to δ_s . 120
- Figure 4.21 Proportional residence time for *T. longicornis* in the presence of individual and combined cue layers. Layer constituents are velocity (V), density (D), and chemical exudates (C). * indicates a significant effect of single treatments relative to the control as determined with a balanced, nested ANOVA ($p < 0.05$). For combined layers, + indicates significant interactive effects between the layer constituents. 121
- Figure 4.22 Time record of swimming speed for two sample *T. longicornis* paths for the velocity gradient layer treatment (triangle – control and square – treatment). The solid line indicates the average value for all treatment paths (in and out of layer indicated separately) and the dashed line indicates the average value for all control paths. 125
- Figure 4.23 Instantaneous swimming speeds for four sample *T. longicornis* paths plotted against shear strain rate for the velocity gradient layer treatment. The solid line shows the response threshold of 0.025 s^{-1} , or δ_s . The dashed lines show the average swimming speed above and below threshold. Open symbols correspond to pre-contact with the layer, and solid symbols correspond to post-contact. 126

- Figure 4.24 Threshold shear strain rate values for *T. longicornis* in the velocity gradient layer treatment. Data from four sample paths are shown in each figure. $\Delta\mu$ is the difference between the mean swim speed values calculated for data above and below a threshold. $\Delta\sigma$ is the difference between the standard deviation values for swim speed data above and below a threshold value. An abrupt change in $\Delta\mu$ or $\Delta\sigma$ indicates a behavior transition, and hence suggests the threshold value for behavioral response. 128
- Figure 4.25 Normalized distribution of orientation angle for 10 *T. longicornis* paths in the velocity gradient layer. The post-contact distribution is significantly different than the pre-contact distribution via a Kolmogorov-Smirnov goodness of fit ($d_{\max} = 0.359$; $d_{0.05,20} = 0.294$). The orientation angle is defined such that 0° corresponds to horizontal facing either upstream or downstream. 129
- Figure 4.26 Proportional residence time of *T. longicornis* in response to the density gradient layer treatment with varying density jump magnitude. Density gradients are a result of a change in salinity (0, 0.25, 0.5, 1, 2, 4) corresponding to change in $\Delta\sigma_t$ (0, 0.2, 0.4, 0.8, 1.8, 3.1, respectively). 131
- Figure 4.27 Behavioral response of *T. longicornis* to density gradient layer treatment is represented by the number of individuals that cross the gradient layer (sigmoidal curve fit; $R^2 = 0.996$, $p = 0.011$). Sample sizes are the same for all gradient levels ($n = 40$). 132
- Figure 4.28 Proportional residence time of *T. longicornis* in the presence of a chemical exudate layer of either *Tetraselmis* spp. or *Rhodomonas lens*. Concentration of exudate is calculated as the equivalent biomass concentration ($\mu\text{g C L}^{-1}$). * indicates significant difference ($p < 0.05$) of treatment value versus preceding value via S-N-K post-hoc test. 134
- Figure 4.29 Threshold shear strain rate values for *T. longicornis* in combined layers with a velocity gradient: velocity-density (a,b), velocity-chemical (c,d), and velocity-chemical-density (e,f). Data from four sample paths are shown in each figure. (a,c,e) $\Delta\mu$ is the difference between the mean swim speed values calculated for data above and below a threshold. (b,d,f) $\Delta\sigma$ is the difference between the standard deviations for swim speed data above and below a threshold value. An abrupt change in $\Delta\mu$ or $\Delta\sigma$ indicates a behavior transition, and hence suggests the threshold value for behavioral response. 139

Figure 4.30	Proportional residence time in presence of individual cue layers for <i>Calanus finmarchicus</i> . Layer constituents are density (D), velocity (V), chemical exudates (C), and food. Different letters indicate significant differences between treatments via a post-hoc S-N-K test ($p < 0.05$).	142
Figure 4.31	Proportional residence time in presence of individual cue layers for <i>Calanus pacificus</i> . Layer constituents are density (D), velocity (V), and chemical exudates (C), and food. Different letters indicate significant differences between treatments via a post-hoc S-N-K test ($p < 0.05$).	143
Figure 4.32	Threshold shear strain rate values for <i>Calanus</i> spp. in the velocity gradient layer treatment: (a,b) <i>C. finmarchicus</i> , (c,d) <i>C. pacificus</i> . Data from four sample paths are shown in each figure. (a,c) $\Delta\mu$ is the difference between the mean swim speed values calculated for data above and below a threshold. (b,d) $\Delta\sigma$ is the difference between the standard deviations for swim speed data above and below a threshold value. An abrupt change in $\Delta\mu$ or $\Delta\sigma$ indicates a behavior transition, and hence suggests the threshold value for behavioral response.	146
Figure 4.33	Proportional residence time in presence of individual cue layers for <i>Calanus finmarchicus</i> nauplii (NIII-NIV). Layer constituents are density (D) and velocity (V). No significant differences occurred between treatments via ANOVA.	152
Figure 4.34	Proportional residence time in presence of individual cue layers for <i>Eurytemora affinis</i> . Layer constituents are density (D), velocity (V), chemical exudates (C), and food. Different letters indicate significant differences ($p < 0.05$) between treatments via S-N-K post-hoc test.	153
Figure 4.35	Proportional residence time in presence of individual cue layers for <i>Metridia pacifica</i> . Layer constituents are density (D), velocity (V), and chemical exudates (C). Different letters indicate significant differences ($p < 0.05$) between treatments via S-N-K post-hoc test.	155
Figure 4.36	Proportional residence time in presence of individual cue layers for <i>Neocalanus plumchrus</i> . Layer constituents are density (D) and velocity (V). Different letters indicate significant differences between treatments via a post-hoc S-N-K test ($p < 0.05$).	156

- Figure 4.37 Threshold values of shear strain rate for various species in a velocity gradient layer for (a,b) *Metridia pacifica* and (c,d) *Neocalanus plumchrus*. Data from four sample paths are shown in each figure. (a,c) $\Delta\mu$ is the difference between the mean swim speed values calculated for data above and below a threshold. (b,d) $\Delta\sigma$ is the difference between the standard deviations for swim speed data above and below a threshold value. An abrupt change in $\Delta\mu$ or $\Delta\sigma$ indicates a behavior transition, and hence suggests the threshold value for behavioral response. 157
- Figure 4.38 Proportional residence time in the velocity gradient treatment ($U_j = 6.7 \text{ mms}^{-1}$). The controls corresponds to no flow ($U_j = 0 \text{ mms}^{-1}$). * indicates significant difference between treatment and control ($p < 0.05$). 158
- Figure 4.39 Threshold values of shear strain rate for various species in a velocity gradient layer for (a,b) *Candacia ethiopica* and (c,d) *Labidocera madurae*. Data from four sample paths are shown in each figure. (a,c) $\Delta\mu$ is the difference between the mean swim speed values calculated for data above and below a threshold. (b,d) $\Delta\sigma$ is the difference between the standard deviations for swim speed data above and below a threshold value. An abrupt change in $\Delta\mu$ or $\Delta\sigma$ indicates a behavior transition, and hence suggests the threshold value for behavioral response. 160
- Figure 4.40 Proportional residence time in the density gradient treatment. The control corresponds to constant salinity (32 ppt). Treatments contain a layer consisting of a 2 ppt salinity change ($\Delta\sigma_t = 1.8$). * indicates significant difference between treatment and control ($p < 0.05$). 161
- Figure 4.41 Proportional residence time in the phytoplankton chemical exudate (*Tetraselmis* spp.) layer treatment. Concentration is based on equivalent biomass of phytoplankton in $\mu\text{g C L}^{-1}$. The control corresponds to the absence of exudate ($0 \mu\text{g C L}^{-1}$). * indicates significant difference between treatment and control ($p < 0.05$). 163
- Figure 4.42 Proportional residence time in the food (*Tetraselmis* spp.) layer treatment. The control corresponds to the absence of food ($0 \mu\text{g C L}^{-1}$). * indicates significant difference between treatment and control ($p < 0.05$). 165

Figure 5.1	Use of associational cues during foraging by copepods. The individual on the left utilizes cue hierarchy to narrow search region, thus finding resources faster and with better success than the individual on the right, who does not use associational cues. The large light gray oval represents a hypothetical habitat region. The darker oval is the portion of the habitat containing an associational cue such as a velocity or a density gradient. The small white oval is the portion of the habitat containing an associated resource (food, mates, etc.).	171
Figure 5.2	Cue hierarchy for copepod foraging based on experimental results. Percentages of the habitat covered by the cues are estimated based on published <i>in situ</i> observations (Holliday et al. 1998; Dekshenieks et al. 2001; McManus et al. 2003; Cowles 2004).	172
Figure 5.3	Field of view at the beginning of simulation for a model 25 meter water column with 1 meter thick layer located at 10 meters. Each symbol represents an individual model organism.	180
Figure 5.4	Model calibration curve: BIAS factor (γ) for (a) <i>A. tonsa</i> and (b) <i>T. longicornis</i> .	183
Figure 5.5	Field of view after 24 hours of simulation for <i>A. tonsa</i> for a model 25 meter water column with 1 meter thick layer located at 10 meters. Each symbol represents an individual model organism.	185
Figure 5.6	Aggregation of <i>A. tonsa</i> based on the model simulation. The solid line is the proportion of copepods in the layer with the layer present. The dashed line corresponds to the proportion of copepods in the same region with no layer present (i.e. no behavioral cue).	186
Figure 5.7	Aggregation of <i>T. longicornis</i> based on the model simulation. The solid line is the proportion of copepods in the layer with the layer present. The dashed line corresponds to the proportion of copepods in the same region with no layer present (i.e. no behavioral cue). The reference horizontal solid line shows the proportion of the model region covered by the model layer.	187
Figure 6.1	Schematic of copepod aggregation behind an obstruction (e.g. a coral head) in flow, for passive aggregation and/or active behavioral aggregation in response to either turbulence, light, or velocity gradients.	192

LIST OF SYMBOLS

c	instantaneous concentration
c'	turbulent concentration fluctuation
C	mean concentration
D_x	molecular diffusion coefficient
g	gravitational acceleration
N	Brunt-Väisala or buoyancy frequency
P	static pressure or significance value
Re	Reynolds number
Ri	gradient Richardson number
S	strain rate
S_e	standard error
T_R	proportional residence time
u	inst. longitudinal velocity
u'^2	turbulent or r.m.s. longitudinal velocity
U	mean longitudinal velocity
v	inst. transverse velocity
v'^2	turbulent or r.m.s. transverse velocity
V	mean transverse velocity
x	longitudinal coordinate
x_o	virtual origin
y	transverse coordinate
δ	layer half-width (various subscripts)
ε	turbulent dissipation rate
λ	Taylor microscale
ν	kinematic viscosity
ρ	fluid density

SUMMARY

In the current study, behavioral responses of several species of calanoid copepods to mimics of oceanographic structure associated with thin layers (or patchiness) were observed and evaluated in the context of foraging and aggregation. Experiments were conducted in two phases, layer characterization and behavioral assays. During layer characterization experiments, a specially-designed plane jet apparatus was constructed to create laboratory mimics of observed *in situ* thin layer characteristics. Isolated factors and combinations of thin layer constituents (velocity, density, chemical exudates – primary and secondary metabolites from living phytoplankton, and/or food) were used in behavioral assays to determine how copepods reacted to isolated and combined gradients as experienced in the field. Behavioral markers such as proportional residence time (amount of time in layer divided by total time in field of view), swimming speed, turn frequency, and orientation distribution were used to evaluate subtle changes in copepod behavior that could lead to increased foraging efficiency and/or aggregation.

All of the tested species of copepods exhibited behavioral responses (increased proportional residence time, increased swimming speed and turn frequency) associated with area-restricted search behavior to either one of the physical gradients (flow velocity or fluid density), but not both. This was the first observation of copepods using a physical gradient in foraging behavior. Similar responses were observed for chemical exudate layer experiments. Food layers induced feeding responses from all tested species (increased proportional residence time, decreased swimming speed). Observed responses to various combinations of gradients suggested that some copepods employ a cue

hierarchy to locate food-rich areas. Velocity or density gradients acted as initial cues for narrowing search regions, whereas the response to chemical exudates negated the initial response to the physical gradient. Additionally, most species of copepods tested rarely crossed a strong density gradient; a behavior which could also lead to aggregation, especially when superimposed on rhythmic movements such as diel vertical migration. A simple foraging model was formulated to illustrate how such behavioral changes can lead to observed aggregations at larger temporal and spatial scales. These results suggest that individual responses to oceanographic structure may have far reaching influence on population dynamics, succession, and biodiversity in coastal and pelagic ecosystems.

Chapter 1 Introduction and Motivation

Historically, ecological patterns in the plankton have been attributed to large-scale physical forcing; however, recent studies and observations have led to a realization that behavioral interactions between organisms and physical or chemical features at fine-to-intermediate scales may also be important (Franks, 1995; Yamazaki et al., 2002; Gallagher et al., 2004). The specific and important processes controlling distribution and patchiness by physical forcing are relatively well known (reviewed in Franks, 1995). Conversely, the relative importance of oceanographic gradients with respect to zooplankton behavior is not well understood, especially at the individual level, although recent advances in field observation techniques have greatly improved (Cowles, 2004; Genin et al., 2005). A disparity in the scales of patchiness also arises when considering contributions of physical forcing and zooplankton behavior to observed patterns of abundance. Physical forcing often drives pattern and patchiness at large (m to km) scales (Abraham, 1998; Seuront and Lagaduec, 2001). However, for zooplankton at fine to intermediate scales (cm to m) increased deviation from physical models is observed. Hence, patterns at small scales are often attributed to zooplankton behavior, although behavioral mechanisms, ecological function, and concurrent cascading impacts on community structure are relatively unknown.

The ability of copepods to locate patches of high productivity is directly linked to survival (Mullin and Brooks, 1976; Daro, 1988). Hence, behavioral responses of organisms at fine to intermediate scales will influence population dynamics and

community structure (Alldredge et al., 2002; Cowles, 2004). Ephemeral food patches in the ocean are often associated with steep gradients in physical and chemical properties such that behavioral adaptations that limit search to these regions may be advantageous (Poulet and Ouellet, 1982; Buskey, 1984; Daro, 1988; Tiselius, 1992; Saiz et al., 1993; Bohdanský and Bollens, 2004). Many observations suggest that a large proportion (>75%) of phytoplankton biomass in a water column can be concentrated into one or a few well-defined regions (Holliday et al., 2003). These patches, often termed thin layers, may be tens of centimeters thick, possibly less (Cowles et al., 1998), and are commonly associated with boundaries separating different bodies of water (often associated with gradients in flow velocity, fluid density, chemical composition, Hanson and Donaghay, 1998; Dekshenieks et al., 2001; Cowles, 2004). Zooplankton, such as copepods, are known to aggregate at or near these boundaries (Holliday et al., 1998), but basic questions regarding copepod foraging behavior and sensory response to oceanic structure remain unanswered. Association between physical gradients and food presence provides a cue that foraging copepods can utilize to focus searches near regions likely to have high concentrations of resources. Once the copepod is in the proximity of a physical gradient, the scales of interactions may be appropriate for chemical sensing or direct contact with food particles. Can copepods sense and thus utilize environmental gradients (physical and chemical) associated with thin layers to narrow searches for food, mates, or other resources? If so, which oceanographic features do copepods utilize to cue area-restricted search behavior thus improving foraging efficiency?

No study to date has used an individual-based approach to examine whether and how copepods utilize oceanic structure. Reported *in situ* values of strain rate and density steps in the thin layers literature (e.g. Dekshenieks et al., 2001) are lower than escape response thresholds (e.g. Fields and Yen, 1997a), but well above physiological limits (Yen et al., 1992; Fields et al., 2002). Similarly, chlorophyll concentrations in thin layers are much higher than exudate concentrations known to elicit swarming responses in many copepod species (Poulet and Marsot, 1978; Poulet and Ouellet, 1982). The influence of physical and chemical gradients on individual copepod behavior has not been previously examined, and until recently, resolution of *in situ* measurements was not sufficient to define appropriate field conditions for simulation in the laboratory (Cowles, 2004). In this thesis, fluid dynamic techniques are utilized to mimic oceanic structure in order to assess the behavioral responses of individual copepods to gradients of flow velocity, fluid density, chemical exudates, and food particles and how these responses compare to known behaviors that may lead to aggregation, such as area-restricted search behavior. This thesis provides the groundwork to begin assessments of the importance of copepod behavior on larger-scale ecological processes (aggregations of higher trophic level organisms, Wishner et al., 1998; Nevitt, 2000; nutrient cycling, Miller et al., 1995; primary production, Dagg and Turner, 1982; Dam and Peterson, 1993) that may even affect coyote populations in the desert (Rose and Polis, 1998; Hay and Kubanek, 2002).

Chapter 2 Literature Review

This chapter reviews literature on thin layers, fluid dynamics, and copepod behavior. First, the characteristics of thin layers and patchiness experiments are outlined to introduce the topic and to illustrate the issues and state of the field. Second, fluid dynamic literature is reviewed in the context of thin layer development, persistence, and structure. Third, copepod sensory systems that may be important in recognizing and utilizing oceanographic structure are discussed in the context of foraging and aggregation. This review then synthesizes each of the above sections within the thesis framework and creates a foundation for the next chapter on methodology and design.

2.1 Observations of thin layers

Vertically thin (cm scale) patches of oceanographic structure, often called “thin layers”, were undiscovered as recently as fifteen years ago due to limited resolution of sampling technologies. In many cases, the exact thickness of thin layers is still unresolved for similar reasons, but advances (resolution, incorporation of instrumentation to slow-drop devices) in field instrumentation technology have significantly improved our knowledge of these features (e.g. Cowles and Desiderio, 1993; Holliday et al., 1998, 2003; Jaffe et al., 1998). Thin layers are currently believed to be on the order of centimeters to meters thick vertically and have been documented to extend for tens of kilometers horizontally. These layers occur over a wide range of depths (4-40 meters), and are most commonly associated with the pycnocline (Dekshenieks et al., 2001). Figure 2.1 shows measurements of a thin layer identified by particle absorption

techniques (Dekshenieks et al., 2001). Plankton assemblages in these layers can be an order of magnitude more concentrated than the surrounding environments, and are often dominated by a single species (Nielsen et al., 1990; Cowles et al., 1998; Dekshenieks et al., 2001; McManus et al., 2002; Cowles, 2004).

2.1.1 Properties of thin layers

Thin layers occur over a wide range of conditions and depths, and are often defined by gradients of physical, chemical, and biological constituents. Gradients in flow properties such as fluid density or velocity often define physical parameters of thin layers (Osborn, 1998; Dekshenieks et al., 2001). Similarly, concentrations of oxygen, nitrite, chemical exudates from living phytoplankton, or marine snow provide chemical signatures (Hanson and Donaghay, 1998; Alldredge et al., 2002). Table 2.1 reports the range of conditions, constituents, and parameters of documented thin layers.

Density or velocity gradients characterize the physical properties of thin layers. Density gradients occur due to changes in fluid temperature and/or salinity. Density can change as much as a few sigma-t units over a few centimeters. Velocity gradients occur when patches of fluid slide past each other, or by shearing from internal waves, and are best quantified by strain rate (S , [s^{-1}]). Documented shear ($\frac{\partial u}{\partial y}$) ranges from 0.01 to 1.0 s^{-1} , but it is important to note that this is fundamentally different than the fluid dynamic shear strain rate ($\frac{1}{2}\left(\frac{\partial v}{\partial x} + \frac{\partial u}{\partial y}\right)$), and resolution limitations in the field may also hinder

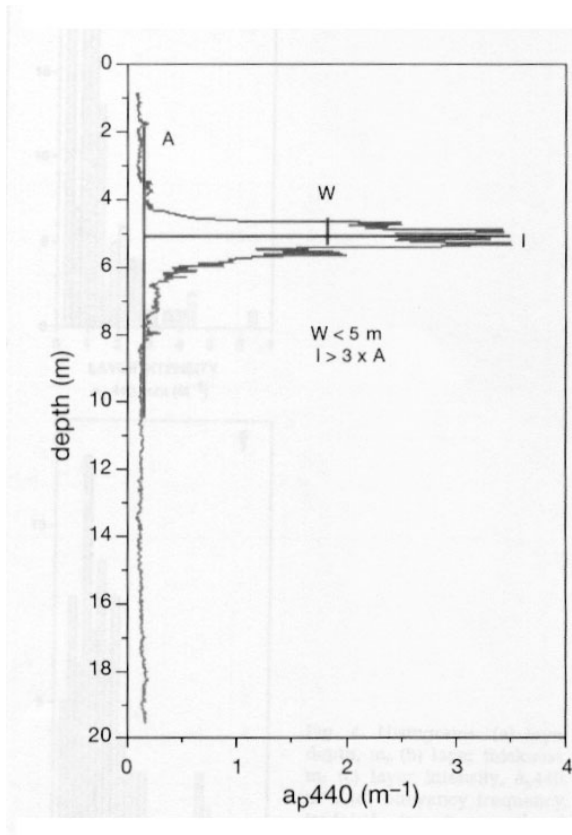


Figure 2.1 Sample profile showing a thin layer. This example is for particle absorption measured by Deksheniaks et al. (2001).

Table 2.1 Physical and biological characteristics of observed thin layers.

Depth (m)	Thickness (cm)	Temperature (°C) (Δt through layer)	Salinity (ppt)	Composition	Reference
10	10-50	11-14 (0.5-1)	N/A	Unspecified phytoplankton	Cowles et al., 1998
3	10-40	11-14 (1-2)	29-29.5	Nitrite, Oxygen, Iron (II)	Hanson and Donaghay, 1998
~10	~50	N/A	N/A	<i>Calanus pacificus</i>	Holiday et al., 1998
7-8	N/A	N/A	N/A	<i>Oithona</i> <i>Centropages</i> <i>Chaetoceros</i>	Davis et al., 1992
5-20	10-200	10-13 (1-2)	29-30	<i>Chaetoceros</i> <i>Pseudo-nitschia</i> <i>Thalassiosira</i>	Rines et al., 2002 McManus et al., 2003
2-25	10-400	10-14	N/A	Unspecified phyto- and zooplankton	Deksheniaks et al., 2001

these estimates. Because horizontal variation is small, the $\frac{\partial v}{\partial x}$ -term is negligible in comparison to the other term, so the relationship between oceanographic shear and fluid dynamic shear strain rate is a factor of 2. Thin layers are often located at the pycnocline (Dekshenieks et al., 2001) suggesting that the mixing between surface and deep waters plays an important role in thin layer formation. However, these layers also occur at small-scale density or velocity gradients throughout the water column (Cowles, 2004).

Gradients in nitrite, iron(II), and dissolved oxygen provide documented examples of the chemical characteristics of thin layers (Hanson and Donaghay, 1998). These layers may be very important in pelagic ecosystems, where nitrogen and iron may be limiting resources for primary production. The chemical properties of thin layers are suspected to develop from physical interactions, and likely arise due to mixing of nutrient-rich deep waters with nutrient deficient surface waters (Franks, 1995), or the accumulation of marine snow at a density gradient (Alldredge et al., 2002).

Dense assemblages of plankton are often associated with the physical or chemical gradients described above. These layers may not perfectly coincide with fine-scale physical or chemical structures, but they are often closely associated and may overlap by a few centimeters (Cowles, 2004). Biologically, thin layers often possess organism concentrations ten times higher than the surrounding environment, and thus are likely to be important features in the pelagic seascape. Phytoplankton layers appear to form within the physical layer via entrapment, thus promoting a bloom. This is supported by evidence that many thin layers are dominated by a single phytoplankton species (Cowles

et al., 1998; Rines et al., 2002). Zooplankton aggregations near phytoplankton layers are hypothesized to result from foraging or aggregation behaviors suggesting that thin layers provide reliable environmental cues about resource abundance and availability, but could also occur due to similar physical forcing believed to form phytoplankton patchiness.

2.1.2 Field studies

Small-scale aggregations of zooplankton have been observed for a number of years, and most observations were done via *in situ* observation by SCUBA divers or direct sampling (Haury, 1976; Hamner and Carleton, 1979; Ueda et al., 1983; Alldredge et al., 1984; Mackas and Louttit, 1988; Ambler et al., 1991; Incze et al., 2001). Until recently, direct sampling of pelagic ecosystems has been limited to plankton tow nets, and interval sampling through the use of rosettes. These techniques can not resolve spatial gradients on the order of tens of centimeters or smaller (Bjornsen and Nielsen, 1991). The use of optical and acoustic techniques to determine and quantify the presence of phytoplankton and zooplankton aggregations *in situ* is vital in the documentation of thin layers (Davis et al., 1992; Cowles et al., 1998; Holliday et al., 1998; Jaffe et al., 1998). Cowles and Desiderio (1993) outlined and implemented an optical technique for characterizing phytoplankton composition based on fluorescence of photosynthetic pigments (chlorophyll and phycoerythrin). Attaching fluorometers (response frequency of 10-25 Hz) to a slow free-falling device (10-30 cm/s fall velocity) allowed resolutions on the order of centimeters. Cowles et al. (1993) demonstrated the validity of this technique in the assessment of thin layer composition. Incorporation of this technique

with devices containing flow, temperature, salinity, and chemical concentration profilers has provided the characteristic information summarized in Table 2.1 (Deksheniaks et al., 2001; Cowles et al., 1998). Similarly, Holliday et al. (1998), Jaffe et al. (1998), and Genin et al. (2005) utilize video imaging and acoustical techniques to identify and quantify fine-scale zooplankton distributions.

Field measurements of the velocity gradient characteristics are particularly difficult. Resolution restrictions of field velocity measurements (~ 20 cm at best; often closer to 1 m) suggest that strain rates estimated in the ocean may be much higher than reported. For example, Deksheniaks et al. (2001) utilized an acoustic Doppler current profiler (ADCP) with a minimum bin size of 1 m. For a strain rate equal to 0.05 s^{-1} , this corresponds to a change of 5 cm s^{-1} over the 1 m distance. A velocity change of this magnitude under density stratified conditions is likely to occur over a shorter distance, as evidenced by Cowles (2004). For instance, if the recorded change in velocity really occurred over a distance of 10 cm, then maximum strain rates would be equal to 0.5 s^{-1} . This is an extreme example, but it illustrates the need for higher-resolution field measurements.

Because of resolution limitations and cost of equipment, thin layers have been documented only in a few regions, but they are suspected to occur globally. These areas cover both pelagic and coastal environments, and suggest that thin layers are an important features in plankton communities worldwide, and thus may play vital roles in a variety of ecological and biogeochemical cycles. Most studies of thin layers have occurred in the

northeast Pacific off the coast of Oregon [USA] (Cowles and Desiderio, 1993; Cowles, 2004 and the San Juan Islands near Washington [USA] (Dekshenieks et al., 2001; Cowles et al., 1998), and some studies have occurred in the Baltic Sea (Tiselius, 1998). Other observations of thin layers have also been documented in the Gulf of Mexico near Destin, FL, in the Ogeechee River Estuary, GA, in Monterrey Bay, CA, and on Georges Bank, Gulf of Maine (McManus, *pers. comm.*). Although the regional observations of thin layers are limited, the characteristics and parameters associated with their occurrence (see Table 2.1) suggest that further research in other regions, especially in warmer latitudes with more intense stratification, may prove rewarding.

2.1.3 Laboratory studies

Although much work has been done on the responses of zooplankton to various environmental cues (Harder, 1968; Buskey, 1984; Hamner, 1988; Yen et al., 1992; Yen et al., 2004), there is a dramatic deficiency in laboratory studies aimed at supporting the hypotheses developed from field observations of thin layers. Mullin and Brooks (1976) made general calculations combined with field sampling to suggest that zooplankton could not survive within a homogenous mixed layer because concentrations of food particles are too low to support a population or even an individual. Daro (1988) later proposed that if zooplankton could efficiently locate high resource patches, then survival was possible. However, the impacts of patchiness and thin layers on zooplankton aggregation have remained elusive.

Tiselius (1992) utilized small density differences to create patches of phytoplankton (*Thalassiosira weissflogii*) in a quiescent tank. Behavioral responses of the copepod, *Acartia tonsa*, were examined using video recordings and evaluated for response time, net-to-gross displacement ratio, and frequency of feeding. Results of the study suggest that this copepod can utilize either density differences or chemical exudates from *T. weissflogii* to perform area-restricted searches and remain in the high resource layer. Although no chemical cue was identified, the author attributed the response to exudates from the phytoplankton. However, this study did not distinguish between the three signaling cues (density, physical contact with food, and chemical compounds), and the influence of patchiness on copepod fitness were inconclusive (Saiz et al., 1993).

Other studies concerning the impacts of patchiness on zooplankton foraging behavior have provided similar results. Bochdansky and Bollens (2004) did not observe significant impacts of patchiness on copepod fecundity, or on aggregation for the copepod *Acartia hudsonica* using thin layers of the diatom *Skeletonema costatum*. However, the scale of the individual experiments may not be sufficient to produce dramatic changes in individual fitness. In a hypothetical 25 meter upper ocean water column, >75% of the phytoplankton biomass can be concentrated into one or a few meter-thick thin layers (Holliday et al. 1998). These high levels of patchiness lead to phytoplankton concentrations adequate to support zooplankton populations in approximately 4 to 16% of the habitat. This suggests that experiments that adequately assess the importance of patchiness must be at scales that mimic search regions in the field. The use of two meter water column with a 26 cm thin layer constitutes

concentrations of food that can support zooplankton in these experiments at 13% is close to that experienced in the field. However, an individual can cover the vertical length of the tank in 100 seconds (2 meter column, swimming speed $\sim 2 \text{ mm s}^{-1}$ for *A. hudsonica*), and can thus always find the layer food in a relatively short amount of time. In the hypothetical water column mentioned above, an individual may have to cover as many as 20 meters before locating a resource patch. Hence, energetic expenditure is ten-fold larger than that of many current patchiness experiments.

Clay et al. (2004) observed higher densities of larval Pacific herring, *Clupea pallasii*, in the presence of food patches associated with mild density gradients, but did not directly assess individual fitness. Ignoffo et al. (2005) showed that the rotifer, *Brachionus plicatilis*, aggregated in food patches, but redistributed once the food patch was depleted, and that rotifers selectively chose thin layers based on dominant species of food resources. This study also isolated the impacts of density and food presence on rotifer aggregation, and showed that rotifers would aggregate at density gradients without food presence. However, food presence alone was not isolated from density gradients, so responses to individual cues and the interactions of the combinations of cues cannot be directly evaluated. These experiments also may suffer from inadequate scaling as mentioned above.

2.1.4 Thin layer formation

Several mechanisms are suspected to be involved in the formation and persistence of thin layers. Physical mechanisms hypothesized to contribute to thin layer formation include shearing by internal waves, vertical shear flows, horizontal intrusions, and turbulent mixing (reviewed in Franks, 1995). Internal waves have received the most attention at this time, predominately from a modeling standpoint (Franks, 1995). Turbulent mixing, stratification, and shear flows also contribute to the formation and longevity of thin layers, but these factors have received little experimental or theoretical attention.

Franks (1995) describes a model for thin layer formation based on internal wave shear. In this model, variations in horizontal velocities are a result of near-inertial internal waves created at the mixed layer/deep ocean interface resulting in along isopycnal patchiness (Franks, 1995). This model assumes phytoplankton as passive particles, and that internal waves have constant frequencies and amplitudes. Despite these simplifications, this model provides evidence for the physical formation of thin layers by internal wave shear. The model shows that a vertical patch can be spread and thinned creating a vertically thin, but horizontally expansive patch along a density discontinuity.

Traditional shear flows (mixing layers, fluid body intrusions) are another important factor in thin layer formation. Mixing layers are defined as regions at the

interface between two fluid layers that have different flow velocities. Increased turbulent mixing occurs at the interface as the two fluid layers slide past each other. These layers often contain different concentrations of a passive scalar quantity. The mixing layer profiles consist of a smooth transition between these concentration limits (Gutmark and Wygnanski, 1976; Bashir and Uberoi, 1975; Davies et al., 1975). At the pycnocline, where the mixed surface layer interfaces with nutrient-rich deep ocean waters, mixing layer formation is likely to provide a mechanism for the formation of nutrient-rich layers. Consequently, the physics of free shear flows has significant impacts on the structure, reliability, and availability of the environmental cues associated with thin layers.

Biological factors such as *in situ* growth, differential grazing, and behavior are often responses to phenomena that occur after the formation of a thin layer by physical mechanisms. *In situ* growth of phytoplankton often results from entrapment of organisms in a nutrient-rich thin layer formed by the physical mechanisms described above. Phytoplankton in such a layer are able to grow and reproduce more quickly than those in the surrounding environs, thus creating a peak in productivity as evidenced by fluorescence readings (Cowles et al., 1998). Zooplankton responses to oceanographic structure may also influence thin layer formation. Behaviors such as predator avoidance and preferred habitat selection may lead to thin layers of zooplankton in certain regions. Additionally, zooplankton able to exploit high concentration phytoplankton patches through sensory adaptation and foraging ability will experience advantages over competing species. Aggregations of zooplankton species in the neighborhood of measured peaks in fluorescence suggest that some species can exploit chemical or

mechanical cues associated with thin layers (Holliday et al., 2003; Rines et al., 2002; Davies et al., 1992). Sinking and accumulation have also been shown to account for thin layers of marine snow (Alldredge et al., 2002).

2.2 Properties of free shear flows

Velocity gradients, flow instabilities, and turbulence often are observed in a defined region between two fluid layers sliding past each other. These flows are often called “free shear flows” due to the absence of fixed or solid boundaries. Common free shear flows in the open ocean include plane jets (i.e. fluid body intrusions) and plane shear layers (i.e. the surface mixed layer sliding past the deep ocean layer; see Figure 2.2). Flow rates, strain rates, and velocity profiles associated with thin layers suggest that the laminar plane jet is the appropriate flow model for laboratory research. Although almost all oceanic flows are turbulent, shear strain rates associated with thin layers are often much less than 1.0 s^{-1} , and strong stratification acts to suppress vertical mixing creating well defined gradients. Therefore, for application in the laboratory, the laminar plane jet appears to most closely mimic field conditions conducive to thin layer occurrence and persistence. However, at larger scales, it is the physics of turbulent shear layers that leads to the development of thin layers.

The majority of research on planar jets has been conducted in the turbulent regime due to relevance to many engineering and high Reynolds number natural flows (Forthmann, 1936; Tennekes and Lumley, 1972; Brown and Roshko, 1974; Gutmark and

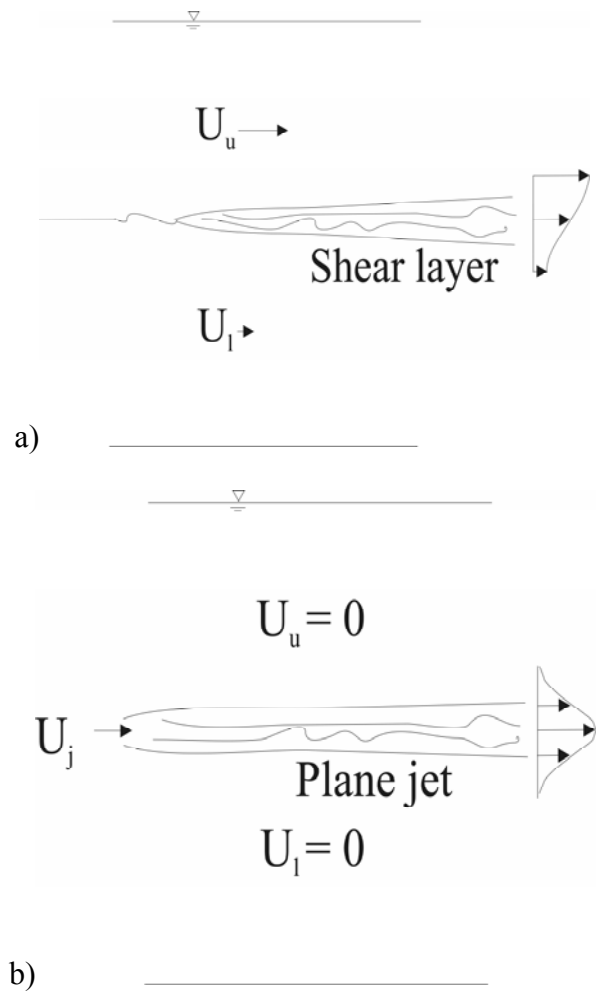


Figure 2.2 Common oceanic free shear flows. a) a plane mixing layer and b) a plane jet.

Wyganski, 1976; Dimotakis, 1991). These studies show that planar jets exhibit self-similar behavior (Gutmark and Wygnanski, 1976), grow linearly with distance from a virtual origin (Forthmann, 1936; Tennekes and Lumley, 1972; Gutmark and Wygnanski, 1976), have Gaussian velocity profiles with maximums on the jet centerline proportional to the square-root of distance downstream (Forthmann, 1936; Gutmark and Wygnanski, 1976), and exhibit saddleback turbulent stress profiles (Gutmark and Wygnanski, 1976). Mixing in these flows is attributed to turbulent entrainment with scalar profiles also growing linearly but slightly faster or slower than velocity profiles because heat diffuses faster than momentum and most chemical scalars diffuse slower in water (Bashir and Uberoi, 1975; Davies et al., 1975, Jenkins and Goldschmidt, 1976; Fischer et al., 1979; Roberts and Mathews, 1987). Table 2.2 summarizes the universal conclusions for turbulent plane jets, including growth rate and centerline velocity decrease rate. The remainder of this review focuses on laminar plane jets as a model for thin layers.

2.2.1 General analysis of laminar free shear flows

As with all fluid dynamics problems, free shear flows are governed by the continuity and Navier-Stokes equations, and many simplifications can be made based on boundary layer analysis. The flow is assumed to be two-dimensional and steady. Additionally, order of magnitude arguments suggest that the diffusion terms are dominated by variation in the y -direction, therefore the other terms are dropped. Hence, the equations for laminar plane jet flow follow as:

Table 2.2 Major conclusions of turbulent plane jet research.

Relationship	Experimental values	Reference
$\frac{\delta}{x} = C_1$	$C_1 = 0.09 - 0.11$	Forthmann, 1936 Gutmark and Wygnanski, 1976
$U_M = C_2 \left(\frac{D}{x}\right)^{1/2}$	$C_2 = 0.3 - 0.45$	Hussain and Clark, 1977 Ramaprian and Chandrasekhara, 1985 da Silva and Metais, 2002 DNS
$\frac{\delta_c}{x} = C_3$	$C_3 = 0.125$	Bashir and Uberoi, 1975 Davies et al., 1975 Fischer et al., 1979
Velocity self-similarity	$\frac{x}{D} \geq 5$	Gutmark and Wygnanski, 1976
Turbulent stress self-similarity	$\frac{x}{D} \geq 30 - 40$	
Saddleback profile for turbulent stresses		
Kolmogorov microscale grows with distance downstream		
$\eta = (\nu^3 / \varepsilon)^{1/4}$		

$$\frac{\partial U}{\partial x} + \frac{\partial V}{\partial y} = 0 \quad (2-1)$$

$$U \frac{\partial U}{\partial x} + V \frac{\partial U}{\partial y} = -\frac{1}{\rho} \frac{\partial P}{\partial x} + \nu \frac{\partial^2 U}{\partial y^2} \quad (2-2)$$

$$\frac{\partial P}{\partial y} = 0 \quad (2-3)$$

The absence of fixed boundaries allows for self-similarity in free shear flows. Hence, at sufficient distances from the nozzle, these flows all possess the same characteristics and profile shapes when employing the appropriate scaling. For these reasons, theoretical solutions for the mean flow are available (e.g. Bickley, 1937) with validation and coefficients derived from experimental analysis. Laminar planar mixing layer flows are often unstable except at low Reynolds numbers (less than approximately 50) resulting in coherent vortical structures eventually transitioning to turbulence. In the case of two fluid layers of different density with a planar interface, this flow corresponds to the classic Kelvin-Helmholtz instability configuration.

2.2.2 Laminar plane jet properties

Bickley (1937) derived an analytical solution of the transverse velocity profile in a laminar jet (form reported by Sato and Sakao, 1964) as:

$$\frac{u}{U_o} = \operatorname{sech}^2\left(\frac{ay}{\delta}\right) \quad (2-4)$$

The growth rate of the laminar plane jet follows the functional form:

$$\delta = a \left(\frac{48\nu^2 x^2}{M} \right)^{1/3} \quad (2-5)$$

where

$$M = \int_{-\infty}^{\infty} U^2 dy \quad (2-6)$$

is the initial jet momentum flux, δ is the half-velocity width, a is a constant equal to 0.81136, and ν is the kinematic viscosity, (Andrade, 1939; Sato and Sakao, 1964). The mean centerline velocity, U_M , decreases with distance downstream as:

$$U_M = \left(\frac{3M^2}{32\nu x} \right)^{1/3} \quad (2-7)$$

Andrade (1939) supported the theoretical analysis of Bickley (1937) experimentally using flow visualization. Jet profiles at five distances from a plane jet source are shown in Figure 2.3. Self-similarity is demonstrated in Figure 2.4, where the non-dimensional profile is shown with data from Andrade (1939).

Equations (2-4), (2-5), and (2-7) are based on flow from a point source. To adapt these formulas to a real jet, a virtual origin must be established due to the non-zero width of the jet nozzle (Andrade, 1939; Kotsovinos, 1976; Bradshaw, 1977; Revuelta et al.,

2002). The location of the virtual origin is weakly dependent on the experimental set-up, and more specifically the nozzle flow conditions.

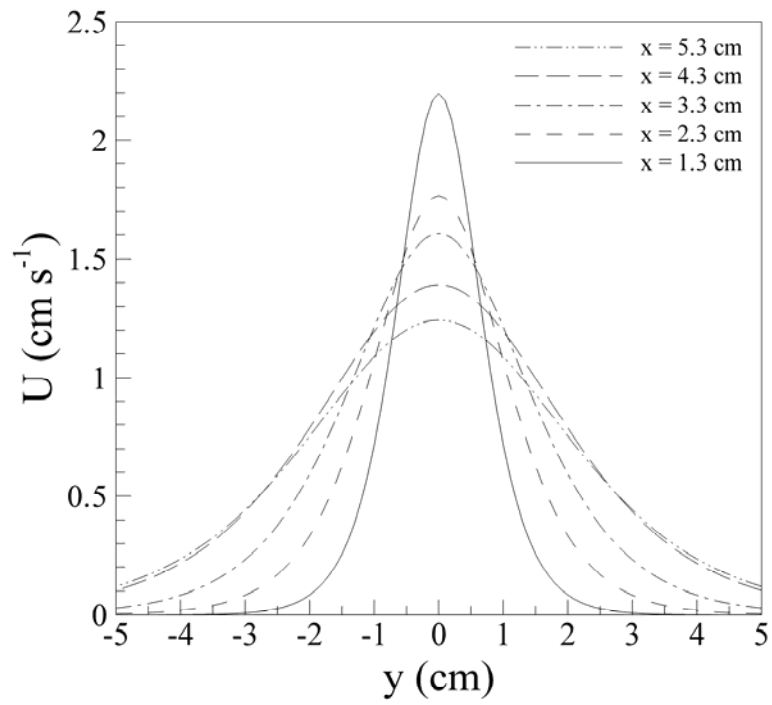


Figure 2.3 Velocity profiles of a Bickley jet (adapted from Andrade, 1939).

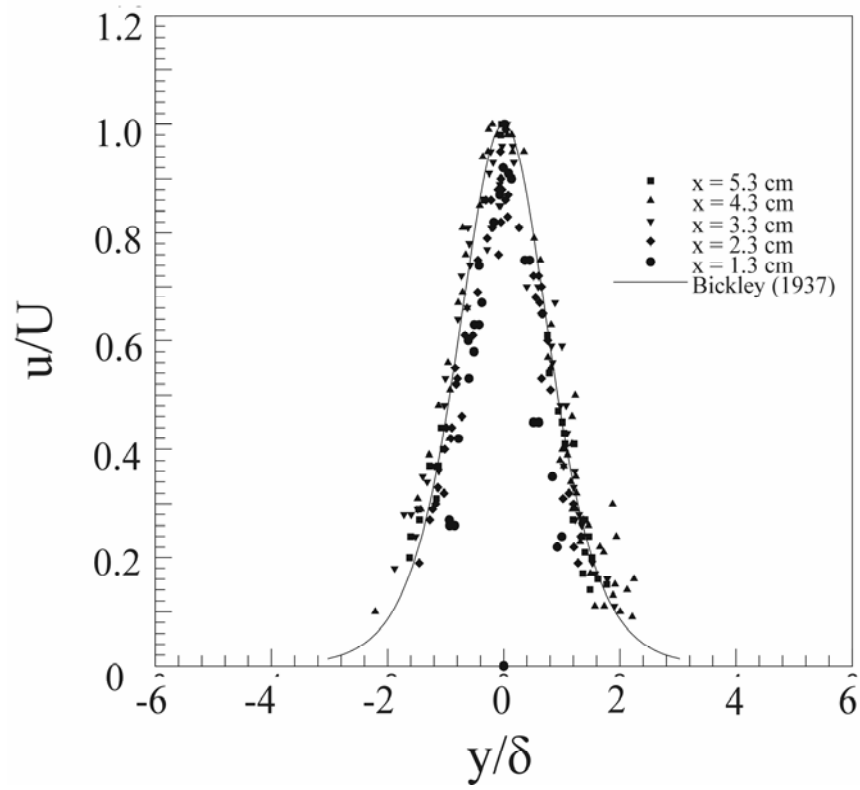


Figure 2.4 Self-similar velocity profiles of a Bickley jet (adapted from Andrade, 1939).

The location of the virtual origin is dependent on the exit velocity profile, which is generally a Poiseuille (parabolic) profile or a top-hat profile depending on the state of the boundary layer at the nozzle exit (Reveulta et al., 2002). Flow conditioners are employed in many experiments to ensure a nearly top-hat profile (Hussein, 1994). Most experimental investigations in the last twenty years have utilized a 5th-order polynomial contraction shape and various flow-conditioning screens to insure a top-hat profile with very thin boundary layers and no flow separation in the contraction (Mehta and Bradshaw, 1979; Hussein, 1994).

Further experimental and theoretical work on the laminar plane jet has focused on instability analysis, and transition to turbulent flow (Pai, 1951; Tatsumi and Kakutani, 1958; Sato and Sakao, 1964; Cormi, 1974; others). Sato and Sakao (1964) evaluated the transition to turbulence of planar jets at low Reynolds number. These investigators used a hot-wire anemometer to measure the velocity in laminar plane jets and confirmed the results of earlier investigations. For Reynolds numbers based on jet nozzle width and exit velocity ($Re_j = Ud/\nu$) less than 10, the jet is laminar and stable (Tatsumi and Kakutani, 1958). For the Re_j range between 10 and approximately 50, periodic velocity fluctuations were observed near the jet, but these instabilities dissipate quickly, and the jet returns to a steady laminar flow at sufficient distances from the nozzle. For Reynolds numbers exceeding 50, the jet becomes turbulent in the far field (distance at which the jet geometry ceases to affect flow). Sato and Sakao (1964) also assessed the affects of disturbances on the transition to turbulence. Disturbances in the form of sound waves

were introduced and found to have contradictory affects (amplification or damping) on velocity fluctuations depending on the frequency of the excitation.

Later investigators (Ikeda, 1977; Ho and Huerre, 1984; Hsiao and Huang, 1990) demonstrated the effects of excitation and the presence of various frequency limits via hot-wire or laser Doppler anemometry techniques. Three modes have been defined as the suppression mode, the shear layer mode (Zaman and Hussain, 1980), and the preferred mode (Crow and Champagne, 1971). Each mode is associated with a particular range of Strouhal number ($St = f\theta/U$, where θ is defined as the momentum thickness of the layer, and f is the excitation frequency). Excitation can act to reduce (suppression mode) or amplify turbulent fluctuations (preferred mode), or promote coherent flow structure (shear layer mode) (Rajagopalan and Ko, 1996; Hsiao and Huang, 1990).

2.2.3 Characteristics of mixing

Mixing is the result of molecular diffusion, shear dispersion, and turbulent motions. Molecular diffusion and shear dispersion are the only mechanisms of mixing for laminar flows with concentration gradients,. In these flows, shear fields stretch concentration gradients and effectively increase molecular diffusion. Molecular diffusion in the transverse direction follows the Fickian model, and flux can thus be calculated directly as:

$$J = -D_x \frac{\partial c}{\partial y} \quad (2-8)$$

where J is the flux of a scalar quantity, and D_x is the molecular diffusion coefficient.

However, for turbulent flows, mixing is a result of irregular vortical motion. These motions create steep gradients in scalar concentrations that allow diffusion to act much more quickly than in laminar flow conditions. Although time-averaged concentrations of scalars in a turbulent shear flow are smooth, instantaneous concentrations fluctuate irregularly (Webster et al., 2003). Mixing in turbulent flows has been extensively studied for many years; however, the fine-scale nature of this process is still not well understood (Webster et al., 2001).

2.2.4 Effects of density differences

Stratification also can have a significant effect on free shear flows such as mixing layers or plane jets (Chu and Baddour, 1984; Fischer et al., 1979). The strength of stratification is often quantified by the buoyancy frequency (N , Eqn. 2-9), and the gradient Richardson number is a measure of stability in stratified flows (Eqn. 2-10).

$$N = \sqrt{-\frac{g}{\rho_o} \frac{\partial \rho}{\partial y}} \quad (2-9)$$

$$Ri = \frac{N^2}{\left(\frac{\partial u}{\partial y}\right)^2} \quad (2-10)$$

Chu and Baddour (1984) observed that shear flows under stable stratification approached a “neutrally stable state” where turbulent kinetic energy was neither lost nor gained. This stable-state is associated with the critical gradient Richardson number (~ 0.25) reported by Hazel (1972). For stable-state flows, the turbulent intensity decreases due to removal of energy by viscous dissipation. The result is a reduction in mixing and entrainment, and consequently an upper limit is set on the thickness of the shear flow.

Roberts and Mathews (1987) illustrate the confined growth and onset of turbulent collapse for axisymmetric jets in stratified fluids. In a similar study, Roberts et al. (2001) utilize planar laser induced fluorescence to estimate dilution in a neutrally-buoyant collapsed round jet. These fully turbulent flows begin to collapse for $x/l_N < 3.5$ and have fully collapsed at $x/l_N = 1.4Re^{1/4}$, where $l_N = M^{1/4}/N^{1/2}$ and M is defined as the jet momentum flux and is constant. Dilution is also reduced in these flows, resulting in finite layers of relatively higher concentration. The results of these studies suggest that stratification plays a major role in limiting mixing efficiency of free shear flows.

Although turbulence is a dominating factor in oceanic mixing (Turner, 1991), thin layers form in regions of intense stratification (Dekshenieks et al., 2001), where vertical motions are highly suppressed and mixing is often dominated by molecular diffusion or shear (Franks, 1995). Turbulent mixing is important during high stress events that are not conducive to thin layer formation and persistence; during these events thin layers are

quickly dissipated (Cowles, 2004; Donaghay et al., 2005). Hence, responses of zooplankton to thin layer properties should be based on low turbulence, highly stratified conditions that are most easily modeled in the laboratory using the laminar plane jet.

2.2.5 Limitations of past studies

The principles developed through these free shear flow studies provide an excellent framework for describing large-scale shear flows in oceanic environments, but they do not characterize features at the scale of individual organisms such as copepods. Also, many of these studies were conducted for Reynolds numbers much larger than those experienced by these organisms. Most studies were conducted in air at Reynolds numbers much larger ($O(10^4)$) than those experienced in shear flows in the open ocean. Typically velocities in oceanic layers range between 0.01 and 50 cm/s compared to 900 and 1500 cm/s or greater for the lab experiments, which is a difference of up to five orders of magnitude. Shear flows and mixing layers at these low flow speeds are laminar or transitional, and turbulent fluctuations may be sufficiently suppressed by stratification.

2.3 Zooplankton behavior

Environmental cues and individual behavioral responses play important roles in structuring pelagic communities (Hamner, 1988; DeMott and Moxter, 1991; Mackas et al., 1993; Fernandez and Acuna, 2003; Genin et al., 2005), and understanding the types and scales of various cues is important in developing an appreciation for the cascading affects of ecological interactions (predator-prey, mating, habitat choice). Vertical

migration and preferred depths in the water column are influenced by phototactic, chemical, mechanical, and visual cues (Bollens et al., 1994; Mackas et al., 1993, Manning and Bucklin, 2005). Escape responses from predators are elicited from both mechanical and chemical cues (Fields and Yen, 1997a,b; Kiørboe et al., 1999; Viitasalo et al., 1998; Fields et al., 2002). Foraging and feeding behavior also are mediated by responses to chemicals and hydrodynamic disturbances from prey items (Paffenhofer, 1998; Kiørboe et al., 1999). Mating and reproductive behavior often are direct responses to the presence of fluid dynamic or chemical cues from a mate (Strickler, 1998; Yen et al., 1998). In short, almost all types of behavior exhibited by planktonic organisms are related to environmental cues such as hydrodynamic disturbances, ambient light levels, and chemical exudates from conspecifics or prey.

2.3.1 Natural history

The sub-Class Copepoda of the phylum Crustacea comprises some 11,500 known species. Copepods are believed to be the most numerous multicellular organisms on Earth, outnumbering insects (Mauchline, 1998). Within the Copepoda, the Order Calanoida is made up of 12 superfamilies, of which the species in this study are members of the Centropagoidea or the Megacalanoidea. *Acartia tonsa* (Centropagoidea Acartiidae), *Eurytemora affinis* (Centropagoidea Temoridae), and *Temora longicornis* (Centropagoidea Temoridae) are dominate omnivores of the coastal habitats of the Eastern Atlantic ocean, and their distribution covers most of the Northern Atlantic. *Candacia ethiopica* (Centropagoidea Candaciidae) and *Labidocera madurae*

(Centropagoidea Pontellidae) are tropical, predatory copepods that feed predominately on other copepods and zooplankton. *Calanus* spp. (Megacalanoidea Calanidae) are often the largest copepod members of a plankton community ranging from 1-5 mm in size. A general sketch of the calanoid copepod, *Temora longicornis* is given in Figure 2.5.

All species of calanoid copepods exhibit similar life history traits. Individuals sexually reproduce, hatch from eggs, then go through a series of larval stages before entering the terminal adult stage. Most calanoids hatch as a first nauplius stage (NI) and progress through five molts to the NVI stage, although some stages are skipped among different species (e.g. *Labidocera* and *Pseudodiaptomus*; Mauchline, 1998). After the NVI stage molt, the copepod enters the initial copepodid juvenile stage (CI) then progresses through five more molts to the CVI or adult stage.

A. tonsa is a common euryhaline diel vertical migrator of plankton communities in many regions worldwide including areas where thin layers have been documented (Ogeechee River estuary, Georgia, USA; Holliday et al., 2004). *A. tonsa* is an important consumer of autotrophs in many of the world's coastal habitats with clearance rates (volume of food cleared) of adults at $80 \mu\text{m}^3$ ingested per copepod per day (Saiz et al. 1992) preferring large, single spherical or elliptical algae. Adults of this species are 0.75 - 0.85 mm in total length, and swim at speeds between $1-4 \text{ mms}^{-1}$. *A. tonsa* employs a hop-sink swimming pattern (Figure 2.6c) when not feeding, and utilizes a feeding current to entrain and capture prey items. As a generalist omnivore, *A. tonsa* prefers prey such as many species of diatoms and other phytoplankton as well as most microzooplankton (e.g

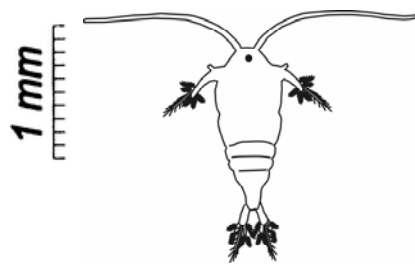


Figure 2.5 Sketch of the omnivorous calanoid copepod, *Temora longicornis*.

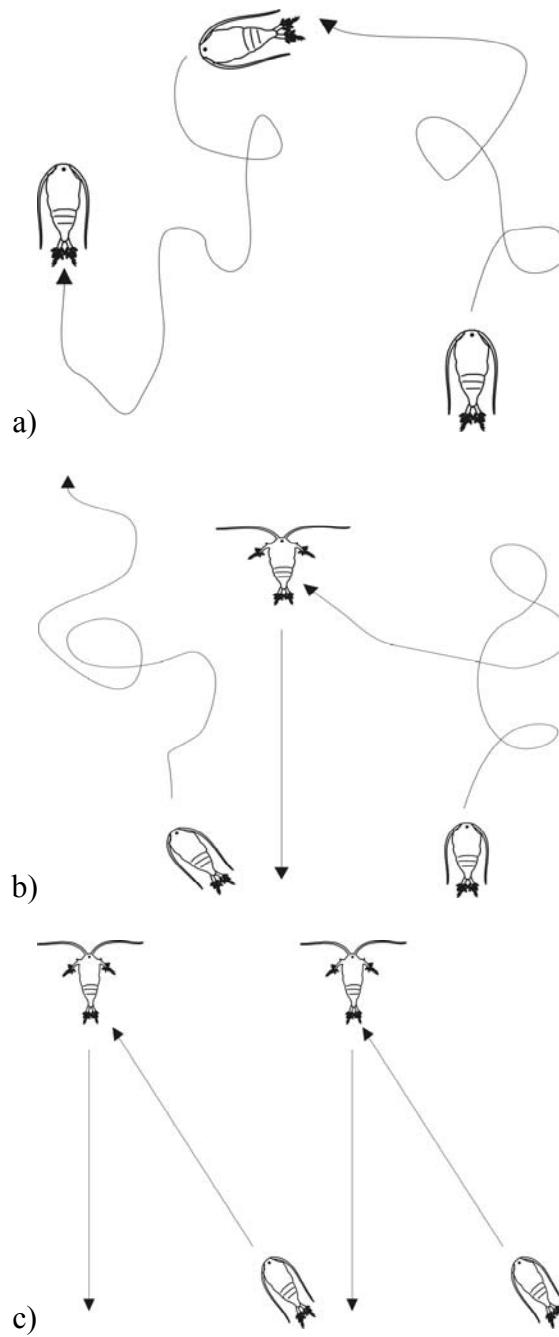


Figure 2.6 Swimming patterns of calanoid copepods: a) cruise style, b) cruise-sink style, c) hop-sink style.

protists, Mauchline, 1998). Generation times for *A. tonsa* are typically around 12 days but may vary between 9-40 days with 4-11 generations per year. Individuals typically mature in about 30 days and can live up to 70 days for females and 14 days in males (Mauchline, 1998).

Calanus, *Neocalanus*, and *Metridia* spp. often are the dominant, large copepods in many high latitude environments. *C. finmarchicus* lives in the North Atlantic, and *C. pacificus* is its counterpart in the mid-latitudes of the Pacific. *Neocalanus plumchrus* and *Metridia pacifica* are spatially, but not temporally sympatric species that occupy the North Pacific and Gulf of Alaska. Often the largest copepods in a community, *Calanus* spp. are very important to local fisheries and aggregations can lead to whale presence or aggregation at feeding grounds (see Wishner et al., 1988). Additionally, most *Calanus* spp. are predominantly herbivorous and can exert top-down control on phytoplankton communities (Dagg and Turner, 1982). *Calanus* spp. utilize a combination hop-sink/cruise-sink style swimming pattern (Fig. 2.6b,c), cruising from 1-10 mms^{-1} , and can exceed speeds of 50 mms^{-1} during predator escape responses using their antennules for propulsion. Generation times for *Calanus* and *Neocalanus* spp. vary greatly, from as little as 20-40 days (*C. finmarchicus*; *C. pacificus*) to as many as 110-120 days (*C. hyperboreus*; Mauchline 1998) with as few as one generation per year.

T. longicornis is a dominate member of coastal plankton communities throughout both the Atlantic and Pacific Oceans (Bigelow, 1926), is an important grazer in these waters (individual clearance rates at 72 μm^3 ingested per copepod per day; Mauchline,

1988), and is a vital food source for many commercial fisheries. Peak abundances are observed in the Northeastern Atlantic in the spring and summer months (Mauchline 1998). Adults are larger than 1 mm total length (Figure 2.5) and swim in a cruise style (Figure 2.6b) at speeds from 2 - 12 mms⁻¹ with escape velocities approaching 30 mms⁻¹. Generation times range between 15 - 45 days, with most around 25 days for *T. longicornis* with 3-6 generations occurring per year. These copepods are known to use hydromechanical and chemical signals for a wide range of ecological functions (Yen et al., 1998; Yen et al., 2004). Additionally, strain rate escape response thresholds for *T. longicornis* are known to be on the order of 1 s⁻¹ (Titelman and Kiørboe, 2003a,b), well below reported values of strain rate associated with thin layers (Dekshenieks et al., 2001; Cowles, 2004).

Eurytemora affinis is closely related to *Temora longicornis*, and many of the distribution regions overlap. However, *E. affinis* is more euryhaline and is often near regions of high freshwater input (e.g. Great Lakes, St. Lawrence River estuary). *E. affinis* adults are typically around 1.0 to 1.5 mm in total length and swim at 2-5 mms⁻¹ in a cruise-style pattern. Prey items preferred by *E. affinis* include most non-deterrent nanoplankton species as well as smaller microzooplankton. Generation times for *E. affinis* are between 19 - 36 days with up to 3 generations per year.

Candacia ethiopica and *Labidocera madurae* are important copepod predators in tropical waters of the Atlantic Ocean. *C. ethiopica* is found throughout the Atlantic and Indian Oceans, while *L. madurae* is found worldwide (Mauchline, 1998). Adults of both

species are about 2 mm in total length, with generation times on the order of 30 days and approximately 3-5 generations per year.

2.3.2 Mechanical signals and responses

Fluid mechanical signals are used by a wide variety of organisms during prey detection (e.g. spiders, Bleckmann and Rovner, 1984; Barth et al., 1993, 1995; fish, Coombs and Janssen, 1990; Janssen and Corcoran, 1993; seals, Dehnhardt et al., 2001; zooplankton, Kiørboe et al., 1999; Kiørboe and Visser, 1999) and predator avoidance (e.g. fish, Janssen, 2003; zooplankton, Haury, 1976; Yen and Fields, 1992; Fields and Yen, 1997a,b; Kiørboe and Visser, 1999). Documented behavioral responses of zooplankton to velocity variations include escape reactions, prey strike, and increased turning during movement (Weissburg, 1997; Fields and Yen, 1997a, b). These behaviors are elicited by variations in flow characteristics that bend setae or hairs on the surface of the organism (Fields et al., 2002; Yen et al., 1992). These sensory appendages, located over the entire body and concentrated on the antennules, generate neural signals in response to physical deflection (Fields et al., 2002). The setae bend when the tip moves relative to the body of the zooplankton. In order to cause a physical deflection, there must be a difference in the relative motion of the organism and its sensory appendage.

It has been proposed that organisms potentially respond to three types of flow disturbances; acceleration, vorticity, and deformation (Kiørboe et al., 1999). The acceleration vector of a flow is formally described as:

$$a_i = \frac{\partial u_i}{\partial t} + u_1 \frac{\partial u_i}{\partial x_1} + u_2 \frac{\partial u_i}{\partial x_2} + u_3 \frac{\partial u_i}{\partial x_3} = \frac{\partial u_i}{\partial t} + u_j \frac{\partial u_i}{\partial x_j} \quad (2-11)$$

where the subscripts i and j are each implied to be 1, 2, and 3 for a three-dimensional flow. The time-derivative term is called the “local acceleration” and corresponds to the time rate of change of the velocity. The spatial derivative terms are called the “convective acceleration” and correspond the rate of change of the velocity of a fluid element moving through a gradient of velocity. However, acceleration is not generally considered an important cue for zooplankton behavior (Kjørboe et al., 1999; Fields and Yen, 1997a,b). Therefore, vorticity and deformation have received much more examination in copepod behavior research.

In order to understand the physical difference between vorticity and deformation, it is important to review basic descriptions of velocity gradients. The decomposition of a general three-dimensional velocity gradient follows as:

$$\frac{\partial u_i}{\partial x_j} = e_{ij} + \frac{1}{2} r_{ij} \quad (2-12)$$

where

$$e_{ij} = \frac{1}{2} \left(\frac{\partial u_i}{\partial x_j} + \frac{\partial u_j}{\partial x_i} \right) = \begin{bmatrix} \frac{\partial u_1}{\partial x_1} & \frac{1}{2} \left(\frac{\partial u_2}{\partial x_1} + \frac{\partial u_1}{\partial x_2} \right) & \frac{1}{2} \left(\frac{\partial u_3}{\partial x_1} + \frac{\partial u_1}{\partial x_3} \right) \\ \frac{1}{2} \left(\frac{\partial u_2}{\partial x_1} + \frac{\partial u_1}{\partial x_2} \right) & \frac{\partial u_2}{\partial x_2} & \frac{1}{2} \left(\frac{\partial u_3}{\partial x_2} + \frac{\partial u_2}{\partial x_3} \right) \\ \frac{1}{2} \left(\frac{\partial u_3}{\partial x_1} + \frac{\partial u_1}{\partial x_3} \right) & \frac{1}{2} \left(\frac{\partial u_3}{\partial x_2} + \frac{\partial u_2}{\partial x_3} \right) & \frac{\partial u_3}{\partial x_3} \end{bmatrix} \quad (2-13)$$

$$\text{and } r_{ij} = \frac{\partial u_i}{\partial x_j} - \frac{\partial u_j}{\partial x_i} = -\varepsilon_{ijk} \omega_k = \begin{bmatrix} 0 & -\left(\frac{\partial u_2}{\partial x_1} - \frac{\partial u_1}{\partial x_2}\right) & -\left(\frac{\partial u_3}{\partial x_1} - \frac{\partial u_1}{\partial x_3}\right) \\ \left(\frac{\partial u_2}{\partial x_1} - \frac{\partial u_1}{\partial x_2}\right) & 0 & -\left(\frac{\partial u_3}{\partial x_2} - \frac{\partial u_2}{\partial x_3}\right) \\ \left(\frac{\partial u_3}{\partial x_1} - \frac{\partial u_1}{\partial x_3}\right) & \left(\frac{\partial u_3}{\partial x_2} - \frac{\partial u_2}{\partial x_3}\right) & 0 \end{bmatrix} \quad (2-14)$$

where e_{ij} is the strain rate tensor (relative velocity due to deformation), r_{ij} is the rotation tensor (relative velocity due to rotation), and ω_k is the vorticity vector. The subscripts i and j are again implied to be 1, 2, and 3 for a three-dimensional flow. An example velocity field for a simple shear flow and its corresponding components is illustrated in Figure 2.7.

Each flow disturbance type can bend setae as illustrated in Figure 2.8. Several studies have assessed the importance of flow disturbance as an important cue in zooplankton behavior, however it is not sure which one (shear or strain) is predominate in particular behaviors. Using simple physical arguments, Kiørboe et al. (1999) establish a theoretical framework for determining the important signal source for predator-prey interactions. The investigators illustrate the validity of their theoretical predictions, and suggest that velocity differences (fluid shear or strain) provide the most important cues for predator-prey dynamics as previously proposed by Yen and Fields (1992). Aggregations near thin layers suggest that velocity gradient cues may allow foraging zooplankton to narrow search behaviors to these regions (Leising and Franks, 2000).

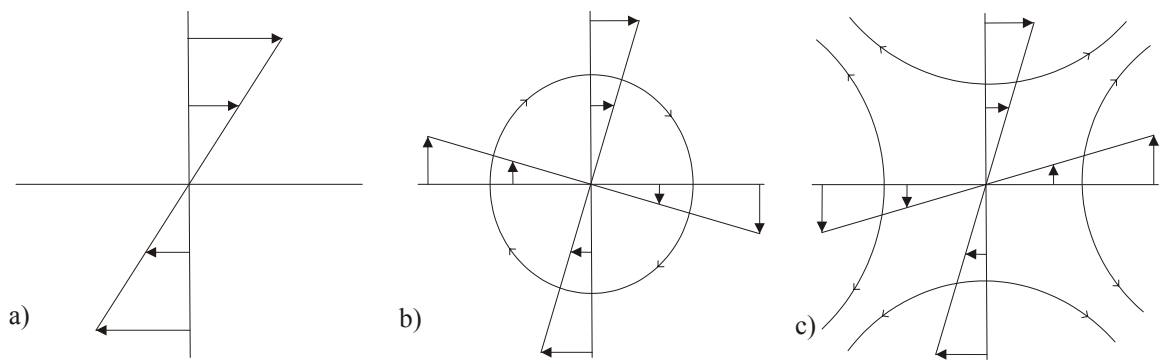


Figure 2.7 Decomposition of simple shear flow. Any flow can be decomposed in rotational (r_{ij}) and deformation (e_{ij}) components. These sketches show a) a simple shear flow with its corresponding b) rotational component, and c) deformation component.

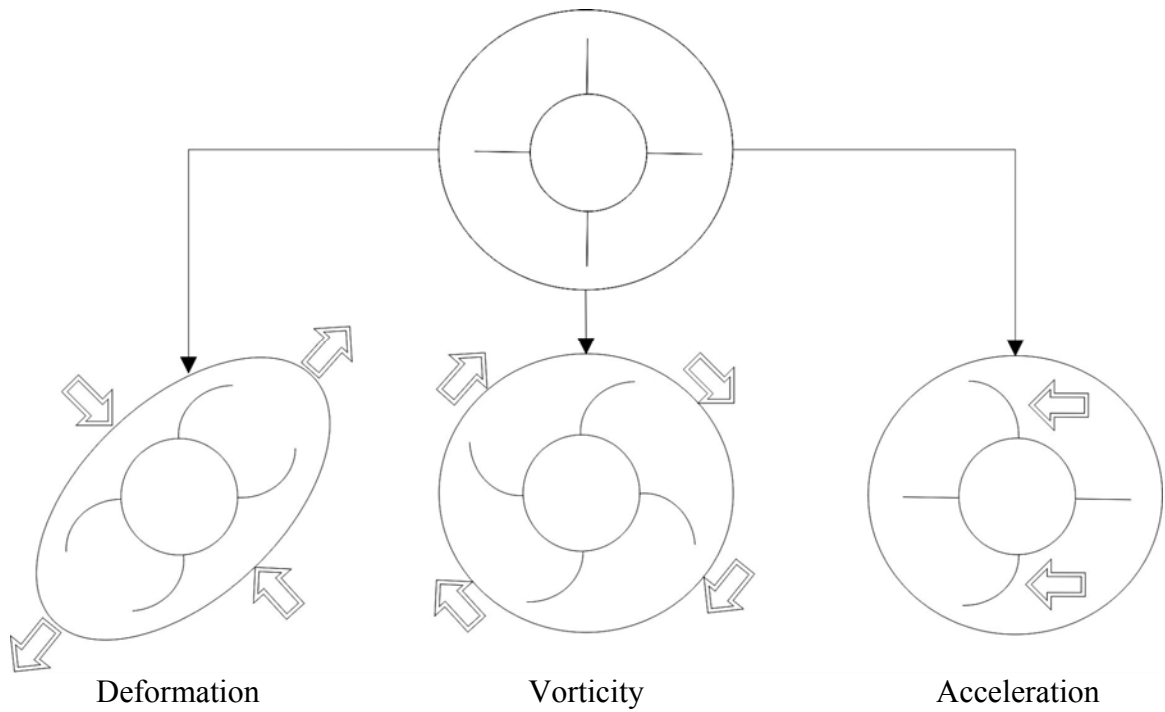


Figure 2.8 Schematic of bending patterns in response to fluid disturbances for an idealized creature with setae (adapted from Kjørboe et al., 1999).

Escape behavior in response to fluid disturbances is the most commonly studied aspect of mechanosensory interactions among copepods (Viitasalo et al., 1998; Kiørboe and Visser, 1999; Fields et al., 2002). In contrast, the use of mechanical signals in foraging and search behavior has received limited attention among zooplankton researchers. The threshold strain rate of escape responses range from 0.5 to 26 s⁻¹ as seen in Table 2.3 (Yen and Fields, 1992; Viitisalo et al., 1998; Kiørboe et al., 1999; Titelman, 2001; Titelman and Kiørboe, 2003a,b). Neurological responses are orders of magnitude lower than those reported to elicit escape responses (Fields et al., 2002). Mechanosensory setae of many copepods are known to respond to fluid velocities as low as 20 μms⁻¹ (Lenz and Yen, 1993; Yen et al., 1992). It is not known whether copepods use weaker signals during foraging and stronger signals as an alert to the presence of a predator.

Ambient flow conditions significantly affect the availability and reliability of hydrodynamic signals. Turbulence acts to dissipate kinetic energy, thus high turbulence levels can quickly diminish hydromechanical signals. Stress or strain from turbulent fluctuations can also act as noise in an habitat, masking hydrodynamic signals. Some authors suggest that copepod size has evolved to utilize specific flow characteristics (Yen and Strickler, 1996), and many copepods have developed adaptive behaviors to remove turbulent noise from their immediate surroundings (Moore et al., 1999; Yen and Strickler, 1996). By creating laminar feeding currents, copepods are able to detect minute variations in the velocity field of oncoming prey items, while large setae on the tips of the antennules protrude out of feeding current enable the detection of larger predators (Yen et

Table 2.3 Escape response thresholds among copepods and nauplii.

Species	Threshold strain rate (s⁻¹)	Hydrodynamic disturbance	Reference
<i>Acartia hudsonica</i>	0.80	Tethered <i>Temora longicornis</i>	Yen and Fields, 1992
<i>Acartia tonsa</i>	1.19-2.49	Flow from suction pipette	Kjørboe et al., 1999 Fields and Yen, 1997
<i>Acartia tonsa</i> nauplii	4.85		Fields and Yen, 1997
<i>Calanus helgolandicus</i>	0.52-3.24		Titelman and Kjørboe, 2003
<i>Centropages typicus</i>	2.60-2.79		Fields and Yen, 1997
<i>Euchaeta rimana</i>	2.05		Fields and Yen, 1997
<i>Eurytemora affinis</i>	1.88-2.65		Titelman and Kjørboe, 2003
<i>Euterpina acutifrons</i>	1.92-4.25		Fields and Yen, 1997
<i>Labidocera maduræ</i>	25.8		Fields and Yen, 1997
<i>Oithona</i> sp.	4.05		Fields and Yen, 1996
<i>Pleuromamma xiphias</i>	3.6		Titelman, 2001
<i>Temora longicornis</i> nauplii	2.78-3.96		

al., 1992; Lenz and Yen, 1993; Yen and Strickler, 1996; Fields et al., 2002). These currents may be disturbed by turbulence, therefore these organisms may be forced to rely on other types of cues to locate high resource patches and feed effectively. As with foraging tactics employed by other organisms (e.g. fish, Pohlmann et al., 2001; wasps, Tumlinson et al., 1993; Vet et al., 1999), zooplankton likely employ a suite of hydromechanical and chemical cues.

Density gradients can alter sinking and or swimming speed and consequently change the velocity of the animal relative to the surrounding fluid. Thus, organisms may sense density gradients in a similar fashion as a hydrodynamic disturbance or velocity gradient. Changes in density can provide cues or act as barriers to migrating zooplankton that lead to aggregation at these boundaries (Harder, 1968; Tiselius et al., 1994; Lougee et al., 2002). Harder (1968) observed that *T. longicornis* aggregated to a density gradient in absence of a salinity gradient, but did not aggregate to a salinity gradient without a density change, which suggests that the response is likely to be mechanically and not chemically mediated.

2.3.3 Chemical signals and responses

Chemical cues are known to play important roles in mating (Doall et al., 1998), predation (Weissburg et al., 2002), and predator avoidance (De Meester et al., 1999) among copepods. Many species of plankton also are known to utilize chemical information to cue predatory behavior and diel vertical migration (Hamner and Hamner,

1977; Hamner et al., 1983; Poulet and Marsot, 1978; Poulet and Oullet, 1982). Plankton are known to adjust vertical migration depths and cycles in response to chemical signals (Bollens et al., 1994; Dodson et al., 1997). Also, male copepods respond to mating cues by following coherent odor trails until the female is located (Yen et al., 2004; Doall et al., 1998; Strickler, 1998). Copepods could use this or similar behaviors to locate prey as well. Exudates from phytoplankton contain compounds such as amino acids, which attract foraging copepods and cause swarming (Poulet and Oullet, 1982), and other forms of chemical cues are also available.

The types of chemicals used as cues range from simple amino acid or ammonia by-products to complex and highly specific secondary metabolites (Zimmer and Butman, 2000). To date, isolation of attractive chemical cues has remained elusive. Chemical signals may provide information about the size, location, and identity of the sender, and this information must be transported through the environmental medium (Dusenbery, 1992). Therefore, turbulence and other hydrodynamic characteristics can have a profound affect on the availability and reliability of chemical information (Zimmer and Butman, 2000; Weissburg, 2000). Because of the size of many zooplankton, the hydrodynamic characteristics are often challenging to quantify due to the transitional regime near Reynolds numbers of unity (Yen, 2000). However, in thin layers, density stratification acts to suppress turbulent motions. At the intermediate scales of zooplankton foraging, velocity gradients, chemicals, and food patches are often in temporally and spatially well-defined regions (Mitchell and Okubo, 1988).

Early investigations on the chemosensory behavior of zooplankton focused on the ability of these organisms to follow scent trails and locate prey (Hamner and Hamner, 1977; Poulet and Oullet, 1982; Hamner et al., 1983), but these studies often were not conducted under relevant field conditions (e.g. artificially high concentrations). Later studies provided a framework for the use of chemical cues by copepods that forage via feeding currents (Jiang et al., 2002; Moore et al., 1999). These studies suggest that a copepod can utilize chemical cues to sense a food particle and then direct it into the center of its feeding current, thus increasing the likelihood of capture.

More recent investigations on the chemosensory abilities of copepods have suggested that hydromechanical cues may be more important than chemical cues in prey detection and capture (Svensen and Kiørboe, 2000). At the range of copepod-prey interactions, chemical cues may not provide adequate information about speed, size, and location. Nevertheless, chemical cues may assist in area-restricted search behavior required to survive in a patchy environment (Leising and Franks, 2000). Average concentrations of prey in the open ocean are not sufficient for many species to meet daily requirements (e.g. *Calanus pacificus*, Mullin and Brooks, 1976); however, patches of high phytoplankton productivity can support zooplankton survival (Daro, 1988). Thus, chemical exudates from high concentrations of phytoplankton may provide the general cue for area-restricted searches, while mechanosensory information provides the cue for attack and capture of prey.

2.3.4 Cue hierarchy and associations

Most studies on copepod foraging have focused on large-scale (meters) or small-scale behaviors (mm). Large scale behaviors such as diel vertical migration occur at the scale of the water column. Small scale behaviors occur once a food particle or mate is within the immediate sensory vicinity of the foraging organism (although this scale is harder to accurately define). However, at intermediate scales, copepods are likely to have adapted search strategies to improve overall fitness. Such strategies include area-restricted search behaviors, and the use associational cues embedded in a cue hierarchy.

Many organisms utilize a cue hierarchy by associating different environmental or biological characteristics with a particular resource (Tumlinson et al. 1993; Vet, 1999). Associational cues help organisms deal with the disparity of scales that arises from reliability-detectability dilemma. The reliability of a cue is a measure of its degree of association with the target or goal. An example of a highly reliable cue is the volatile chemicals released by an apple (the smell). This cue almost without fail signifies the presence of an apple. However, it is difficult to smell an apple from a long distance. The detectability of a cue is a measure of its availability at specific spatial and temporal scales. For the apple case, the smell would have low detectability at large distances, whereas as a visual cue would be detectable since the apple is bright red. However, at large distances, the visual cue has lower reliability. In the search for an apple, an organism will employ more detectable, less reliable cues during initial searches, and then focus on less detectable, more reliable cues as the search area narrows. Thus, animals utilize a suite of sensory pathways in a hierarchy to improve foraging at particular scales.

The use of a cue hierarchy has been most well established in terrestrial arthropods (Tumlinson et al., 1993). Many organisms, including humans utilize cue hierarchies in a variety of behaviors. For example, parasitic wasps utilize the cue hierarchy shown in Figure 2.9. In this schematic, a parasitic wasp first utilizes cues associated with a particular plant species. Once such a plant is found, the wasp uses cues associated with fruiting bodies on the plant to further minimize search areas. Finally, once on the fruiting body, the scales of interaction are appropriate for direct location of a mate. In aquatic systems, blue crabs (*Callinectes* spp.) utilize flow velocity cues to direct movement, and chemical cues to ultimately locate prey (Weissburg, 2000).

Density and velocity gradients are more common, easily detectable cues for foraging at larger scales than chemical exudates or phytoplankton presence alone that warrant brief searches for other information thus focusing the search region, reducing energetic expenditure, and improving individual fitness (Hamner, 1988; Cowles, 2004; Gallager et al., 2004). Physical gradients are more common than chemical exudate gradients, and therefore meet the criteria for detectability at larger scales. Additionally, momentum dissipates faster than scalar quantities (exudates, phytoplankton cells), thus velocity gradients often surround chemical exudate or food patches (Cowles, 2004). Gallager et al. (2004) proposed that aggregations at these layers are a result of copepods using this information to narrow search regions. In contrast, waterborne chemical exudates provide more reliable, but possibly less available cues that also induce swarming and area-restricted search behavior (Poulet and Marsot, 1978; Poulet and

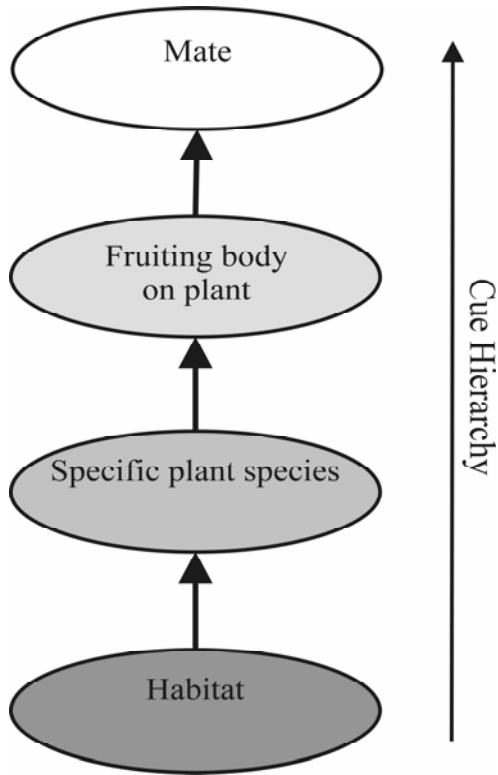


Figure 2.9 Idealized cue hierarchy for a parasitic wasp (adapted from Tumlinson et al., 1993).

Ouellet, 1982). Finally, contact cues (mechanical or chemical) with individual prey cells are likely to provide the most reliable, close range cues that initiate feeding response (e.g. Tiselius, 1992). This detectability-reliability issue has been thoroughly addressed for specialist insects in terrestrial systems, and suggests that foraging individuals employ a host of cues to improve search success and foraging efficiency (Vet, 1999).

2.3.5 Aggregations and patchiness

Aggregative behavior in zooplankton is often credited either to physical processes or to behavior (Banas et al., 2004). Physical processes such as internal waves, currents, stratification, and turbulence, may affect aggregations, but only at large spatial and temporal scales. However, behavioral interactions that promote aggregations and swarming act at small scales that may not be observed by typical oceanographic or biogeography studies. Behavioral responses that lead to aggregations are attributed to either social interactions (Yamazaki, 1993), or individual-based responses to environmental cues (Okubo and Anderson, 1984; Okubo, 1986). These types of behavior differ in that the former is a response to signals/cues that are the product of animals at certain density; whereas the latter is the result of attraction to an external cue (see Ambler et al., 1991, Banas et al., 2004). Zooplankton may exhibit social behavior during mating, but responses to environmental cues such as light, flow characteristics, or chemical odors appear to be the primary driving forces behind zooplankton swarms (Banas et al., 2004). Zooplankton interaction with environmental conditions is directly affected by their ability to perceive and respond to mechanical and chemical information in their surroundings.

The interaction of these processes at relevant scales affects observed community structure and, therefore is an important aspect of plankton ecology.

On large scales, advective motions of currents can act to transport organisms into general areas. On smaller scales, turbulent motions mix passive particles. Abraham (1998) illustrates how turbulent advection can explain plankton patchiness at large scales (order of kilometers), but variation at small scales is also present. Phytoplankton closely follow distributions of passive scalar quantities, while zooplankton show intense variability even at the smallest scales. The patchiness, described at the inertial scales by Abraham (1998), is the result of turbulent transport, or behavioral responses (Mackas et al., 1993). The strength of this process is often defined by the turbulence intensity or the turbulent diffusivity. Surface winds play an important role in the variation of turbulence through the water column, with the highest turbulent intensity near the surface and lowest in the pycnocline (Yamazaki and Osborn, 1988). Density stratification acts to attenuate vertical velocity fluctuations, and thus may aid in creating vertical aggregations of passive particles in regions of uniform density (Alldredge et al., 2002).

It is increasingly apparent that organism behavior may be equally or more important than turbulence and flow conditions in defining large-scale patterns. Spectral analysis of time records of chlorophyll concentration in the open ocean closely follows the $5/3$ -power law for the inertial subrange of turbulent spectra (Platt, 1972). In contrast, Powell and Okubo (1994) and Abraham (1998) found that spectral analysis of zooplankton density does not follow a $5/3$ -power law. These investigators suggest that

aggregative behavior increases the variance at small scales. Thus small-scale interactions of actively foraging, mobile consumers can have significant cascading effects on distributions and patchiness.

Random walk models have been used to attempt to explain foraging and aggregative behavior (Okubo, 1986). Initial models utilized Fickian diffusion in the form of attraction to simulate aggregative behavior (Okubo, 1972). Later techniques utilized density estimation parameters from a Lagrangian viewpoint, but still neglected animal behavior and responses to environmental cues (Yamazaki and Haury, 1993). Dynamic Lagrangian equations using autocorrelation techniques have also been employed to model aggregative behavior with some success, but these models still neglect other environmental parameters (Yamazaki and Okubo, 1995).

Okubo (1986) uses an individual-based model to assess aggregative behavior and maintenance. Banas et al. (2004) provide an experimental validation of this type of model based on data from aggregations of daphnids and *Temora longicornis*. Phototaxis is known to maintain swarms in some cyclopoid copepods as well (Ambler et al., 1991). Zooplankton are also known to respond to hydrodynamic disturbances and chemical scents (see Sections 2.3.2 and 2.3.3). However, other than phototaxis, these cues have not been experimentally evaluated as cues for aggregative behavior.

The impacts of patchiness on individual fitness are not known. As discussed in Section 2.1.3, the scales of patchiness experiments in the laboratory may not be

appropriate to resolve these issues. At the scale of a water column, energetic expenditures of foraging will be much greater than those resulting from searching a 2 meter tall tank (17 cm × 10 cm cross section; Bochkansky and Bollens 2004; Ignoffo et al., 2005), and assessing patchiness on relative percentages of the habitat with sufficient resources will not capture this energetic scale.

Harder (1968) and Lougee et al. (2002) suggest that aggregation at density discontinuities boundaries may be due to energetic advantages while suspended in the water column. More dense fluid requires less effort to maintain vertical position; however, a lighter fluid requires less inertial input to swim. Bochkansky and Bollens (2004) and others suggest that density gradients may also act as a positive cue for limiting search behavior. On the other hand, density differences may simply act as a physical or behavioral barrier to vertical migration (Harder, 1968; Hamner, 1988; Leising, 2001). The mechanisms and motivations of copepod aggregation at physical discontinuities remain unresolved.

2.4 Conclusions

The ability of zooplankton, in particular various species of copepods, to associate the characteristics of thin layers with high food availability will provide significant advantages for survival. Characteristics of thin layers that may be available to copepod include velocity, turbulence, density, or chemical gradients. Each of these signals may elicit area-restricted search behavior thus promoting aggregation. Many of these cues are well studied at scales relevant to prey capture among biologists and at large scales by

engineers and oceanographers. Observations generally have not been reported at scales that demonstrate aggregative behavior among foraging zooplankton. Experimental support for the hypotheses proposed by Leising and Franks (2000) will require a definition of the scales at which these cues can be effective and determination of those that are predominant in eliciting aggregative behavior and creating observed patchiness in the open ocean.

Reported strain rates in thin layers range from 0.01 to 1.0 s⁻¹ (Dekshenieks et al., 2001), but may be higher due to instrument resolution limitations. This range appears within the neurological limits of organisms, but behavioral responses have not been directly observed or tested. Copepods may also be able to detect thin layers via differences in their descent velocity due to steep density gradients. Another physical characteristic of thin layers, especially in the pycnocline is attenuated turbulence. Copepods may be able to recognize a reduction in velocity fluctuations. Although Svensen and Kiørboe (2000) suggest that chemical cues may not be adequate for direct prey capture, these types of signals may provide key information about search areas. The presence of compounds associated with thin layers may key foraging zooplankton to high resource patches.

The goals of the present study are to isolate and analyze the importance of the various cues in the formation of zooplankton aggregations associated with thin layers. A carefully-designed planar jet apparatus is used in the laboratory to isolate the effects of strain rate, density gradients, and chemical gradients. Additionally, these cues can be

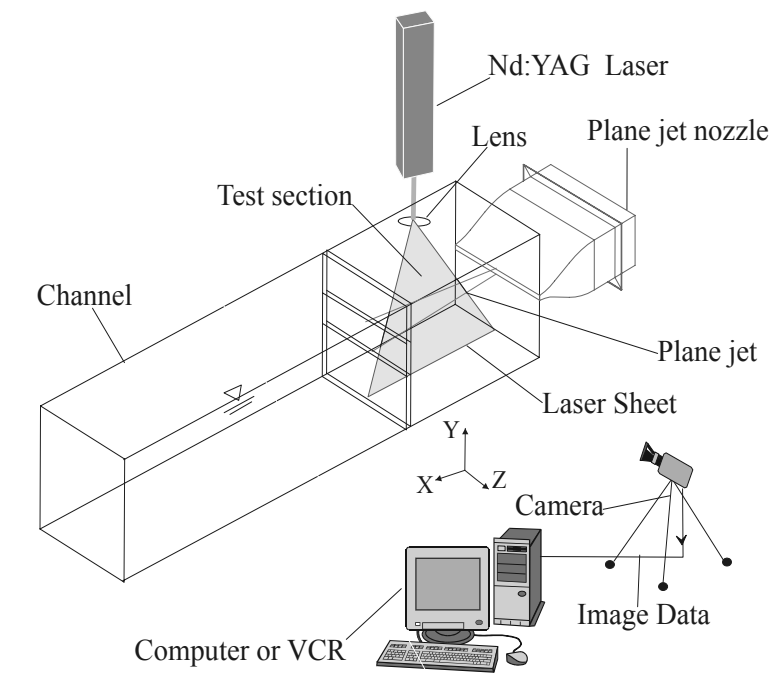
combined to better understand how foraging copepods exploit thin high-resource patches, and thus impact pelagic ecosystem processes.

Chapter 3 Methods

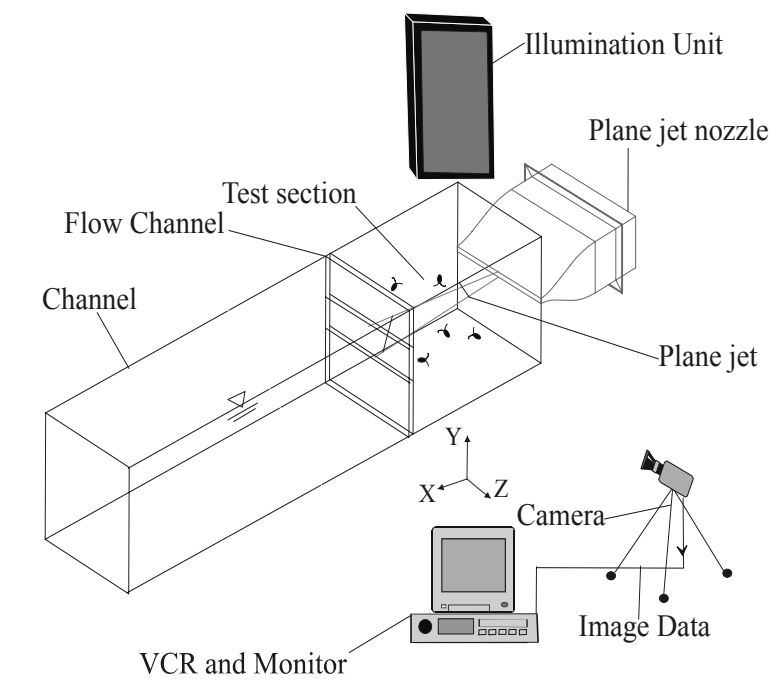
The experiments in this study involved the isolation and quantification of relevant cues associated with thin layers and the behavioral responses of copepods to the simulated environmental gradients. The research was conducted in two phases: flow characterization followed by copepod behavioral assays. Flow characterization was performed using particle image velocimetry (PIV) and planar laser-induced fluorescence (PLIF). These techniques are widely used in fluid dynamics research and allow for the quantification of properties such as local velocity, layer thickness, strain rate, local concentration, and mixing efficiency. This phase of the study allowed for the definition and creation of ecologically relevant conditions for the second phase of the study. Copepod behavioral assays were designed to evaluate the importance of features identified during flow characterization in defining aggregative behavior, and to determine threshold levels that elicited such behaviors.

3.1 Flow system

A plane jet apparatus was used in the experiments to model appropriate velocity, density, chemical, and food gradients associated with thin layers. The apparatus consisted of a long clear acrylic tank (100 cm × 30 cm × 30 cm) with a stainless steel slot jet nozzle (1 cm high × 25 cm wide) mounted on one end (Figs. 3.1-3.3) in the center of the tank (14 cm above bottom). The water depth in the tank was 28 cm. A constant head tank (28 L) drove the flow from the slot jet (Fig. 3.2). The plane jet developed through the center of the tank and flowed into a retrieval unit near the end of the test section (20



a)



b)

Figure 3.1 Plane jet flow system. a) PIV/LIF arrangement and b) behavioral assay arrangement.

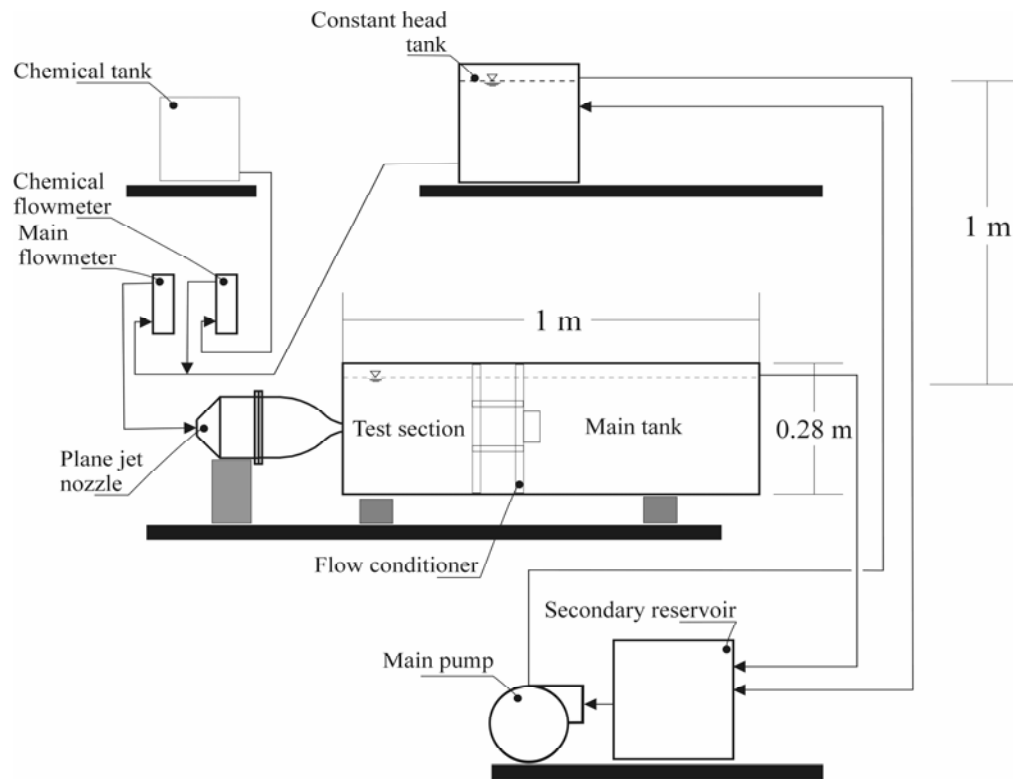


Figure 3.2 Plane jet flow system.

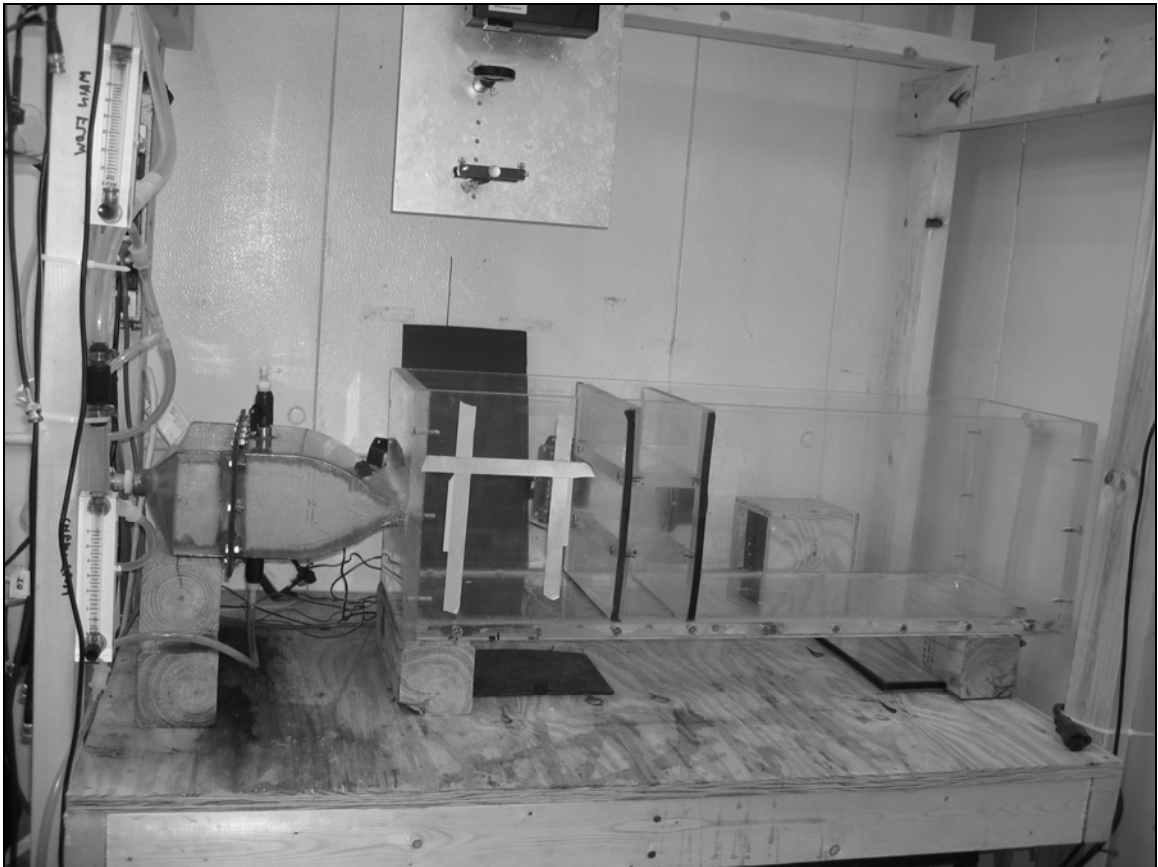


Figure 3.3 Photo of the experimental apparatus showing the plane jet nozzle, test section, main tank, and flow meters.

cm from nozzle exit) where it was transferred to a secondary (isolated) tank (28 L). The flow conditioner (30 cm high \times 25 cm wide with 6 cm \times 25 cm wide contracted opening; see Fig. 3.2 and 3.3) channeled all flow from the jet through a circular opening (50 mm dia.) and prevented recirculation of flow in the test section. A flow straightening edge was placed in the tank 16 cm from the nozzle exit. A remote pump (Dolphin Pumps, #DP-800) returned the water to the constant head tank. Figure 3.1a shows a diagram of the flow system with the set-up for PIV and PLIF measurements and the configuration for the behavioral observations.

In order to insure a top-hat velocity profile at the jet nozzle exit, a 12:1 area ratio contraction was located immediately upstream of the nozzle opening. A 5th-order polynomial defined the shape for the contraction walls, which prevented flow separation in the nozzle (Hussein, 1994). Three flow conditioning screens (stainless steel mesh) with 50% open area were mounted in the straight section of the flow conditioning section to create uniform flow conditions and reduced turbulent fluctuations at the nozzle exit (Mehta and Bradshaw, 1979). Water was supplied to the conditioning section via a 20 mm threaded connection. The conditioning section also had 7 mm threaded connections on the top and bottom for air removal and drainage, respectively.

A coordinate system also is shown in Figure 3.1. The x -coordinate corresponded to the downstream distance with the origin at the nozzle edge. The y -coordinate corresponded to the vertical direction with the origin at the jet centerline, and the z -coordinate was the transverse direction. The 10 cm \times 10 cm observation region was

located 5 nozzle lengths (at $x/D = 5$ or $x = 50$ mm) from the nozzle exit insuring that the jet had achieved a self-similar profile and extends to $x = 150$ mm. Vertically, the region was located in the center of the tank such that the centerline of the plane jet was located at $y = 0$.

3.2 Experimental parameters

The jet was operated in the laminar flow regime in order to simulate conditions associated with thin layers so that important behavioral cues could be determined for zooplankton encountering these environmental structures. Strain rates reported with thin layers are often very low (less than 0.5 s^{-1}), although it should be noted that the resolution of velocity data collected *in situ* is still not adequate to truly resolve these gradients (see Section 2.1.2). Maximum strain rates in the laminar jet are controlled by adjusting the jet Reynolds number, $Re_j = Ud/\nu$. PIV allowed quantification of the target flow conditions over the entire flow field, and because the flow was laminar and steady, these results did not vary in time and were repeatable. Table 3.1 illustrates the range of strain rates and the corresponding flow rates used for physical gradient characterization experiments. For behavioral experiments, the jet exit velocity is chosen to be $U_j = 6.7 \text{ mms}^{-1}$ because this was the lowest flow rate that was laminar and stable during the course of experiments.

Thin layers often develop at the pycnocline or at fine-scale density jumps in the water column (Cowles, 2004). This situation was modeled dynamically as a three layer flow with density stratification in the middle layer. Figure 3.4 shows a schematic

Table 3.1 Sample experimental parameters.

Q ($\text{cm}^3 \text{ s}^{-1}$)	Max Strain Rate at $x = 50 \text{ mm}$ ($S, \text{ s}^{-1}$)	δ_s at $x = 50 \text{ mm}$	Max Strain Rate at $x = 150 \text{ mm}$ ($S, \text{ s}^{-1}$)	δ_s at $x = 150 \text{ mm}$	Re_j
10.5	0.10	17.7	0.06	27.4	33
12.6	0.19	17.8	0.08	27.5	39
14.7	0.28	17.6	0.10	27.5	46
16.8	0.35	17.7	0.12	27.6	52
18.9	0.51	17.6	0.15	27.7	60

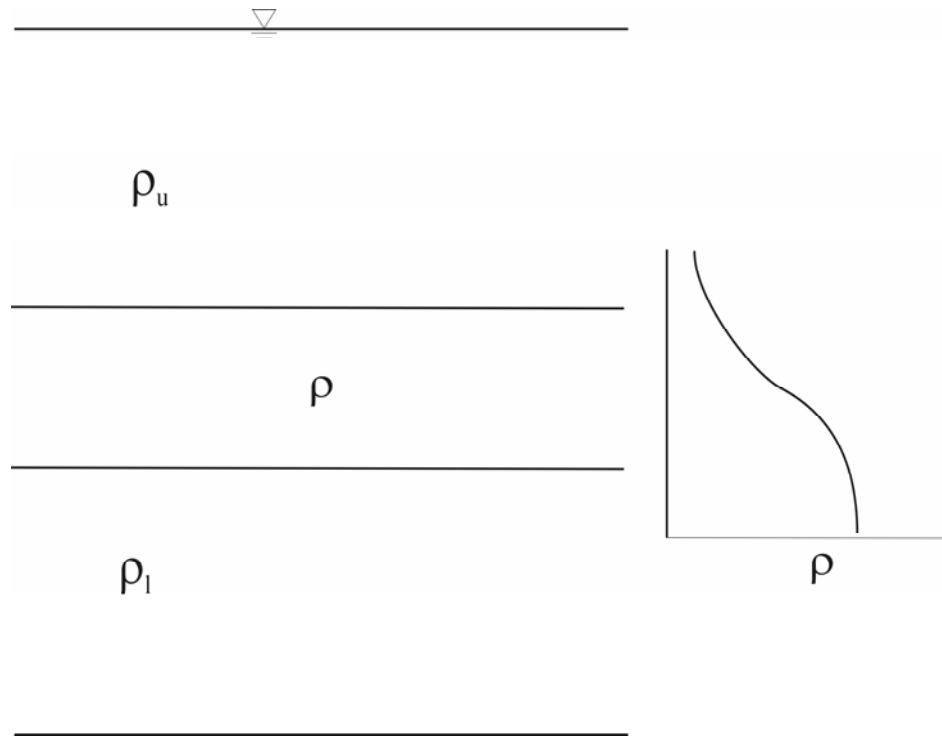


Figure 3.4 Experimental representation of a stratified plane jet layer where $\rho_u < \rho_l$.

representation of the experimental stratified layer. For density gradient experiments, the flow system was filled halfway with a lower density fluid (30 ppt at 12 °C) and then filled slowly from below with a higher density fluid (32 ppt at 12 °C) corresponding to a 2 ppt salinity change at constant temperature. In addition to this base case, salinity changes of 0.25, 0.5, 1.0, and 4.0 ppt were also tested with an upper layer always at 30 ppt to examine thresholds and density gradient strength effects on organism behavior. Temperature gradients were not examined because of the difficulty in maintaining such gradients over time periods sufficient for behavioral observations. The strength of the density gradient is expressed as the buoyancy frequency, N , and is calculated as:

$$N = \sqrt{-\frac{g}{\rho_o} \frac{\Delta\rho}{2\delta_s}} \quad (3-2)$$

In this discrete formulation, $\Delta\rho$ is the density difference between the upper and lower fluid ($\rho_1 - \rho_2$), ρ_o is the effective reference density $(\rho_1 + \rho_2)/2$, and δ_s is the layer half-width.

Density layers were created in the experimental tank by first filling to the centerline with the less dense fluid. Next, the more dense fluid (or bottom layer) was slowly introduced via a pump (Dolphin Pumps, #DP-385) through the drain port at the bottom of the tank. The lower-layer fluid slowly raised the less dense fluid with minimal mixing. The result was a density discontinuity in the middle region of the tank. For physical characterization, the bottom layer was seeded with a known concentration of a

fluorescent dye (Rhodamine 6G) and PLIF was used to quantify the profile of the density gradient layer.

Chemical or food gradient layers were created by adding a known concentration of tracer dye solution (matched salinity, 30 ppt) at a specified flow rate to the plane jet nozzle via a secondary pump (Dolphin Pumps #DP-385) upstream of the primary flow meter. Characterization of chemical or food gradient layers was conducted using Rhodamine 6G as a tracer dye. Dye advection across the experimental section of the tank was timed, and the flow was stopped once the dye reached the flow conditioner at the end of this region. The jet momentum was allowed to dissipate for ten minutes before measurement of the gradient layer using PLIF. This procedure created a distinct chemical layer in the middle of the test section without the use of density gradients as employed in many previous thin layer or patchiness studies (Tiselius 1992; Bochdansky and Bollens 2004; Clay et al. 2004), and isolated the chemical cue for behavioral experiments. Estimated dilution of the tracer dye solution was done by using PLIF calibrations over a range of flow rates from the secondary pump. The dilution, D , was equal to the total flow rate, Q_T , divided by the tracer solution flow rate, Q_S ($D = Q_T/Q_S$) because the tracer solution is added upstream of the primary flow meter. Main flow from the constant head tank was set at $16.8 \text{ cm}^3 \text{ s}^{-1}$, and the secondary flow rate was set at $4.2 \text{ cm}^3 \text{ s}^{-1}$ and therefore resulted in a dilution factor of 4.0. The concentration of Rhodamine 6G in the tracer dye solution was set at $200 \text{ } \mu\text{g L}^{-1}$ so that C_o (initial concentration of dye at nozzle exit) was equal to $50 \text{ } \mu\text{g L}^{-1}$. Several calibration experiments were run to insure that the effluent from the nozzle was thoroughly mixed as it entered the test section.

Combined cue layers were created using combinations of the above techniques. Velocity-chemical layers used the main flow at $16.8 \text{ cm}^3 \text{ s}^{-1}$ in combination with the secondary pump (dye tracer), or gravity feed to prevent cell lysing (phytoplankton, or phytoplankton exudates) at a flow rate of $2.1 \text{ cm}^3 \text{ s}^{-1}$. These flow rates resulted in a dilution ratio of 8, so initial concentration of solution was scaled accordingly (for tracer dye, $400 \mu\text{g L}^{-1}$). Reservoir water was not recirculated over the course of experiments to prevent concentration increases in the model layer. Velocity-density model layers were created by filling the tank, reservoir, and constant head tank just over half full with 30 ppt artificial seawater. Denser (32 ppt) seawater was then pumped into the tank through the drain fitting until the density jump was aligned with the bottom of the slot jet nozzle (0.5 cm below the mid-point of the tank). Once full, the plane jet was turned on at an exit velocity of 6.7 mm s^{-1} , just as in the velocity-only layer experiments. Density-chemical layers were created by using the methods described above for the velocity-chemical layer, but with the secondary pump at $4.2 \text{ cm}^3 \text{ s}^{-1}$, and a dilution ratio of 4. Tracer solution concentration was $200 \mu\text{g L}^{-1}$ as in chemical-layer only experiments. The density gradient was created as in the density-chemical layer, by filling the tank with two different salinity fluids (30 and 32 salinity). Once the chemical layer passed through the flow conditioner, both pumps were turned off, and residual momentum from the jet was allowed to dissipate. These methods resulted in a thin layer of chemical concentration with a density gradient on the lower boundary. Finally, velocity-density-chemical layers were created in the same fashion with the secondary pump set at $2.1 \text{ cm}^3 \text{ s}^{-1}$, which yields a dilution ratio of 8 as in the velocity-chemical layer.

3.3 Physical measurement techniques

3.3.1 Particle image velocimetry

Data acquisition for particle image velocimetry (PIV) consisted of capturing sequential images of light scattered from particles suspended in a flow. The particles must be small and close to neutrally-buoyant in order to insure that the particles follow the fluid motion. For this investigation, titanium dioxide particles with diameter of less than 5 μm were used for flow seeding. Illumination was provided by a pair of Nd:YAG lasers (New Wave Minilase III; 532 nm wavelength, 50 mJ per pulse) that were mounted above the tank on a sliding bracket (see Figure 3.1a). The laser beam was focused with a 1 m focal length spherical lens and expanded with a -12.6 mm cylindrical lens creating a thin sheet through the observation region.

An eight-channel pulse generator (Berkeley Nucleonics Corporation 500D) sequenced the laser firing with the shutter of a CCD camera (Kodak Megaplug ES 1.0; 8-bit, 1018×1008 pixels). The camera had a 105-mm lens (Nikon AF Micro Nikkor). The images captured by the camera corresponded to the $10 \text{ cm} \times 10 \text{ cm}$ observation region of the test section (see Section 3.1) and had a resolution of roughly $100 \mu\text{m}/\text{pixel}$.

The image capture system was operated through a computer running the Windows 2000 operating system. A Coreco image capture board provided the interface between the camera and the computer. Image sequences were captured using Video Savant 3.0

software (IO Industries) and were stored real-time on the hard drive array. A typical image sequence was 500 images taken at a sampling rate of 20 Hz for a period of 25 seconds.

The displacement of the particles between consecutive images was determined via a spatial correlation performed for 16×16 pixel sub-windows. Spatial correlations were calculated using the cross-correlation function as:

$$R_{II}(x, y) = \sum_{i=-K}^K \sum_{j=-L}^L I(i, j) I'(i + x, j + y) \quad (3-6)$$

where $I(i, j)$ and $I'(i, j)$ are the representative light intensity of the individual pixels in the first and second images, respectively. The computation of this function, actually performed in wavenumber space, yielded a correlation peak that signifies the average planar shift for all particles in the sub-window. The location of the correlation peak was realized within $1/20^{\text{th}}$ of a pixel for an 8-bit image by employing a Gaussian peak fit (Raffel et al., 1998). The displacement vector was divided by the time delay between laser pulses (e.g. 0.05 s) to produce the velocity vector. The correlation was repeated until the entire image as been covered, yielding an instantaneous two-dimensional velocity vector field. The correlations, peak fits, and post-processing were performed using analysis software developed by Dasi (2004).

Sources of error or measurement uncertainty included typical experimental sources such as aliasing and background noise, but more specific to this technique were

loss of particle pairs, inaccurate correlations, and too few particles per interrogation sub-window. In consecutive images, particles may either leave the imaging frame, or pass completely through the laser sheet. This results in a loss of particle pairs, and can reduce the correlation peak as well as introduce bias into the correlation field. Correction factors were employed to remove bias errors, and adjustments to experimental parameters such as the time step can alleviate other sources of error (Raffel et al., 1998).

For the laminar plane jet flow used in this study, out-of-plane loss of pairs did not make a significant contribution to error and uncertainty. Similarly, in-plane loss of pairs was minimized using small time steps or large interrogation windows. In this study, the resolution was sufficient to capture velocity gradients at the scale of individual copepods ($<100\ \mu\text{m}$), therefore interrogation windows of 16×16 pixels are used, with a time step of 0.05 s. These parameters allowed for losses on the order of 5% of the entire vector field. The code developed by Dasi (2004) was verified using numerical simulations of PIV data fields, therefore alleviating issues pertaining to inaccurate correlations. Velocity measurements for turbulent flows were within $\pm 2\text{-}3\%$ of actual values (Webster et al., 2001), and may be better due to minimal out-of-plane loss in this laminar flow.

3.3.2 Planar laser induced fluorescence

Planar laser induced fluorescence (PLIF) relies on the principle that the intensity of light emitted by a fluorescent dye is proportional to its concentration and the incident light intensity. This technique allowed for the capture of images of the instantaneous

scalar field, and thus allows for the evaluation of chemical signal structure. Using this technique allowed investigators to measure the instantaneous concentration distribution.

Rhodamine 6G was used as the dye with a peak absorption of 530 nm and a peak emission of 560 nm (Acroumanis et al., 1990). The laser and camera arrangement for PLIF was the same as described for PIV. The emitted light was in the yellow-orange wavelengths, and the camera had an optical cut-off filter (Tiffen color 21) allowing the emitted light to pass, while blocking the green laser light. The intensity of the emitted light was linearly proportional to the concentration of the dye. Thus, in order to convert raw image intensity data to concentration, calibration curves were developed prior to each experiment. Using a small container set in the tank, a time series of images of the emitted light from six known concentrations (0, 5, 10, 15, 20, 25 $\mu\text{g L}^{-1}$) were captured. These images were averaged and a least-squares regression was applied to obtain a calibration curve for each individual pixel (Webster et al., 2003).

PLIF was also used to characterize the density gradient layer experiments. To obtain salinity (or density) profiles, 50 $\mu\text{g L}^{-1}$ of Rhodamine 6G was added to the more dense lower fluid prior to pumping into the tank. The molecular diffusion coefficient of Rhodamine 6G ($\sim 10^{-9} \text{ m}^2 \text{ s}^{-1}$) and salt ($\sim 10^{-9} \text{ m}^2 \text{ s}^{-1}$) are essentially the same making this a valid technique over the time scales of these experiments (Webster et al. 2003). Once the tank was full, data was collected in the same fashion as described above.

Measurement uncertainty in PLIF arises primarily from pixel saturation, calibration procedures, and repeatability of laser sheet intensity (Webster et al., 2001). It is important to utilize tracer concentrations below camera saturation levels for a particular experiment, thus the ideal combination of laser intensity, lens aperture, and dye concentration was found via trial-and-error. Concentration profiles can be obtained within $\pm 3\%$, and possibly better due to the laminar condition of the flow in this study (Webster et al., 2001).

3.4 Biological observation techniques

3.4.1 Organisms and cultures

A. tonsa were collected near the Skidaway Oceanographic Institute outside of Savannah, GA, USA. *T. longicornis* were collected from Stony Brook Harbor and the Gulf of Maine, and shipped overnight to Atlanta, GA. Copepods shipped to Atlanta were sorted and placed in five gallon buckets for culture in the environmental room where the experimental apparatus was setup. *C. ethiopica* and *L. madurae* were collected from coastal waters near Key Largo, FL, USA at the National Undersea Research Center run by the University of North Carolina – Wilmington, USA. *Calanus* sp. (*C. finmarchicus* [adults and nauplii] – Gulf of Maine, *Neocalanus* spp. – Gulf of Alaska, and *C. pacificus* – Monterey Bay, CA) were also collected and shipped overnight to Atlanta, GA. *A. tonsa* and *T. longicornis* were kept in culture at Georgia Tech. Culture media consisted of

prepared filtered seawater (Instant Ocean). Table 3.2 shows copepod collection locations, ambient temperatures at collection, and sizes for all tested species.

Copepod cultures were fed either *Tetraselmis* sp., or *Rhodomonas lens* (two co-occurring phytoplankton species) every few days, except for the twenty-four hours prior to experiments. Only adult copepods were used in experiments except for *C. finmarchicus* nauplii experiments (stage NIII-IV) which contained only juveniles and no adults. All experiments were conducted at constant temperature (± 0.2 °C) corresponding to the ambient water temperature when animals were collected (See Table 3.2).

For chemical exudates experiments, cultured *Rhodomonas lens* and *Tetraselmis* spp. were used as prey for copepods. Attraction to food particle layers of the diatom *Thalassiosira weissflogii* has been partially demonstrated for *A. tonsa* (Tiselius, 1992), and is likely to occur in many other species as well. Phytoplankton cultures were kept at optimal growth temperatures (22-25 °C). Cultures were prepared using filtered sea water (Instant Ocean) and marine culture media (Sigma Guillard's f/2 #G0154).

Chemical solutions were prepared by centrifuging cultures (3000 rpm, 23 °C, 5 min) of known cell concentration and then filtering through a glass fiber filter (0.7 μm). The flow rate of the solution into the jet was adjusted to achieve desired exudate or phytoplankton concentration. Initial experiments involve five concentrations (0, 25, 50, 75, 100, 200 $\mu\text{g C L}^{-1}$) covering the range of reported *in situ* values associated with

Table 3.2 Copepod species, average sizes, ambient temperatures, and collection locations.

Species	Size (mm)	Ambient temp. (°C)	Collection location
<i>Acartia tonsa</i>	~ 1	12	Wassaw Sound, GA
<i>Calanus finmarchicus</i>	3-4	12	Gulf of Maine
<i>Calanus pacificus</i>	2-3	12	Monterrey Bay, CA
<i>Candacia ethiopica</i>	2-3	23	Conch Reef, FL
<i>Eurytemora affinis</i>	~ 1	12	Boothbay Harbor, ME
<i>Labidocera madurae</i>	2-3	23	Conch Reef, FL
<i>Neocalanus plumchrus</i>	4-5	5	Gulf of Alaska
<i>Temora longicornis</i>	1-2	12	Long Island Sound, NY

background and peak concentrations. The control (artificial seawater) is prepared following the same procedure; however, no phytoplankton was present.

3.4.2 Behavioral assays

Behavioral assays were conducted in the same flow apparatus as the flow characterization experiments (arrangement shown in Figure 3.1b). All experiments were conducted using filtered seawater (FSW) or artificial seawater (Instant Ocean). Overlapping PIV and PLIF data with the location of the behavioral response allowed the determination of threshold levels for responses to strain rate stimuli and the effect of chemical exudates and density gradients.

The experiments were performed for the conditions quantified by the physical measurements. Responses to controls and isolated stimuli were evaluated for all species with responses to combined cues also run for two species, *Acartia tonsa* and *Temora longicornis*. Table 3.3 shows the different parameters for each stimuli experiment. Control experiments, with no signal of any type, were conducted for statistical comparisons.

Experiments consisted of adding thirty to seventy individual copepods (based on species and size to avoid overcrowding) into the test section of the flow system. The animals were allowed to acclimate for one hour. The experiments began after the 1 hour acclimation period. Copepods were allowed to swim freely in the tank, and their

Table 3.3 Matrix of experimental parameters for the behavioral trials. Copepod species were either subjected to isolated cues (Trials 1-5), or to all isolated and combined experiments (*A. tonsa* and *T. longicornis*, Trials 1-9). Two replicates were performed for each treatment.

Trial	Velocity ($U_j = 6.7 \text{ mm s}^{-1}$)	Density $\Delta\sigma_t = 1.8$	Chemical Exudates ($C = 200 \mu\text{g C L}^{-1}$)	Food ($C = 200 \mu\text{g C L}^{-1}$)
Isolated Cue Trials				
1 (control)	N	N	N	N
2	Y	N	N	N
3	N	Y	N	N
4	N	N	Y	N
5	N	N	N	Y
Combined Cue Trials				
6	Y	Y	N	-
7	Y	N	Y	-
8	N	Y	Y	-
9	Y	Y	Y	-

positions in the 10 cm × 10 cm observation section were recorded for a period of two hours. During an experiment, between zero and 10 copepods were typically present in the observation window (mode around 2). A mesh filter (50 μm) was attached to the overflow at the end of the main tank to prevent copepods from traveling through the entire system and being visually sampled more than once.

A filtered illumination box (fluorescent 14W cool light with Kodak Safelight #2A filter passing 640 nm), or infrared diodes were mounted behind the tank allowing for clear visualization of the organisms. The species tested did not exhibit phototactic behavior at these wavelengths (>700 nm; Tiselius, 1992; *pers. obs.*). Video recordings were made with a CCD video camera (Pulnix model TM-745, 768 × 494 pixels) and recorded to VHS tape for later analysis. Two-hour video recordings of the test section (10 cm × 10 cm) allowed for calculation of proportional residence time in the layer, pre-contact and post-contact swimming speeds, turn frequency in the layer and out of the layer, and feeding bouts. Each of these factors or similar measures has been used to evaluate behavioral responses to environmental stimuli (Buskey, 1984; Tiselius, 1992). Two replicates of each experiment were performed and 20 or 50 paths taken from each experiment for analysis.

Two-dimensional paths of swimming organisms were taken from VHS format and converted to data files containing coordinate positions using ExpertVision software (MotionAnalysis Corp.) at 15 Hz. This frame rate was selected because it provided sufficient displacement between frames to accurately assess swimming speed. The

displacement of an animal swimming at 0.5 cm s^{-1} was roughly 1 pixel between consequent frames for the image resolution of our system. Swimming speed calculations were not sensitive to the time interval of measurement for these settings. The digitized paths were filtered to remove paths with escape responses and paths that did not cross into the layer at least once during the time in the observation window. This resulted in a loss of between 0 and 10 paths for most trials. For turn frequency and density gradient crossing tests, the first forty accepted paths were selected. A typical path lasted approximately 60 seconds for all experiments. Analysis of individual paths consisted of calculating proportional residence time, swimming speed, and turn frequency. Proportional residence time is the ratio of time in the layer relative to the total time in the viewing window and therefore ranges from 0 to 1. This normalization eliminates bias associated with differences in viewing time as a result of either animal movements or ambient flow velocity.

Swimming speed was defined as the speed relative to the flow velocity for copepods in the velocity gradient layer treatments, and actual (raw) swimming speed for other treatments. Turn frequency was defined as the number of turn events per second where a turn event was defined as a change in direction of motion of more than 15 degrees. Each of these kinematic parameters was computed for the overall path, the portions of the path in versus out of the layer, and pre-contact versus post-contact with the gradient layer.

A second set of behavioral experiments consists of exposing individual copepods to the layer and recording the response of each when the layer is contacted. Only *Candacia ethiopica* and *Labidocera madurae* were exposed to these experiments. Responses were recorded as either positive (remain in layer by actively swimming), negative (escape response), or no response. For each experiment fifty individuals were selected, with twenty-five being administered the treatment and twenty-five as control. Each copepod was removed via a pipette and was allowed to sink out of the pipette into the field of view at natural sinking rates. Sample paths are shown in relation to important characteristics of the model thin layer for *C. ethiopica* in Figure 3.5. Three paths are shown, dead, no response, and positive response. Dead animal paths isolate the effects of advection by the plane jet. Comparison of dead animal tracks to positive responses shows that increased proportional residence time is achieved by counteracting the natural sinking rate, and the organism is eventually taken out of the field of view by the flow. Thus, increases in residence time within the velocity gradient layer can be attributed to behavioral responses and not advection by the flow (Fig. 3.5). Results of drop experiments with *Candacia ethiopica* showed that advection by the flow does not increase proportional residence time, and therefore changes in proportional residence time are only the result of behavioral responses of the organism (Fig. 3.5).

3.4.3 Statistical analyses

Statistical analyses were conducted between treatments and controls for proportional residence time using analysis of variance (ANOVA). ANOVA is a

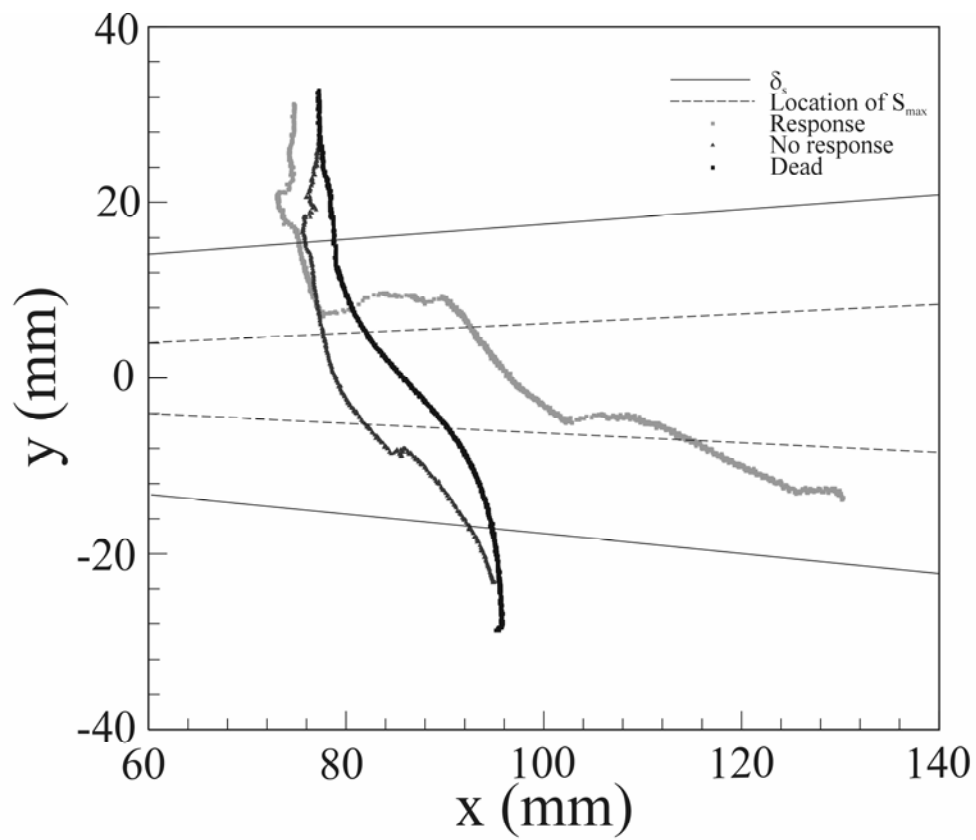


Figure 3.5 Individual paths of living and dead *Candacia ethiopica* in response to model thin layer with flow velocity gradient.

statistical evaluation technique used for hypothesis testing in many (ecological) experiments. ANOVA tests for the equality of the mean values of two or more datasets by comparing the variance within and across treatments. The ANOVA approach, among other uses, allows for comparisons between behavioral responses in the presence of a cue compared to the absence of a particular cue. ANOVA is a convenient and powerful tool for hypothesis testing because it does not require equal sample sizes. The underlying assumptions for ANOVA include random sampling and normal distributions of independent samples, and groups possessing the same variance. Random selection of individuals of the same species and size allows for these assumptions to hold for this study.

Calculations necessary for a single factor ANOVA are presented in Table 3.3. The results of this analysis yield a value corresponding to an F -distribution, calculated as:

$$F = \frac{MS_{groups}}{MS_{error}} \quad (3-7)$$

Critical values of the F -distribution are determined from the group and error degrees of freedom and are used to determine the p -value of the data set for the ANOVA. The p -value is the most commonly reported statistic for ANOVA and provides a measure of difference between data sets. Specifically, the p -value is the probability that the means of the two groups are equal. The p -value varies between 0 and 1. For most biological experiments, p -values less than 0.05 are considered

Table 3.4 Summary of calculations for a single-factor ANOVA (adapted from Zar, 1999).

Source of variation	Sum of squares (<i>SS</i>)	Degrees of freedom (<i>DF</i>)	Mean square (<i>MS</i>)
Total $[X_{ij} - \bar{X}]$	$\sum_{i=1}^k \sum_{j=1}^{n_i} X_{ij}^2 - C$	$N - 1$	
Groups (i.e. among group variation) $[\bar{X}_i - \bar{X}]$	$\sum_{i=1}^k \frac{\left(\sum_{j=1}^{n_i} X_{ij} \right)^2}{n_i} - C$	$k - 1$	$\frac{SS_{groups}}{DF_{groups}}$
Error (i.e. within group variation) $[X_{ij} - \bar{X}_i]$	$SS_{total} - SS_{groups}$	$DF_{total} - DF_{groups}$ $(N - k)$	$\frac{SS_{error}}{DF_{error}}$

indicative of a significant difference between the mean values of two datasets and hence p -values test hypotheses of different behavior response and other differences.

A balanced or general linear model analysis of variance (ANOVA) was used on proportional residence time to examine individual and interactive effects of experimental replicate, velocity, density, and chemical exudates for *Acartia tonsa* and *Temora longicornis*. Significance of individual factors suggests that the organisms are altering their behavior in response to the particular cue. Significant interactive effects show that the response to one factor changes depending on the presence of a second factor, either positively, or negatively.

For species only tested with isolated gradients, ANOVA combined with post-hoc Student-Newman-Keuls (S-N-K) tests were used to determine statistical differences between treatments. Proportional residence time data followed normal distributions and arcsine transform was not warranted because sample sizes were identical with lower variances associated with lower means (Zar, 1999). Two-tailed Fisher's exact tests were employed to evaluate direct comparisons of individuals crossing the density gradient.

Separate ANOVAs were used to determine whether significant differences in proportional residence time occurred as a function of different chemical concentrations or density jump strengths. Post-hoc S-N-K tests were used to test for differences in proportional residence times between adjacent chemical concentrations and density steps because non-linear regression techniques (due to threshold effects) revealed qualitatively

similar results. Regression statistics were used to analyze density gradient data (testing whether an individual crosses the density gradient).

Statistical comparisons of swimming speed and turn frequency were conducted using a single factor ANOVA design to compare pre- and post-contact values separately for each individual treatment or combination of treatments. Kinematic parameters along with associated statistical tests in controls (no gradients) are provided for qualitative comparison. We employed the single factor design to alleviate bias due to varying sex ratios between experiments (males typically swim faster than females; Mauchline, 1998).

Chapter 4 Results

4.1 Model thin layer characterization

The velocity, density, and concentration fields were quantified for the isolated and combined treatments using the methods described in the previous Chapter. In this Section, physical data are presented to define the environment in which the behavioral trials were performed.

4.1.1 Velocity gradient layer

Figure 4.1 shows the ensemble-averaged velocity field recorded during characterization experiments for a Reynolds number of 52 ($Re = U_j D / \nu$; $D = 10$ mm; $U_j = 6.7$ mm s⁻¹; $\nu = 1.27$ mm² s⁻¹). The laminar regime for this flow was verified by minimal particle movement in the transverse direction and small values of the standard deviation of the velocity vectors. Maximum velocities in the observation section decreased from 6 mm s⁻¹ at 50 mm downstream of the jet nozzle to 4 mm s⁻¹ at 150 mm downstream. The corresponding velocity profile at $x = 100$ mm compared well with the analytical solution of Bickley (1937) for a plane jet (Fig. 4.2a).

The local shear strain rate $\left(\frac{1}{2}\left(\frac{\partial u}{\partial y} + \frac{\partial v}{\partial x}\right)\right)$ is shown as contours in Fig. 4.1. The

other components of the strain rate tensor are an order of magnitude lower than the shear component, and therefore are not shown here. The shear strain rate profiles also agreed

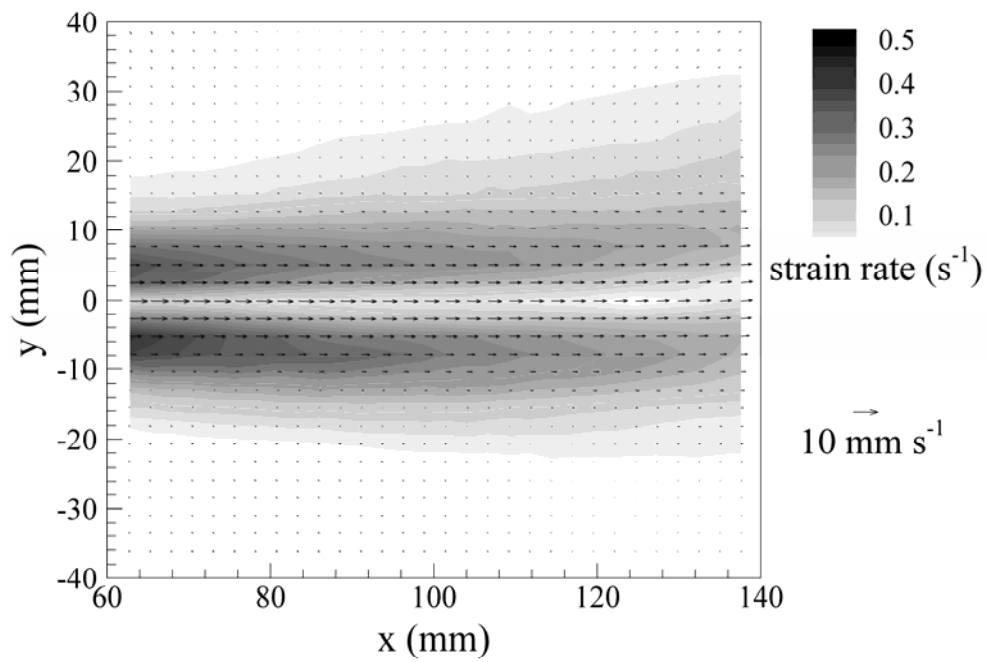


Figure 4.1 Velocity and shear strain rate fields for the velocity gradient layer treatment with $U_j = 6.7 \text{ mm/s}$. Contours show the magnitude of the strain rate.

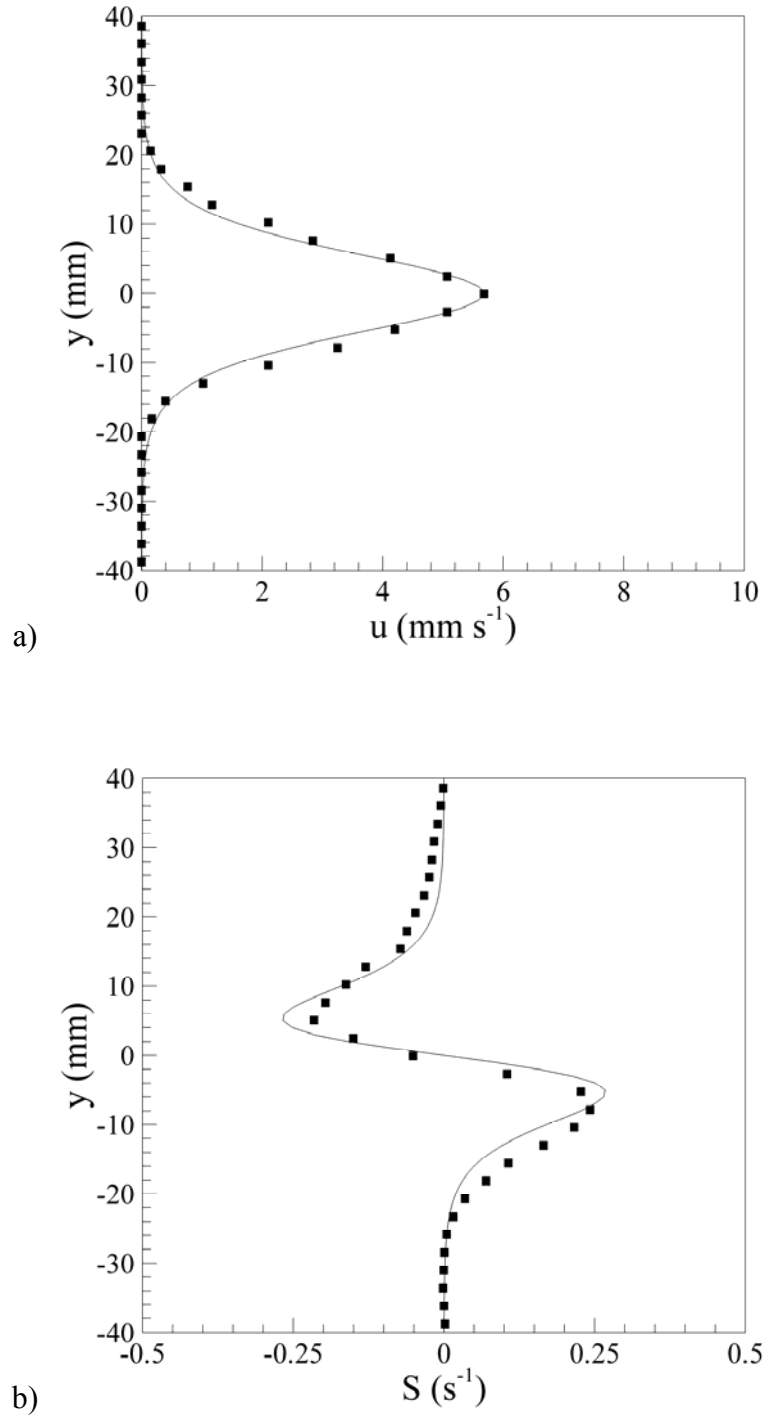


Figure 4.2 Comparison of measured velocity and shear strain rate ($S = \frac{1}{2} \left(\frac{\partial u}{\partial y} + \frac{\partial v}{\partial x} \right)$) profiles (shown with data points) at $x = 100$ mm to the analytical solution of Bickley (1937) indicated by a solid line.

well with the analytical solution (Fig. 4.2b). For the flow rate reported here, the maximum shear strain rate varied from 0.35 s^{-1} (at $x = 5 \text{ cm}$) to 0.12 s^{-1} (at $x = 15 \text{ cm}$) with distance downstream in the observation window. Strain rates across the layer ranged from zero to the local maximum ($0.12\text{-}0.35 \text{ s}^{-1}$) depending on location on the x -axis.

For zooplankton behavior experiments, the boundary or edge of the layer, δ_s , was defined as the location where the shear strain rate crossed the threshold value of 0.025 s^{-1} (Fig. 4.3). Because copepods respond to strain rate, this definition of the boundary of the velocity gradient layer was more relevant for behavioral observations compared to the mean velocity profile half-width, δ , which is traditionally employed as a measure of jet width (e.g. Sato and Sakao, 1964). Across the viewing window, the velocity layer grew linearly with distance downstream from a 17 mm half-width (at $x = 5 \text{ cm}$) to a 27 mm half-width (at $x = 15 \text{ cm}$) as defined by the strain rate threshold above (Fig. 4.3).

Whereas the range of shear strain rates in the apparatus covered the range reported in field estimates, the maximum values ($0.12\text{-}0.35 \text{ s}^{-1}$) exceeded the maximum shear ($\frac{\partial u}{\partial y}$ only) recorded *in situ* for thin layers (0.1 s^{-1} reported by Deksheniaks et al., 2001). However, resolution restrictions of field velocity measurements ($\sim 20 \text{ cm}$ at best; often closer to 1 m) suggest that strain rates estimated in the ocean may be much higher than reported. For example, Deksheniaks et al. (2001) utilize an acoustic Doppler current profiler (ADCP) with a minimum bin size of 1 m. For a strain rate equal to 0.05 s^{-1} , this corresponds to a change in flow velocity of 5 cm s^{-1} over the 1 m distance. The velocity

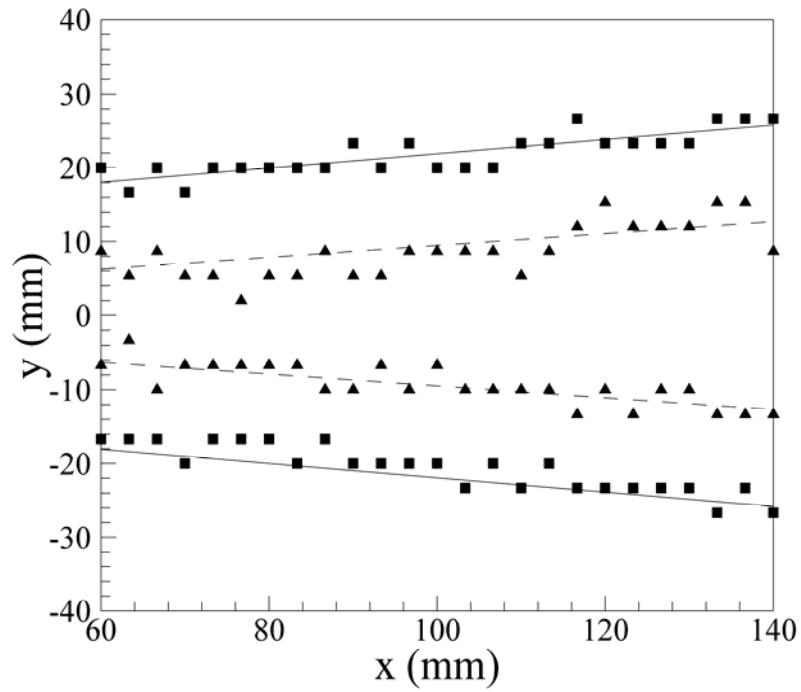


Figure 4.3 The position of the boundary of the layer, δ_s , is indicated by the squares and the solid lines, and is defined by a threshold level of shear strain rate (0.025 s^{-1}). The location of the maximum shear strain rate is indicated by the triangles and dashed lines.

change under density stratified conditions is likely to occur over a shorter distance, as evidenced by Cowles (2004). For instance, if the recorded change in velocity really occurred over a distance of 10 cm, then reported maximum strain rates would be equal to 0.5 s^{-1} (Cowles, 2004). This is an extreme example, but it illustrates the need for higher-resolution field measurements. It should be noted here that the oceanographic definition of shear ($\frac{\partial u}{\partial y}$) is related to, but distinctly different than, the fluid dynamic shear strain rate, $\frac{1}{2}\left(\frac{\partial u}{\partial y} + \frac{\partial v}{\partial x}\right)$, reported in this study. However, because the $\frac{\partial u}{\partial y}$ -term dominated the shear strain rate, these values are similar (numerical values obviously differing by a factor of one half). Additionally, maximum shear strain rates in the model layer were always below reported escape response thresholds (Yen and Fields, 1992; Fields and Yen, 1997a; Titelman, 2001).

4.1.2 Density gradient layer

Figure 4.4 shows an example density profile for the model thin layer two hours after the tank was filled. The upper and lower layers were constant density, and the gradient was entirely contained within the thin layer defined by the strain rate profiles. The upper layer had a salinity of 30 ppt and the lower layer had a salinity of 32 ppt resulting in a density discontinuity of $1.8 \sigma_t$ units. The buoyancy frequency of the layer shown in Fig. 4.4 is 0.147 which corresponds well with observed field conditions (Deksheniaks et al., 2001). Density discontinuities of varying degrees can be created in the model thin layer using the procedure and methods described in Section 3.2. Similar

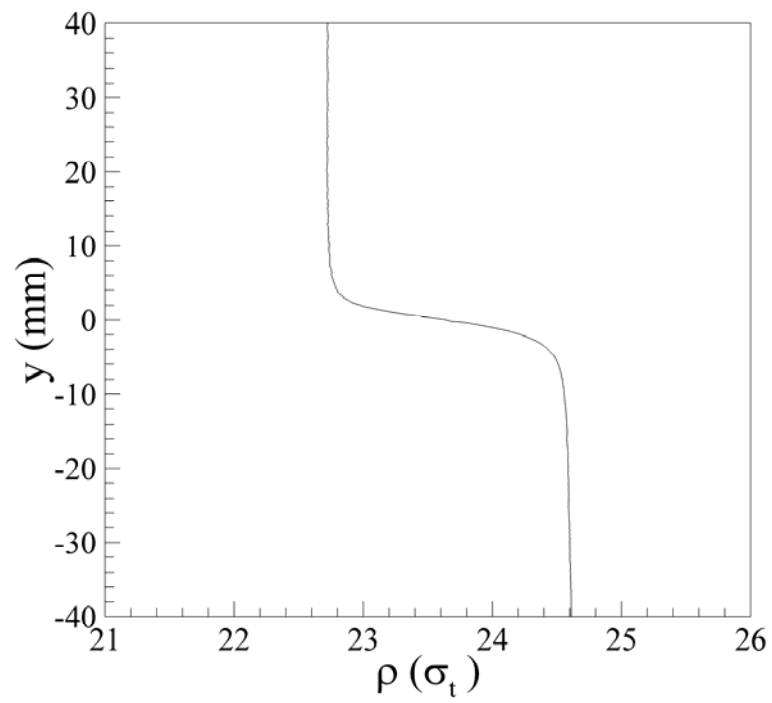


Figure 4.4 Density profile for the $\Delta\sigma_t = 1.8$ density gradient layer treatment (upper layer $S = 30.0$ ppt, lower layer $S = 32.0$ ppt).

profile results were obtained for all density gradients tested in behavioral experiments (0.25, 0.5, 1.0, 2.0, 4.0 ppt salinity change).

4.1.3 Chemical and biological layers

A chemical model thin layer is shown in Fig. 4.5. The concentration within the layer was close to the initial concentration with steep gradients at the edges. The thickness of the stationary chemical layer was nearly constant across the field of view and was equal to 22 mm. Figure 4.6 shows vertical concentration profiles at three x - locations in the field of view. The steep gradients in chemical concentration are the result of the laminar fluid body intrusion method used to create the layer and model field conditions well. The layer is not as thick as the velocity layer due to the fact that diffusivity of momentum is much greater than that of the scalar (e.g. Webster et al., 2001), and the time period for the experiment does not allow for significant diffusion of the chemical component. During the behavioral trials, the non-dimensional concentration (C/C_o) data was employed to specify the source concentration of food and phytoplankton chemical exudates to achieve reported field data levels in the observation region.

4.1.4 Thickness of the gradient layer

For all isolated and combined layer experiments, the thickness of the layers was defined as described in Section 4.1.1 based on the velocity gradient layer. All isolated

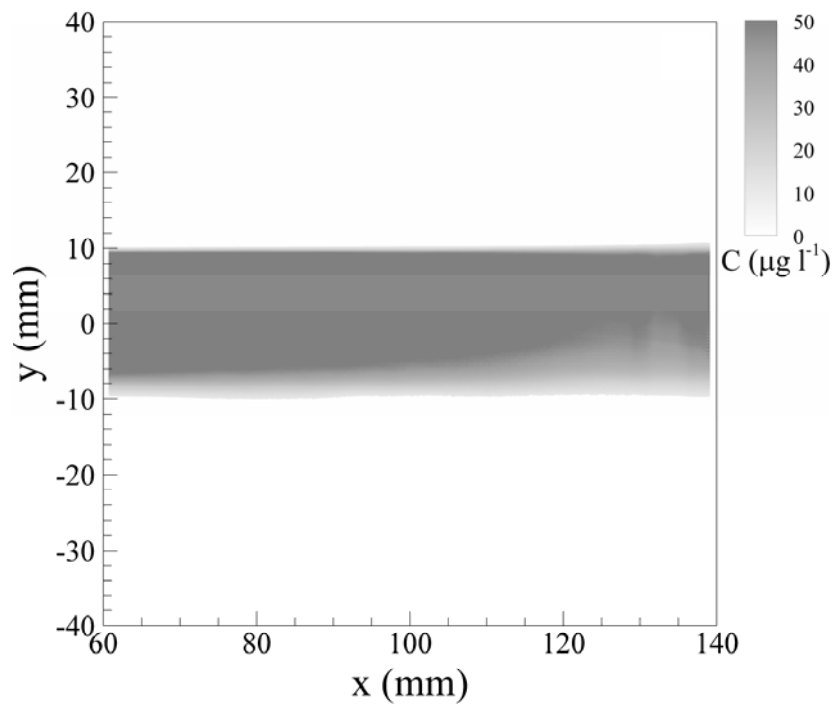


Figure 4.5 Concentration field for the chemical layer treatment.

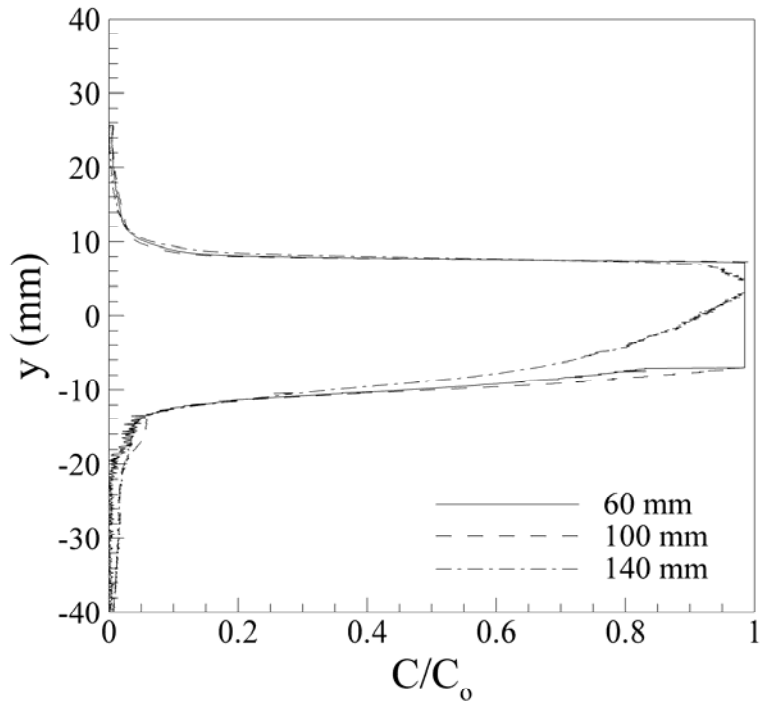


Figure 4.6 Vertical concentration profiles at various x -locations (60, 100, 140 mm) for the chemical layer treatment.

and combined cue layers were contained entirely within the boundaries of the region defined by the 0.025 s^{-1} threshold for the velocity gradient layer experiments (Fig. 4.7). Arrows indicate the boundary of the layer in Fig. 4.7, and in all subsequent profiles shown for combined cue layers (Figs. 4-8 through 4-11). Using the same definition for the thickness of the layer removes possible bias between treatment experiments for proportional residence time data.

4.1.5 Combined layers

Layers of biological activity, chemical concentration, density gradients, and velocity gradients are often found in combination *in situ*. The singular model layers described above were used to isolate the responses to individual cues; however, to understand the function of all cues in the foraging behavior of copepods it is also necessary to create conditions that are relevant to the organism. Therefore, a series of model layers with gradients of two or more of these properties also were developed.

Density acted as a stabilizing force in the velocity-density model thin layer; hence, lower flow rates could be achieved. However, the profile of the jet was asymmetric due to the presence of a density gradient (see Fig. 4.8). The jet grew in a linear fashion, but was skewed slightly with more rapid growth into the less dense fluid or upper layer. Consequently, the velocity gradient was greater and the maximum strain rate was higher in the lower half ($S_{\max}(\text{lower}) = 0.50 \text{ s}^{-1}$ at $x = 50 \text{ mm}$) of the plane jet than the upper half ($S_{\max}(\text{upper}) = 0.39 \text{ s}^{-1}$ at $x = 50 \text{ mm}$). The velocity profile reached a maximum slightly below the original centerline of the jet and decreased quickly to zero in

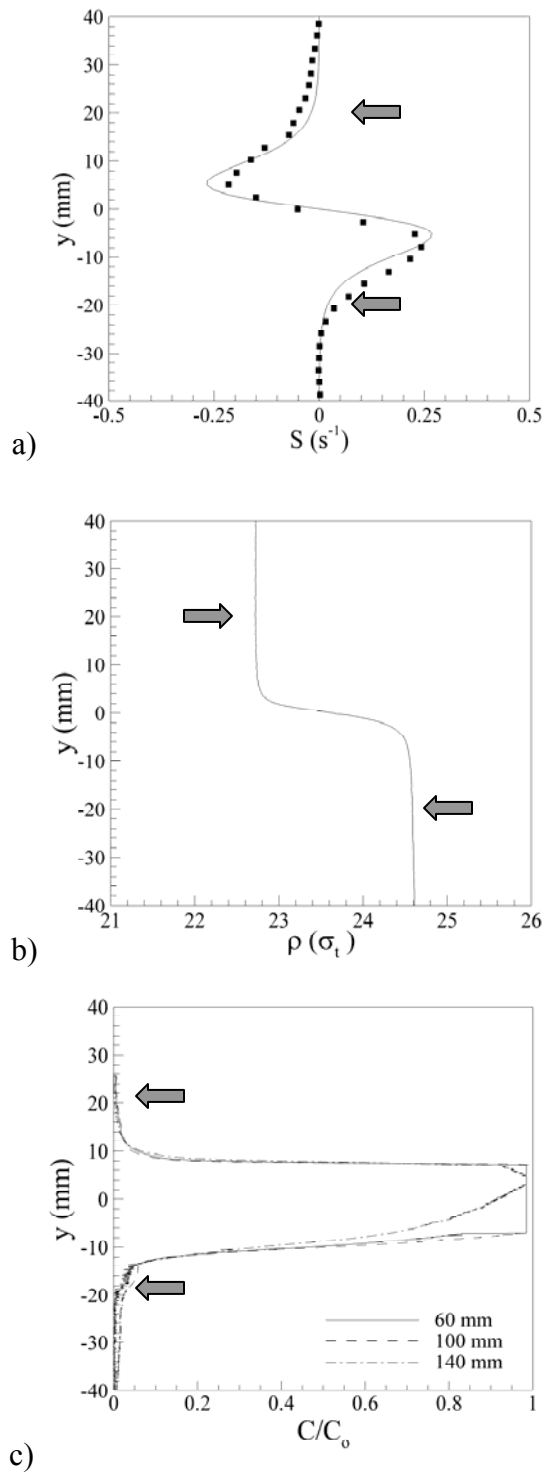


Figure 4.7 Definition of the model thin layer thickness for behavioral experiments with isolated cues. The edge of the layer is defined by the location of a threshold value of the shear strain rate in each case (0.025 s^{-1}) indicated by the arrows.

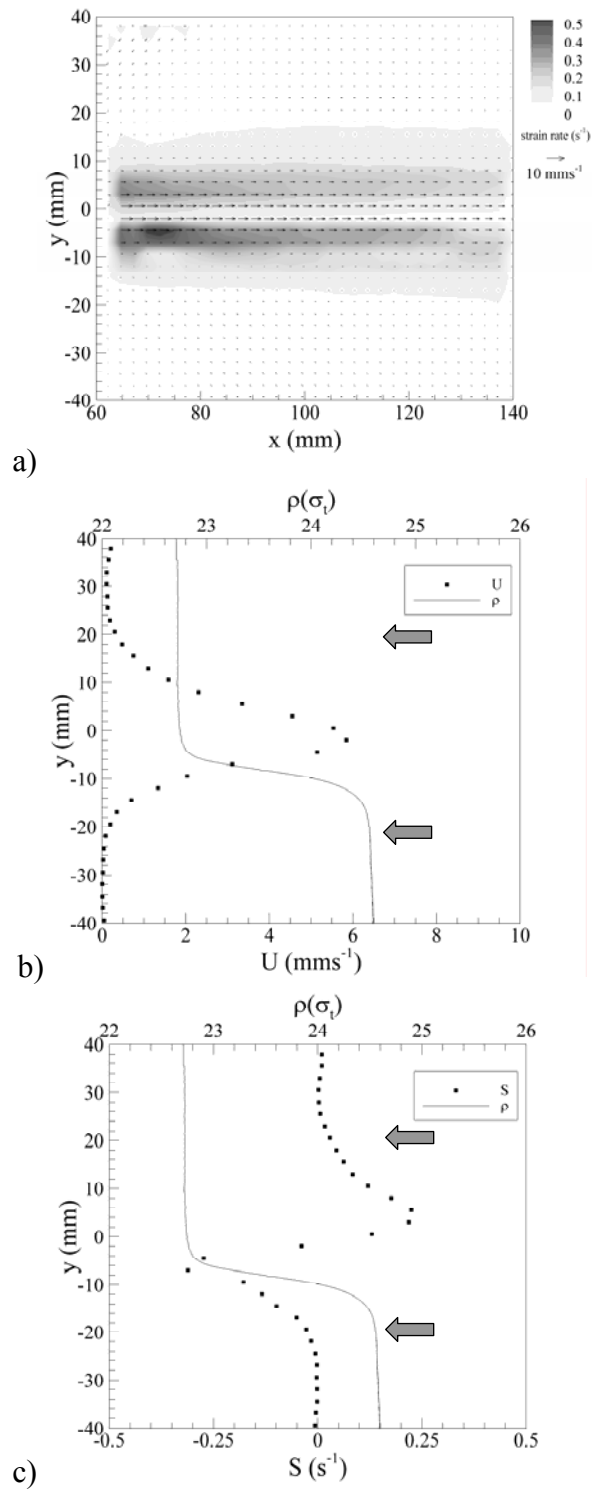


Figure 4.8 Combined velocity-density layer. (a) Vector field, (b) flow velocity and density profile at $x = 100$ mm, and (c) strain rate and density profile at $x = 100$ mm. Arrows indicate edge of layer defined by the 0.025 s⁻¹ threshold.

the bottom layer. Consequently, the combined velocity-density model thin layer is approximately 10% thinner than the velocity model thin layer (ranging from 15 mm to 24 mm), and our behavioral definition of thin layer boundary was not changed (i.e. δ_s at $S = 0.025 \text{ s}^{-1}$ for the velocity model layer). For the above layer, the Richardson number was well above the critical value for stability (i.e. $Ri > 0.25$), as with all *in situ* observations of thin layers (Hazel, 1972; Dekshenieks et al., 2001).

In the combined velocity-chemical layer, the velocity and shear strain rate profiles are broader than the chemical concentration profile, as expected, because momentum diffuses faster than chemical concentration (kinematic viscosity of $\sim 10^{-6} \text{ m}^2 \text{ s}^{-1}$ compared to diffusivity of $\sim 10^{-9} \text{ m}^2 \text{ s}^{-1}$; Fig. 4.9). The velocity and shear strain rate profiles were nearly identical to those for the isolated velocity gradient layer since the presence of Rhodamine 6G in the jet does not significantly affect the flow. Fig. 4.10 shows the vertical profiles for the combined density-chemical layer at $x = 100 \text{ mm}$. The figure illustrates that the combination did not significantly alter the profile characteristics compared to the isolated treatments. Finally, the profiles for the combined velocity-density-chemical layer were similar to the isolated layer treatments, except for the slight narrowing of the velocity profile resulting in increased shear strain rates due to the interaction of flow velocity and the density gradient (Fig. 4.11).

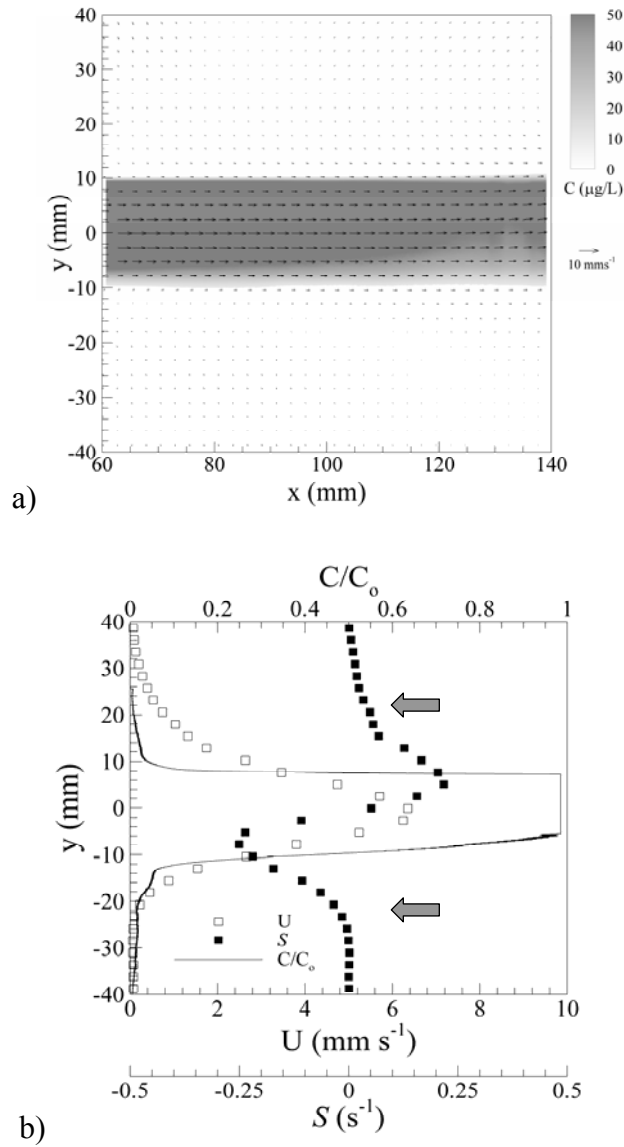


Figure 4.9 Combined velocity-chemical layer. (a) Vector field and concentration contours, and (b) flow velocity, shear strain rate, and concentration profiles at $x = 100 \text{ mm}$. Arrows indicate edge of layer defined by the 0.025 s^{-1} threshold.

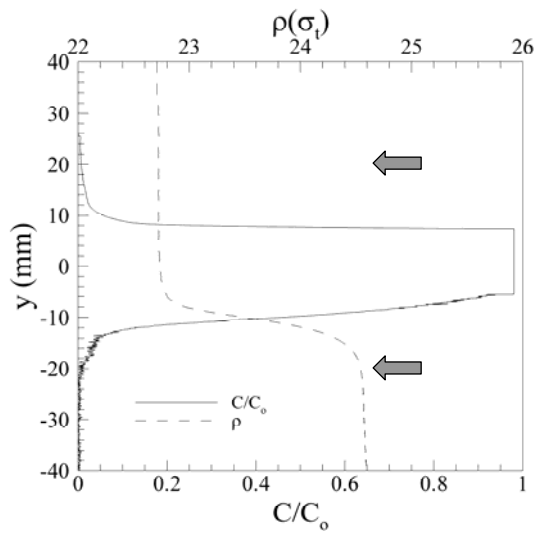


Figure 4.10 Combined density-chemical layer. Density and concentration profiles at $x = 100$ mm. Arrows indicate edge of layer defined by the 0.025 s^{-1} threshold.

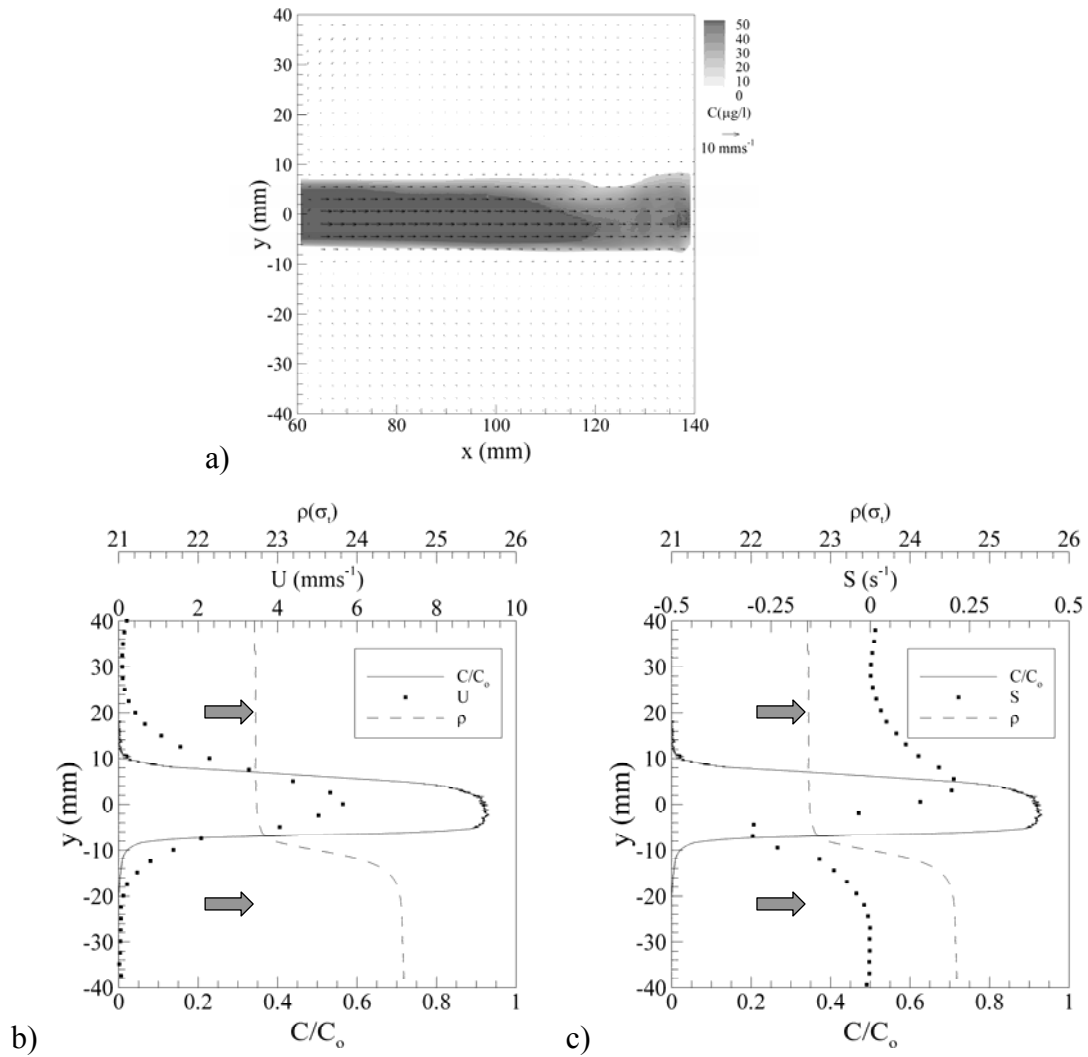


Figure 4.11 Combined velocity-density-chemical layer. (a) Velocity vector field and concentration contours, (b) flow velocity, density, and concentration profiles at $x = 100$ mm, and (c) strain rate, density, and concentration profiles at $x = 100$ mm. Arrows indicate edge of layer defined by the 0.025 s^{-1} threshold.

4.1.6 Synthesis

All layer treatments were repeatable and reliable such that following the experimental protocols described in the Methods yielded layer properties that were identical to those reported in this Section. All layers were fully characterized in the field of view at resolutions relevant to foraging zooplankton. In order to remove layer thickness as a variable in the behavioral observations, the boundary defined by the threshold of shear strain rate for the isolated velocity gradient layer was used to define the thin layer region for all environmental gradients. Importantly, the layer is much larger (~4 cm) than a copepod (~ 0.1 cm), insuring that an individual cannot sense both boundaries of the layer at the same time. Shear strain rate values for the velocity thin layer are in the range of those reported field conditions. Although some velocity gradients are above maxima reported *in situ*, they are of the same order of magnitude, and resolution limitations of field equipment may not allow for the strength of these properties to be accurately determined in the field. Density layers are comparable to those observed in the field covering salinity changes of 0.25-4 ppt for buoyancy frequencies in the layer around 0.15. Chemical gradients also mimic field conditions well, with cell concentrations equal to or less than reported field observations (Cowles 2004). The combined layer experiments also mimic field conditions well.

Shear strain rates for the velocity layer treatment varied from 0 to 0.5 s^{-1} , which is below escape responses for all species tested. Additionally, the maximum values are orders of magnitude above physiological detection limits. Because strain rates vary

continuously across the vertical section of the jet, copepods are exposed to a range of shear strain rate magnitudes, and hence it is not necessary to test several strain rates in this system to determine the threshold strain rate that induces a response.

4.2 *Acartia tonsa* and environmental structure

4.2.1 Responses to the velocity gradient layer

Acartia tonsa exhibited aggregative behavior in presence of the velocity model layer. As seen in Fig. 4.12, *A. tonsa* swimming paths were strikingly different between velocity gradient layers (Fig. 4.12a) and controls (Fig. 4.12d). *A. tonsa* in the velocity gradient layer experiments increased proportional residence time by roughly 25% relative to the no flow control (see Fig. 4.13). *A. tonsa* in control experiments spent about one third of its time in the layer region which is close to the expected value of 0.33 (the layer covers approximately 1/3 of the field of view). The proportional time in the layer increased to 64% in the presence of a velocity gradient ($T_R = 0.64$; $S_e = 0.03$; control $T_R = 0.39$; $S_e = 0.04$). Repeating this experiment with a second group of 70 organisms produced nearly identical results ($T_R = 0.64$ and 0.65 ; $S_e = 0.03$ and 0.04). Proportional residence times in the velocity gradient layer were significantly different from the control for *A. tonsa*, using a general linear model design since data set sizes were not identical (Table 4.1). As discussed further in Section 5.4, the behavior leading to an increase in proportional residence time observed in these experiments also leads to aggregations at relevant time scales near boundaries between fluids with different velocities.

Table 4.1 Results of general linear model (ANOVA) on proportional residence time with four factors (replicate, velocity, density, and chemical) and interactive effects for *A. tonsa*. * indicates significance at $p < 0.05$, and ** indicates significance at $p < 0.001$. Significance shows that the factor or the interaction of the listed factors has an effect on the behavior of the organism with respect to proportional residence time.

Factor	df	Seq. <i>SS</i>	Adj. <i>SS</i>	Adj. <i>MS</i>	<i>F</i>	<i>P</i>
TOTAL	749	39.823				
Replicate	1	0.016	0.001	0.001	0.03	0.871
Velocity (V)	1	3.167	2.290	2.290	52.44	<0.001 **
Density (D)	1	0.335	0.094	0.094	2.14	0.144
Chemical (C)	1	1.735	2.065	2.065	47.30	<0.001 **
Velocity × Density	1	0.156	0.040	0.040	0.93	0.336
Velocity × Chemical	1	1.973	2.050	2.050	46.95	<0.001 **
Density × Chemical	1	0.030	0.039	0.039	0.90	0.342
Velocity × Density × Chemical	1	0.051	0.051	0.051	1.16	0.282
Error	741	32.361	32.361	32.361	-	-

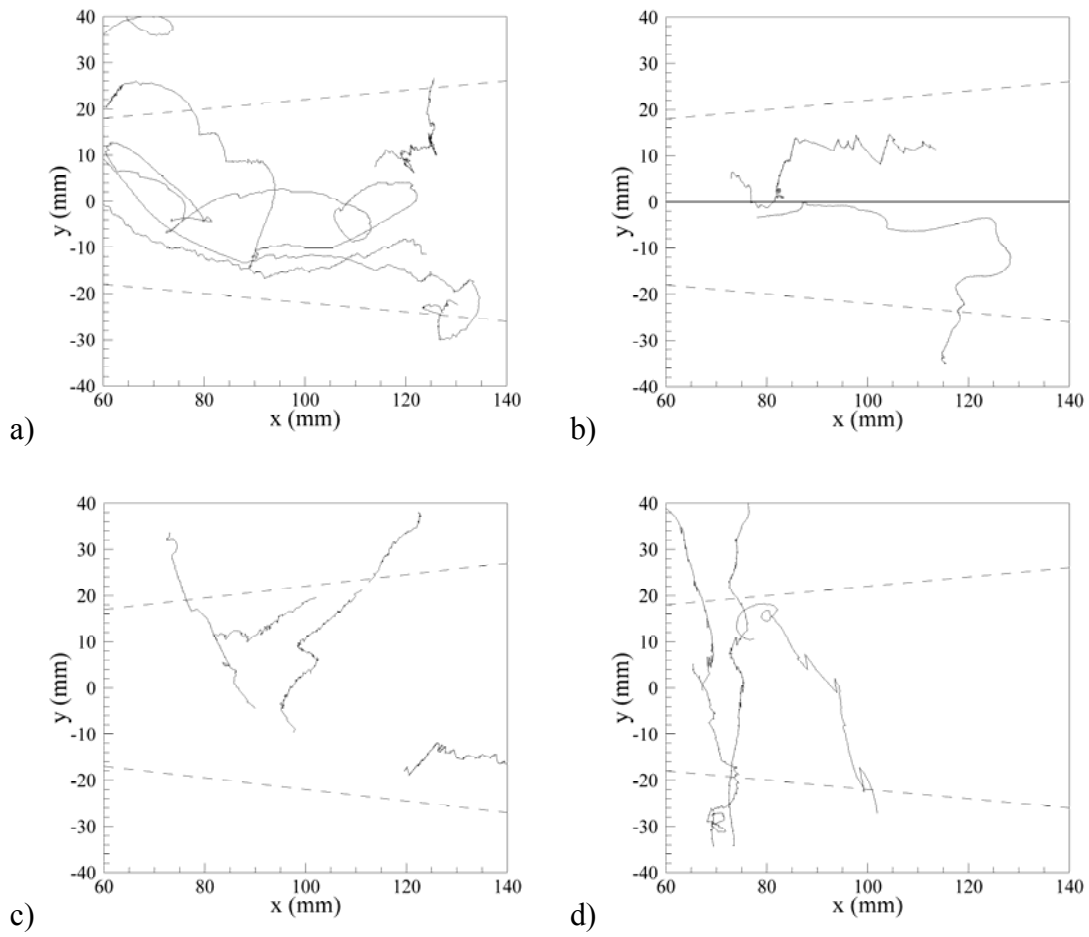


Figure 4.12 Sample paths for *A. tonsa* for the (a) velocity gradient layer, (b) density gradient layer, (c) chemical layer, and (d) control. The dashed lines indicate the edge of the layer corresponding to δ_s .

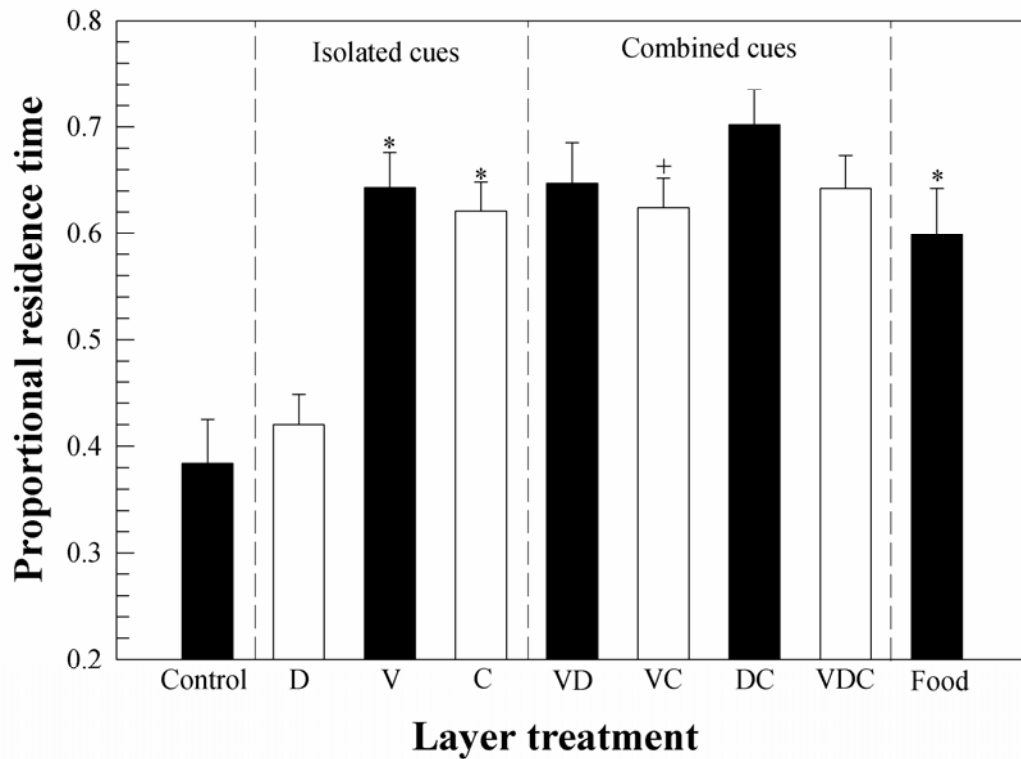


Figure 4.13 Proportional residence time of *Acartia tonsa* in presence of individual and combined cue layers. Layer constituents are velocity (V), density (D), and chemical exudates (C). * indicates a significant effect of single treatments relative to the control as determined with a balanced, nested ANOVA ($p < 0.05$). For combined layers, + indicates significant interactive effects between the isolated layer constituents.

Acartia tonsa significantly increased its relative swimming speed after contact with the velocity gradient layer compared to pre-contact swimming speed (Table 4.2). Comparisons of pre-contact and post-contact swimming speeds for control experiments were not significantly different (Table 4.2). Turn frequency also increased within the velocity gradient layer compared to outside the layer (Table 4.3). These behaviors are congruent with an excited area-restricted search behavior. Statistical evaluations were made only within each experiment and not between experiments because varying sex ratios (males typically swim faster than females) could influence results.

Instantaneous swimming speeds for *A. tonsa* increase when plotted against the local value of the strain rate (Fig. 4.14). In Figure 4.14, the open symbols are pre-contact data points and closed symbols show instantaneous swimming speeds after contact with the velocity gradient layer (vertical solid line; defined by $S = 0.025 \text{ s}^{-1}$). The average swimming speed for *A. tonsa* from these experiments is plotted as a dashed horizontal line for comparison. Instantaneous swimming speeds increase slightly beyond the threshold resulting in an increased average swimming speed for the population. The change is subtle, but important, because these swimming speeds are below escape response swimming speeds. The change in the behavior of the copepod is not related to predator avoidance, and is apparently linked to foraging (Poulet and Oullet, 1982; Yen et al., 1992).

An important objective is to define the threshold response levels for zooplankton in order to determine appropriate conditions and differences between species, to provide

Table 4.2 Swimming speeds for *A. tonsa* pre-contact and post-contact with the model thin layer. * denotes significant differences ($p < 0.05$) between pre-contact and post-contact values by single-factor ANOVA; control values are shown for comparison.

Treatment	n	Pre-contact swimming speed [mm/s] (std err)	Post-contact Swimming speed [mm/s] (std err)	p
Individual cues				
Control	47	2.23 (0.17)	2.15 (0.15)	0.703
Velocity ($U_j = 6.7 \text{ mms}^{-1}$)	47	3.08 (0.17)	3.68 (0.19)	0.009 *
Density ($\Delta\sigma_t = 1.8$)	48	1.82 (0.07)	1.71 (0.06)	0.393
Chemical ($200 \mu\text{g C L}^{-1} \text{ eq.}$)	40	1.91 (0.18)	2.57 (0.14)	0.005 *
Food ($200 \mu\text{g C L}^{-1}$)	42	2.85 (0.19)	1.97 (0.17)	0.001 *
Combined cues				
Velocity-Density	50	3.04 (0.38)	3.93 (0.22)	0.037 *
Velocity-Chemical	40	2.28 (0.20)	3.09 (0.25)	0.016 *
Density-Chemical	41	2.55 (0.15)	3.05 (0.17)	0.031 *
Velocity-Density- Chemical	36	3.13 (0.29)	4.37 (0.26)	0.005 *

Table 4.3 Turn frequency for *A. tonsa* pre-contact and post-contact with the model thin layer. * denotes significant differences ($p < 0.05$) between pre-contact and post-contact values by single-factor ANOVA; control values are shown for comparison.

Treatment	<i>n</i>	Total # turns/ind/s (std err)	In layer # turns/ind/s (std err)	Out of layer # turns/ind/s (std err)	<i>p</i>
Individual cues					
Control	40	0.06 (0.01)	-	-	
Velocity ($U_j = 6.7 \text{ mms}^{-1}$)	40	0.14 (0.02)	0.24 (0.05)	0.09 (0.02)	0.018 *
Density ($\Delta\sigma_t = 1.8$)	40	0.07 (0.03)	0.08 (0.03)	0.06 (0.02)	0.548
Chemical (200 $\mu\text{g C L}^{-1}$ eq.)	40	0.15 (0.03)	0.20 (0.04)	0.02 (0.02)	0.016 *
Food (200 $\mu\text{g C L}^{-1}$)	40	0.09 (0.03)	0.10 (0.03)	0.06 (0.04)	0.493
Combined cues					
Velocity-Density	34	0.08 (0.02)	0.10 (0.02)	0.03 (0.02)	0.071
Velocity-Chemical	37	0.07 (0.02)	0.09 (0.02)	0.04 (0.02)	0.074
Density-Chemical	40	0.07 (0.02)	0.09 (0.04)	0.04 (0.01)	0.039 *
Velocity-Density-Chemical	36	0.06 (0.02)	0.07 (0.02)	0.02 (0.01)	0.022 *

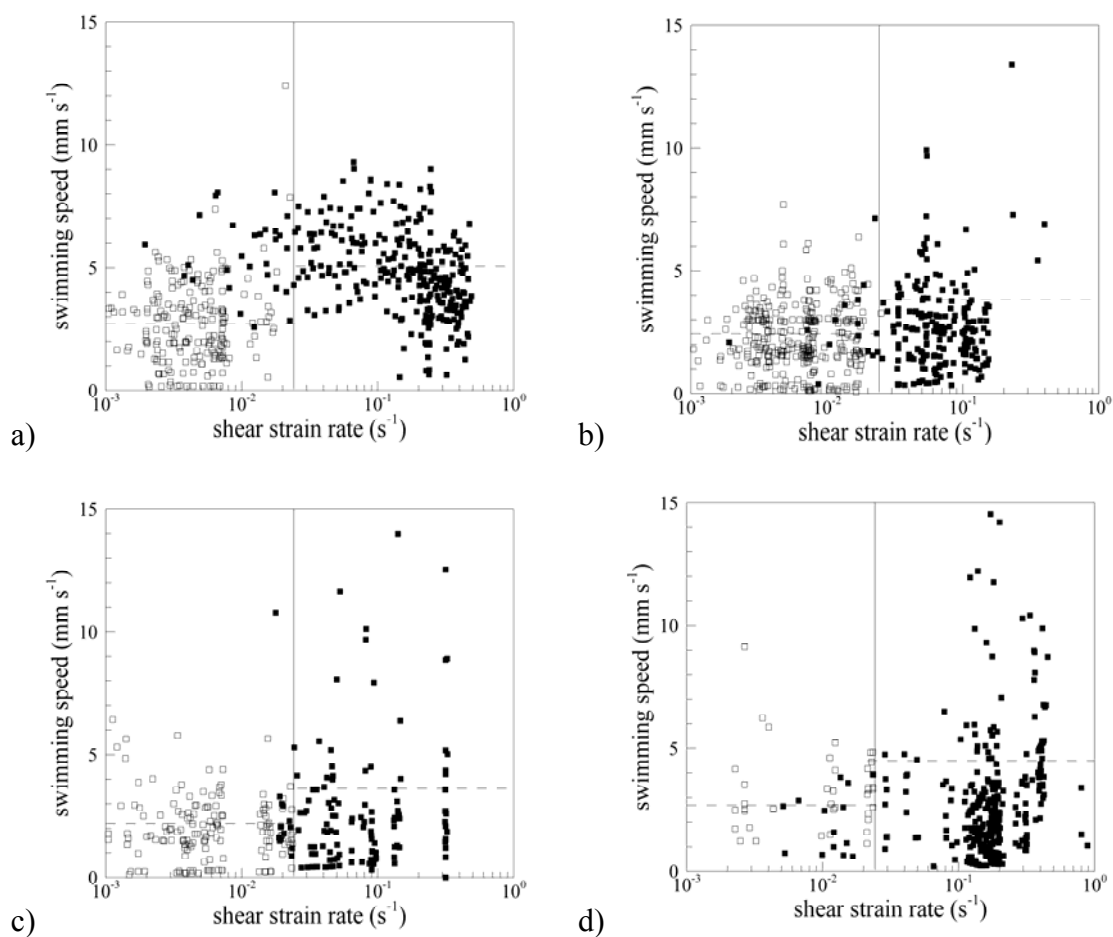


Figure 4.14 Instantaneous swimming speeds for four *A. tonsa* paths plotted against shear strain rate for the velocity gradient layer treatment. The solid line shows the threshold of 0.025 s^{-1} . The dashed lines show the average swimming speed above and below threshold. Open symbols correspond to pre-contact with the layer, and solid symbols correspond to post-contact.

information to models, and to guide field observations. In order to determine the threshold shear strain rate for the above observations, two techniques are employed. Fig. 4.15 shows plots of $\Delta\mu$ and $\Delta\sigma$ for five individual *A. tonsa* paths, where Δ refers to the difference between the statistic calculated for data above and data below the threshold value. To calculate these quantities, the threshold was varied over the range shown in Fig. 4.15 and for each case the average and standard deviation of swimming speed were calculated for data above and below that threshold value. The reported data correspond to the difference between those calculated values. Behavioral thresholds were then defined where $\Delta\mu$ and $\Delta\sigma$ change abruptly, showing the region where the animal behavior is significantly altered. Changes in $\Delta\mu$ and $\Delta\sigma$ indicate a significant alteration of swimming pattern and hence an alteration of behavior in response to the perceived cue. For *A. tonsa*, the behavioral threshold values of shear strain rate range from 0.02 to 0.035 s^{-1} . These values compare well with observed shear strain rates from field observations (Deksheniaks et al., 2001; McManus et al., 2003) and justify our selection of the 0.025 s^{-1} cutoff for the velocity gradient layer.

4.2.2 Responses to the density gradient layer

In contrast to responses to the velocity gradient layer, *A. tonsa* did not exhibit significant aggregative behavior in the presence of the model density gradient layer for $\Delta\sigma_t = 1.8$ (Fig. 4.13). Examination of swimming paths revealed that *A. tonsa* often contacted the density gradient and turned horizontally or swam in the opposite direction (Fig. 4.12b). Proportional residence time in the layer was not increased over the control

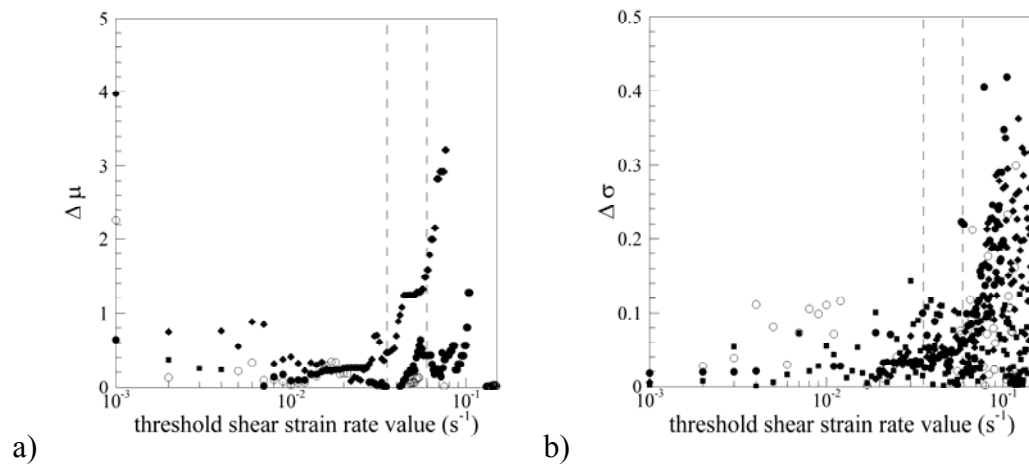


Figure 4.15 Threshold shear strain rate values for *A. tonsa* in the velocity gradient layer treatment. Data from four sample paths are shown in each figure. $\Delta\mu$ is the difference between the mean swim speed values calculated for data above and below a threshold. $\Delta\sigma$ is the difference between the standard deviation values for swim speed data above and below a threshold value. An abrupt change in $\Delta\mu$ or $\Delta\sigma$ indicates a behavior transition, and hence suggests the threshold value for behavioral response.

condition (Fig. 4.13; $T_R = 0.42$). General linear model results were not significant (Table 4.1), suggesting that *A. tonsa* may not utilize density gradients as a cue for area-restricted foraging. Further support is provided by comparisons of swimming speeds and turn frequency. Swimming speeds and turn frequency for *A. tonsa* in response to the $\Delta\sigma_t = 1.8$ density gradient were not significantly different between pre-contact and post-contact with the density gradient (Tables 4.2 and 4.3).

Nevertheless, *A. tonsa* did exhibit a response in the presence of the density gradient; organisms often turned around and swam in the opposite direction when encountering the layer, as if the organism had approached an impenetrable boundary. Comparisons of the number of individuals (out of 40 observations) that cross the density gradient (9 crossing) compared to the control (27 crossing) showed significant behavioral changes in the presence of a density gradient ($n = 40$; two-tailed $P = 0.002$; Fisher's exact test). These behaviors could lead to density gradients acting as boundaries, thus promoting aggregations.

Responses to the range of density gradients showed no significant differences in proportional residence times (Fig. 4.16; $df = 299$, $F = 1.05$, $p = 0.389$; single-factor ANOVA). As discussed above, the number of copepods crossing the layer is influenced by the presence of a density gradient, and the influence appears to depend on the strength of the jump. The first 40 recorded paths for each experiment were scored for cross or did not cross as before to determine the proportion of copepods crossing the gradient. Regression analysis of locale crossing data revealed a lower threshold of $\Delta\sigma_t = 1.6$, with

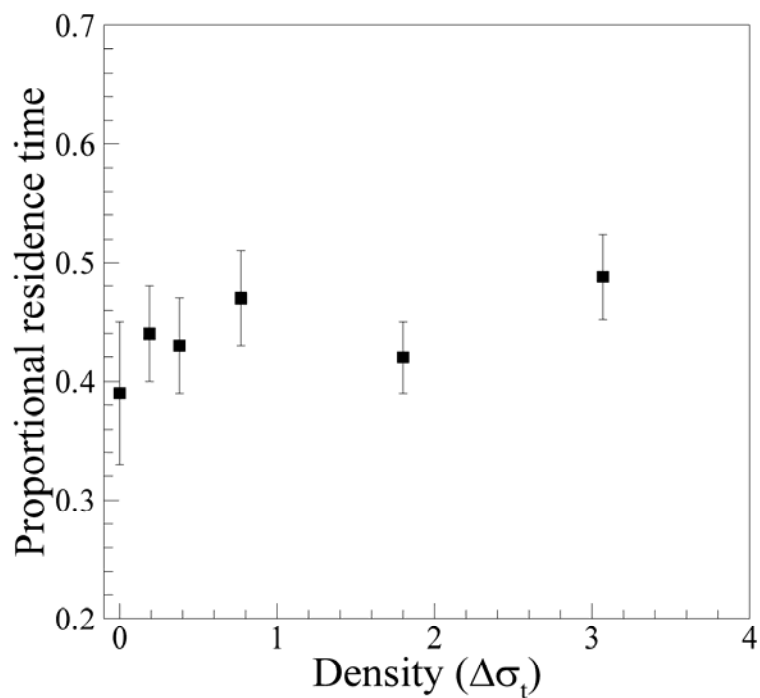


Figure 4.16 Proportional residence time of *A. tonsa* in response to the density gradient layer with varying density jump magnitude. Density gradients are a result of a change in salinity (0, 0.25, 0.5, 1, 2, 4 ppt) corresponding to change in $\Delta\sigma_t$ (0, 0.2, 0.4, 0.8, 1.8, 3.1 respectively).

a saturation response at $\Delta\sigma_t = 2.1$ (Fig. 4.17). Sigmoidal regression was used due to the threshold type response, and residuals from a linear regression were statistically not random (Runs test, $u_{0.20(2),6} = 2$, $u = 2$).

4.2.3 Responses to the chemical/biological gradient layer

A. tonsa significantly increased proportional residence time in the layer for both biological (phytoplankton) layers and chemical exudate (from *Tetraselmis* spp.) layers by adjusting swimming patterns (Figs. 4-12c and 4-13). However, *A. tonsa* responded differently to the biological and chemical exudate layers. *A. tonsa* responded to the chemical exudate layer by significantly increasing swimming speed (Table 4.2) and turn frequency (Table 4.3). This response is similar to that described in Section 4.2.1 for the response of *A. tonsa* responses to the velocity gradient layer and is consistent with an excited area-restricted search response. Conversely, in the biological (or food) layer, *A. tonsa* significantly decreased swimming speed and slightly increased turn frequency. The unique path kinematics in the food layer are the result of *A. tonsa* increasing the frequency and duration of feeding bouts. Similar results were observed by Tiselius (1992).

A. tonsa significantly increased proportional residence time in response to chemical exudate concentration (Fig. 4.18; $df = 299$, $F = 13.08$, $p < 0.001$; single-factor ANOVA). A post-hoc S-N-K test revealed a significant difference only at the highest concentration tested ($200 \mu\text{g C L}^{-1}$; difference = 0.177; minimum significant difference,

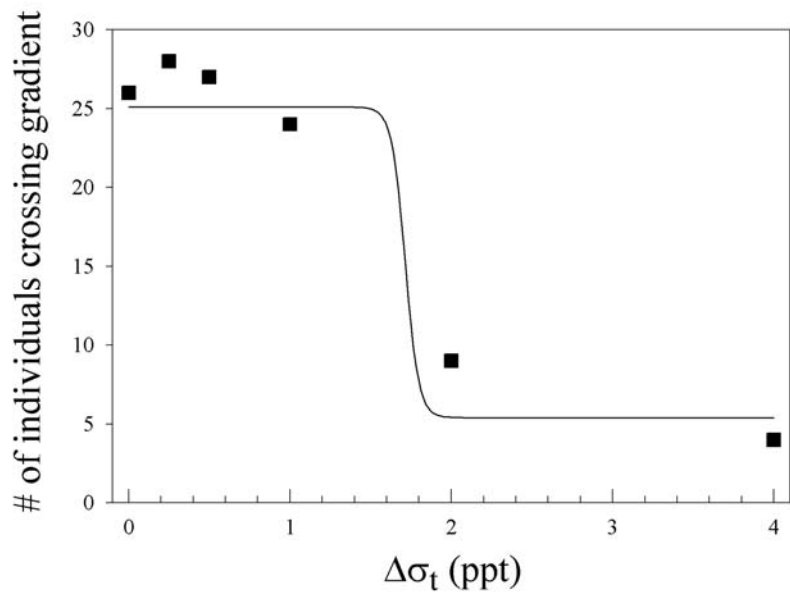


Figure 4.17 Behavioral response of *A. tonsa* to density gradient layer treatment is represented by the number of individuals that cross the gradient layer (sigmoidal curve fit; $R^2 = 0.972$, $p = 0.094$). Sample sizes are the same for all gradient levels ($n = 40$).

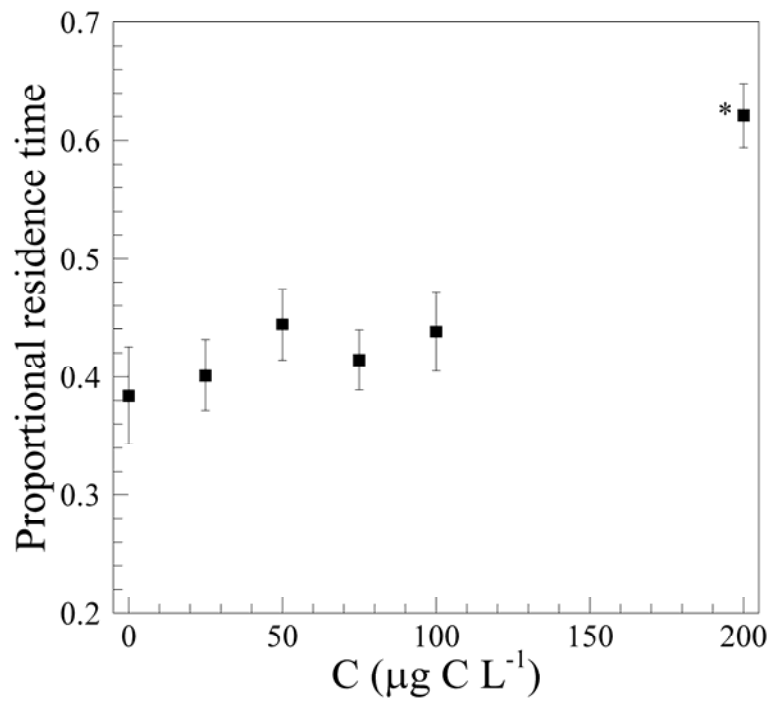


Figure 4.18 Proportional residence time for *A. tonsa* in the presence of a chemical exudate layer of *Tetraselmis* spp. Exudate concentration is calculated as equivalent biomass concentration ($\mu\text{g C L}^{-1}$). * indicates significant difference ($p < 0.05$) of treatment value versus preceding value via S-N-K post-hoc test.

$MSD_{0.05,299,1} = 0.112$). This suggests a behavioral threshold between $100 \mu\text{g C L}^{-1}$ and $200 \mu\text{g C L}^{-1}$ for *A. tonsa* responses to *Tetraselmis* spp. exudates.

4.2.4 Responses to combined layers

Proportional residence times of *A. tonsa* for combined cue treatments were higher than controls in all cases (Fig. 4.13; Table 4.1). Responses by *A. tonsa* to various combinations of gradients revealed significant interactions between velocity and chemical factors, but no interactive effects involving fluid density for proportional residence time (Table 4.1). This interaction shows that the response to a velocity gradient is altered in the presence of a chemical exudate layer. *A. tonsa*, a relationship exists between certain thin layer properties that are strong enough to influence individual behavior. Although density gradients helped strengthen or increase proportional residence time in combination with the other properties, interactions were not significant. *A. tonsa* increased swimming speed and turn frequency for all combined layers (Tables 4.2 and 4.3), likely because either velocity or chemical exudates were present in all combinations.

Threshold responses to velocity gradients were not significantly affected by the presence of an additional cue (Fig. 4.19). However the trend is not as clear as the isolated case, likely due to the fact that responses are not uniquely tied to shear strain rate, and behavior may be driven by a response to another cue. *A. tonsa* responded in a strain rate range between $0.03\text{-}0.05 \text{ s}^{-1}$ compared to $0.02\text{-}0.04 \text{ s}^{-1}$ for the velocity-only experiments

(shown in Fig. 4.15). The velocity and density gradients elicit very different responses from *A. tonsa*, therefore it is not likely that the threshold response would change in such a combination. However, chemical exudates and velocity gradients elicit almost identical responses from *A. tonsa*, but no change in threshold occurred. This is likely due to the shear strain rate profile being wider than the chemical concentration profile in these experiments. The shear strain rate threshold level is located at the edge of the layer and is not coincident with the location of the chemical exudates, which is isolated at the center of the layer (see Sections 4.1.4 and 4.1.5; Fig. 4.9; Deksheniaks et al., 2001; Cowles, 2004).

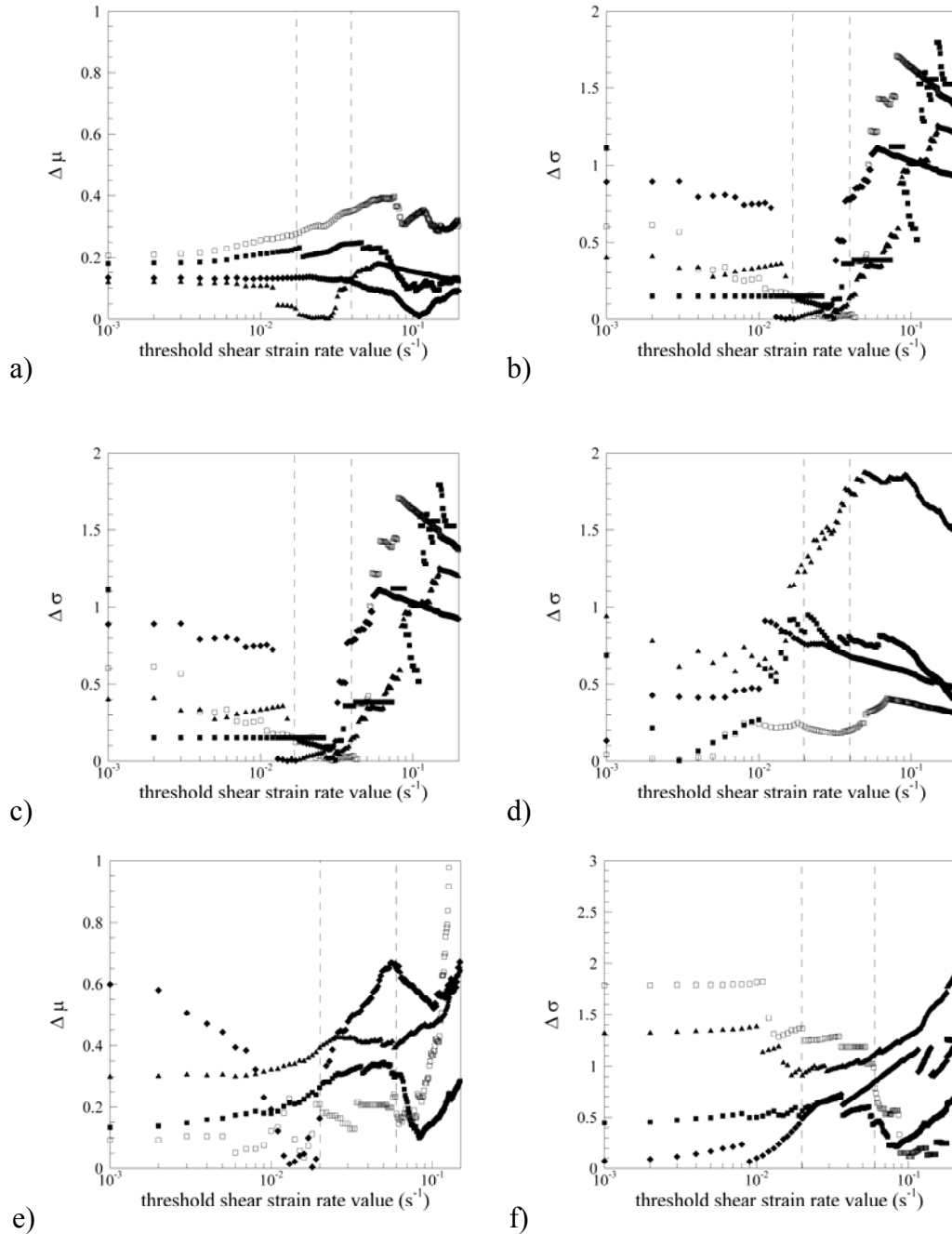


Figure 4.19

Threshold shear strain rate values for *A. tonsa* in combined layers with a velocity gradient: (a,b) velocity-density, (c,d) velocity-chemical, and (e,f) velocity-chemical-density. Data from four sample paths are shown in each figure. (a,c,e) $\Delta\mu$ is the difference between the mean swim speed values calculated for data above and below a threshold. (b,d,f) $\Delta\sigma$ is the difference between the standard deviations for swim speed data above and below a threshold value. An abrupt change in $\Delta\mu$ or $\Delta\sigma$ indicates a behavior transition, and hence suggests the threshold value for behavioral response.

4.3 Temora longicornis and environmental structure

4.3.1 Responses to the velocity gradient layer

Temora longicornis exhibited a significant aggregative behavioral response to the velocity model layer. Fig. 4.20 illustrates differences in typical swimming paths between velocity gradient (Fig. 4.20a) and control layers (Fig. 4.20d). Proportional residence time in the layer increased by approximately 17% in the presence of a shear strain rate over the no flow control (see Figure 4.21 and Table 4.4; $T_R = 0.507$ and 0.340 respectively). Table 4.4 shows that the proportional residence time in the layer increased significantly for the velocity gradient layer treatment compared to the control (balanced ANOVA). The repeatability of these results was excellent, with little or no change in both the means and variances between individual trials ($T_R = 0.507$ and 0.506 ; $S_e = 0.033$ and 0.026). The behavioral change in residence time of *T. longicornis* is ample to produce observed field aggregations and distributions (Hamner, 1988).

The increased residence time arise from a combination of increased swimming speed and turn frequency. Table 4.5 shows that *T. longicornis* increases swimming speed significantly after contact with the layer (6.84 mms^{-1} compared to 5.40 mms^{-1} pre-contact). This increase in swimming speed suggests that *T. longicornis* individuals are behaviorally excited by the layer. The behavioral response is different than the hydromechanical escape response observed by previous researchers (Yen and Fields, 1992a; others) with less than 5 escape responses observed within the layer during video analysis of fifty paths.

Table 4.4 Results of balanced ANOVA on proportional residence time with four factors (replicate, velocity, density, and chemical) and interactive effects for *T. longicornis*. * indicates significance at $p < 0.05$, and ** indicates significance at $p < 0.001$. Significance shows that the factor or the interaction of the listed factors has an effect on the behavior of the organism with respect to proportional residence time.

Factor	df	SS	MS	F	P
TOTAL	799				
Replicate	1	0.022	0.022	0.55	0.459
Velocity (V)	1	1.957	1.957	46.76	<0.001 **
Density (D)	1	0.935	0.935	22.35	<0.001 **
Chemical (C)	1	3.066	3.066	73.25	<0.001 **
Velocity × Density	1	0.008	0.008	0.19	0.664
Velocity × Chemical	1	0.881	0.881	21.03	<0.001 **
Density × Chemical	1	0.359	0.359	8.60	0.003 *
Velocity × Density × Chemical	1	0.022	0.022	0.54	0.465

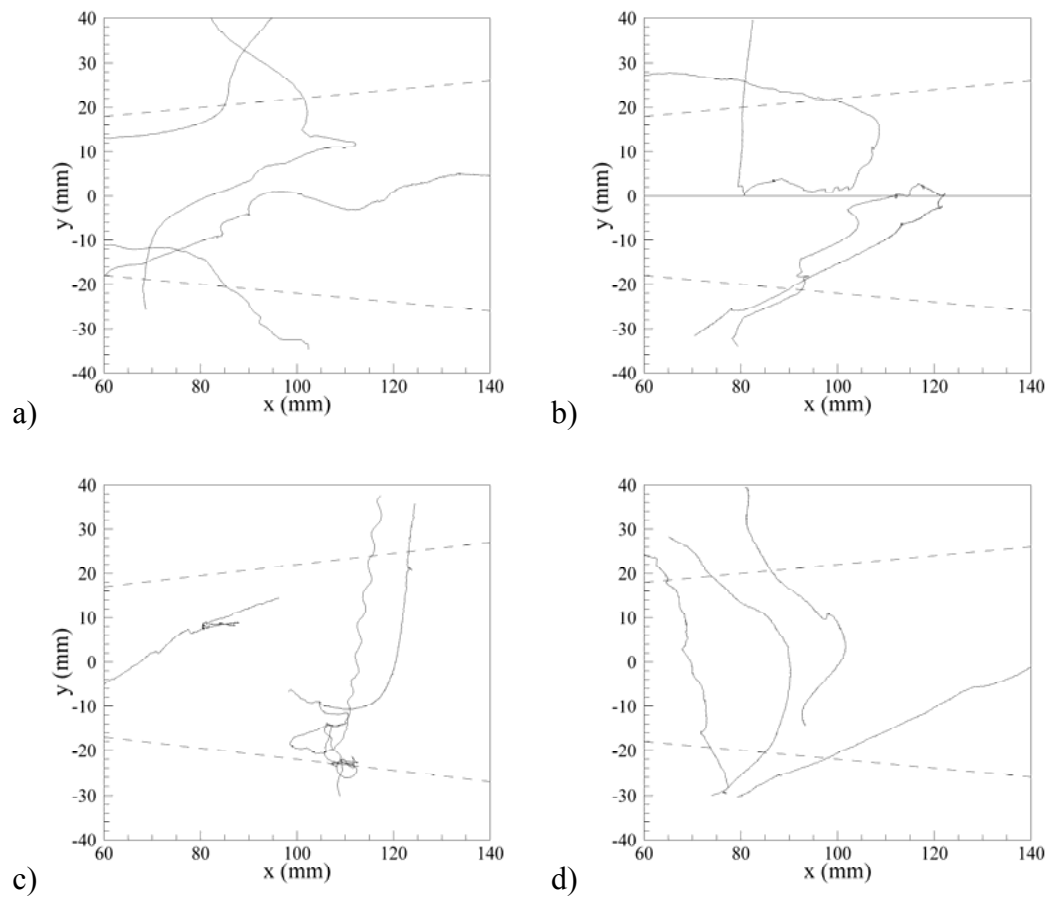


Figure 4.20 Sample paths for *T. longicornis* for the (a) velocity gradient layer, (b) density gradient layer, (c) the chemical exudate layer, and (d) control. The dashed lines indicate the edge of the layer corresponding to δ_S .

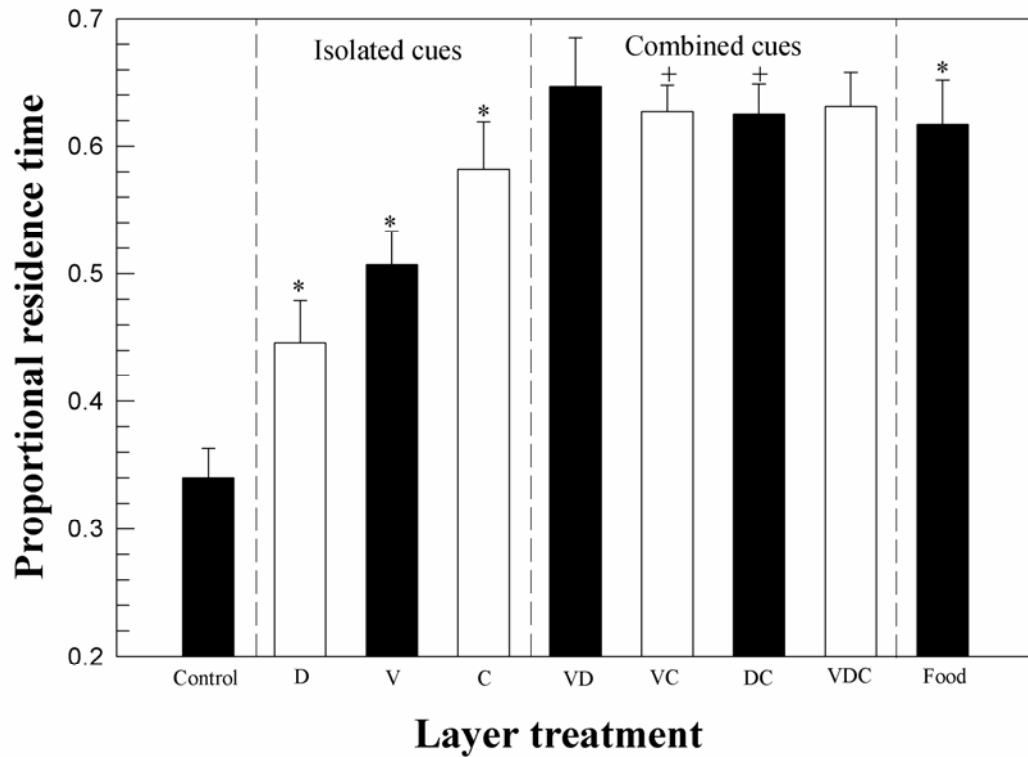


Figure 4.21 Proportional residence time for *T. longicornis* in the presence of individual and combined cue layers. Layer constituents are velocity (V), density (D), and chemical exudates (C). * indicates a significant effect of single treatments relative to the control as determined with a balanced, nested ANOVA ($p < 0.05$). For combined layers, + indicates significant interactive effects between the layer constituents.

Table 4.6 shows the increase in the turn frequency of *T. longicornis* within the velocity gradient layer. In the control experiments, the mean turn frequency is 0.11 and is qualitatively similar to out-of-layer values (0.10) for the treatment experiments. However, while in the velocity gradient layer, *T. longicornis* more than doubled its turn frequency (Table 4.6). This increase in turn frequency allows the excited individual to remain in the region of interest while quickly scanning for resources.

Instantaneous swimming speeds from two sample paths (control and treatment) are plotted on the same time axis in Fig. 4.22. These paths were chosen because both entered the gradient layer region at approximately the same time (labeled). The increase in relative swimming speed in the velocity gradient layer is apparent. Plotting the instantaneous swim speed against the shear strain rate further illustrates the importance of the velocity gradient layer in the behavioral change. Figure 4.23 shows four sample paths

Table 4.5 Swimming speeds for *T. longicornis* pre-contact and post-contact with the model thin layer. * denotes significant differences ($p < 0.05$) between pre-contact and post-contact values by single-factor ANOVA; control values are shown for comparison.

Treatment	n	Pre-contact mm/s (std err)	Post-contact mm/s (std err)	p
Individual cues				
Control	50	4.50 (0.22)	4.76 (0.47)	0.574
Velocity ($U_j = 6.7 \text{ mms}^{-1}$)	46	5.40 (0.41)	6.84 * (0.51)	0.025 *
Density ($\Delta\sigma_t = 1.8$)	48	5.37 (0.24)	5.36 (0.19)	0.990
Chemical ($200 \mu\text{g C L}^{-1}$ eq.)	40	2.41 (0.15)	3.72 * (0.38)	0.001 *
Food ($200 \mu\text{g C L}^{-1}$)	42	3.57 (0.32)	2.71 * (0.17)	0.034 *
Combined cues				
Velocity-Density	50	5.13 (0.40)	6.53 * (0.47)	0.007 *
Velocity-Chemical	37	3.17 (0.31)	4.55 * (0.36)	0.012 *
Density-Chemical	41	3.31 (0.29)	3.97 * (0.15)	0.032 *
Velocity-Density- Chemical	47	4.44 (0.41)	5.51 * (0.30)	0.031 *
Velocity-All Chemical	42	5.36 (0.65)	5.53 (0.48)	0.828

Table 4.6 Turn frequency for *T. longicornis* in all gradients pre-contact and post-contact with the model thin layer. * denotes significant differences ($p < 0.05$) between pre-contact and post-contact values by single-factor ANOVA; control values are shown for comparison.

Treatment	<i>n</i>	Total # turns/ind/s (std err)	In layer # turns/ind/s (std err)	Out of layer # turns/ind/s (std err)	<i>p</i>
<i>Individual cues</i>					
Control	40	0.11 (0.02)	-	-	
Velocity ($U_j = 6.7 \text{ mms}^{-1}$)	40	0.19 (0.03)	0.24 * (0.06)	0.10 (0.02)	0.046 *
Density ($\Delta\sigma_t = 1.8$)	40	0.14 (0.02)	0.13 (0.04)	0.14 (0.03)	0.817
Chemical (200 $\mu\text{g C L}^{-1}$ eq.)	26	0.19 (0.02)	0.23 * (0.04)	0.11 (0.04)	0.048 *
Food (200 $\mu\text{g C L}^{-1}$)	35	0.15 (0.02)	0.16 (0.03)	0.11 (0.04)	0.267
<i>Combined cues</i>					
Velocity-Density	27	0.20 (0.04)	0.22 * (0.04)	0.06 (0.03)	0.008 *
Velocity-Chemical	30	0.21 (0.03)	0.22 (0.06)	0.12 (0.05)	0.167
Density-Chemical	40	0.18 (0.02)	0.22 * (0.04)	0.10 (0.03)	0.042 *
Velocity-Density-Chemical	29	0.17 (0.02)	0.19 * (0.03)	0.08 (0.03)	0.039 *
Velocity-All Chemical		0.18 (0.03)	0.17 (0.02)	0.20 (0.04)	0.742

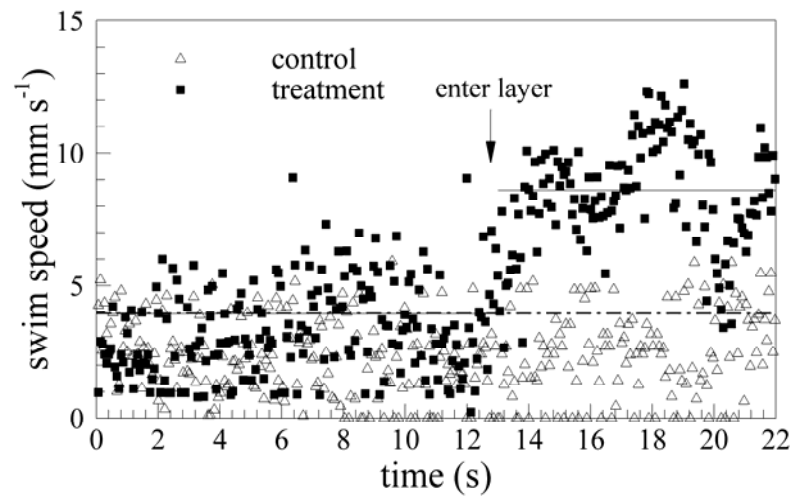


Figure 4.22 Time record of swimming speed for two sample *T. longicornis* paths for the velocity gradient layer treatment (triangle – control and square – treatment). The solid line indicates the average value for all treatment paths (in and out of layer indicated separately) and the dashed line indicates the average value for all control paths.

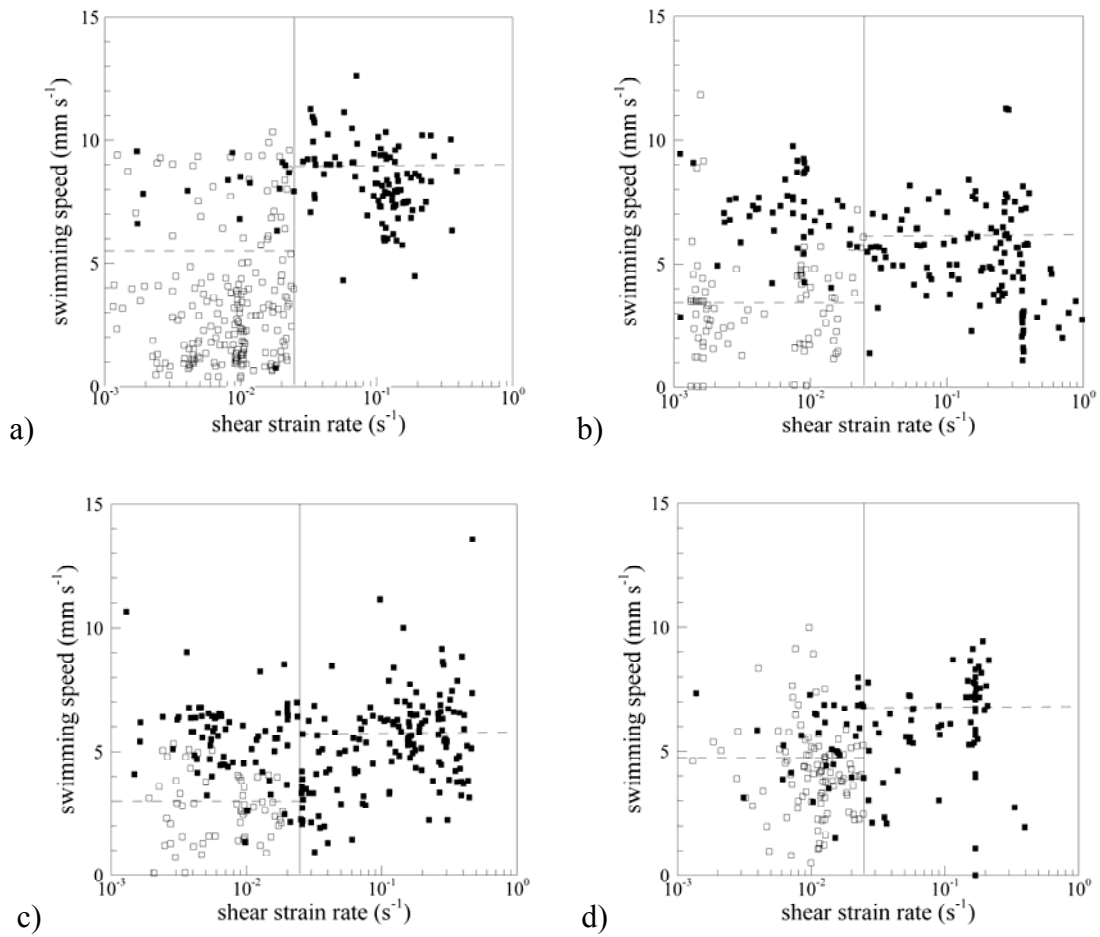


Figure 4.23 Instantaneous swimming speeds for four sample *T. longicornis* paths plotted against shear strain rate for the velocity gradient layer treatment. The solid line shows the response threshold of 0.025 s^{-1} , or δ_s . The dashed lines show the average swimming speed above and below threshold. Open symbols correspond to pre-contact with the layer, and solid symbols correspond to post-contact.

plotted in this fashion. Swimming speeds increase upon contact with the layer (closed symbols), and remain elevated upon exiting the layer.

The threshold shear strain rates for the above observations were determined in the same fashion as for *A. tonsa* (Section 4.2.1). Figure 4.24 shows plots of $\Delta\mu$ and $\Delta\sigma$ for five individual *T. longicornis* paths, where the delta refers to the difference above and below the threshold value. For *T. longicornis*, threshold values of shear strain rate range from 0.03 to 0.06 s⁻¹. Body size corrections to the threshold values are used for larger copepods such as *T. longicornis* because the strain rate value corresponds to the centroid of the copepod. Thus, the antennae are likely to be 0.5 mm from this location. By extrapolating this distance along the axis of the organism, the threshold values are adjusted based on the shear strain rate profile at the appropriate x -location. These values compare well with observed shear strain rates from field observations (Dekshenieks et al., 2001; McManus et al., 2003) and also fit into our definition of the edge of the velocity gradient layer (0.025 s⁻¹).

T. longicornis is a cruise-style swimmer, and therefore the orientation of the body axis is a good indicator of the swimming direction of the organism and vice versa. Figure 4.25 shows the probability density function of the orientation angle with 0° aligned with the horizontal either with or against the laminar jet flow. The post-contact orientation distribution of 10 *T. longicornis* paths shows a significant difference compared to the precontact distribution (Kolmogorov-Smirnov goodness of fit; $d_{\max} = 0.359$; $d_{0.05,20} = 0.294$). The change in the orientation distribution shows that *T. longicornis* individuals

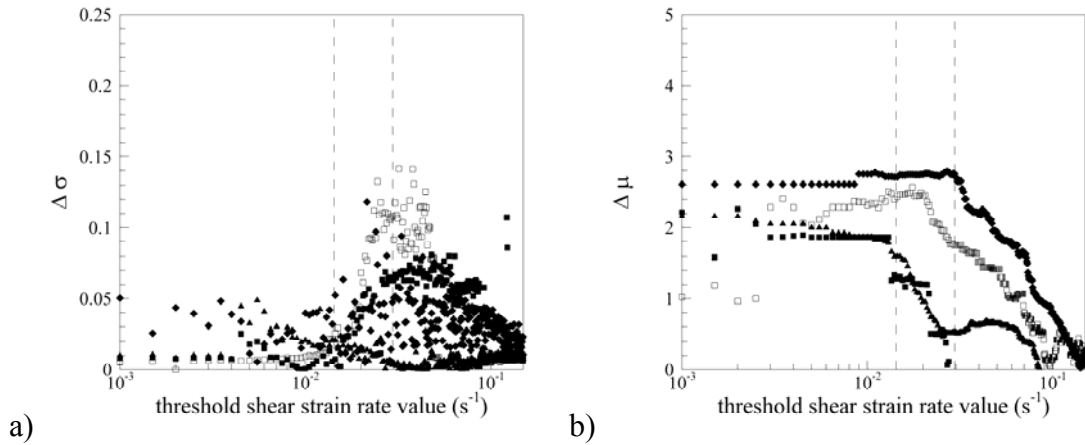


Figure 4.24 Threshold shear strain rate values for *T. longicornis* in the velocity gradient layer treatment. Data from four sample paths are shown in each figure. $\Delta\mu$ is the difference between the mean swim speed values calculated for data above and below a threshold. $\Delta\sigma$ is the difference between the standard deviation values for swim speed data above and below a threshold value. An abrupt change in $\Delta\mu$ or $\Delta\sigma$ indicates a behavior transition, and hence suggests the threshold value for behavioral response.

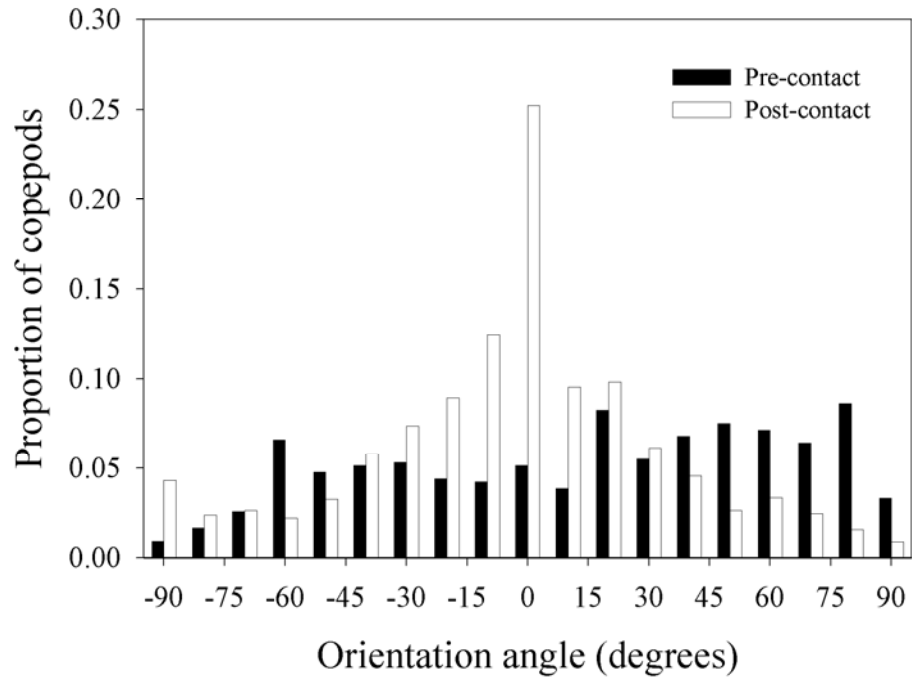


Figure 4.25 Normalized distribution of orientation angle for 10 *T. longicornis* paths in the velocity gradient layer. The post-contact distribution is significantly different than the pre-contact distribution via a Kolmogorov-Smirnov goodness of fit ($d_{\max} = 0.359$; $d_{0.05,20} = 0.294$). The orientation angle is defined such that 0° corresponds to horizontal facing either upstream or downstream.

orient parallel to the flow, which allows the copepod to maintain contact with the velocity gradient layer. The preferred body orientation also places the antennal mechanosensory array in a direction perpendicular to the flow direction, which presumably facilitates sensing the velocity gradient, although the precise sensing mechanism of the setal array is currently unknown. Similar preferential orientation observations have been reported *in situ* for other copepod and zooplankton species (Genin et al., 2005).

4.3.2 Responses to the density gradient layer

Temora longicornis also exhibited a significant aggregative behavior in the presence of a density gradient (Figure 4.21 and Table 4.4). Sample paths for *T. longicornis* in the presence of a density gradient are shown in Fig. 4.20b. Density had a significant impact on the proportional residence time (Table 4.4). However, *T. longicornis* did not increase swimming speed or turn frequency in response to contacting the density gradient layer (Tables 4.5 and 4.6).

Although single factor ANOVA revealed significant differences ($df = 299$, $F = 2.412$, $p = 0.036$) in the proportional residence time for the threshold density experiment, a post-hoc S-N-K test on the proportional residence time data revealed no significant differences for the range of density gradient layer experiments because a minimum significant difference (MSD) was not reached between adjacent treatments (Fig. 4.26; maximum difference = 0.119; $MSD_{0.05,294,6} = 0.120$). Individual copepods often did not cross the gradient layer (Fig. 4.27), and this effect was non-linear with a distinct lower threshold; linear regression showed a non-random distribution of residuals

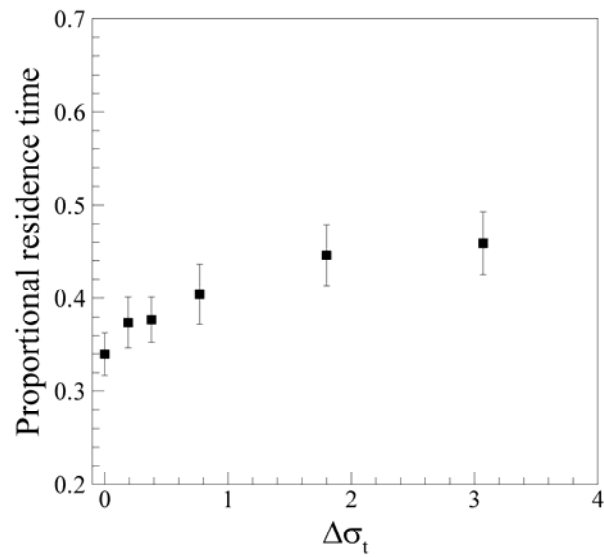


Figure 4.26 Proportional residence time of *T. longicornis* in response to the density gradient layer treatment with varying density jump magnitude. Density gradients are a result of a change in salinity (0, 0.25, 0.5, 1, 2, 4) corresponding to change in $\Delta\sigma_t$ (0, 0.2, 0.4, 0.8, 1.8, 3.1, respectively).

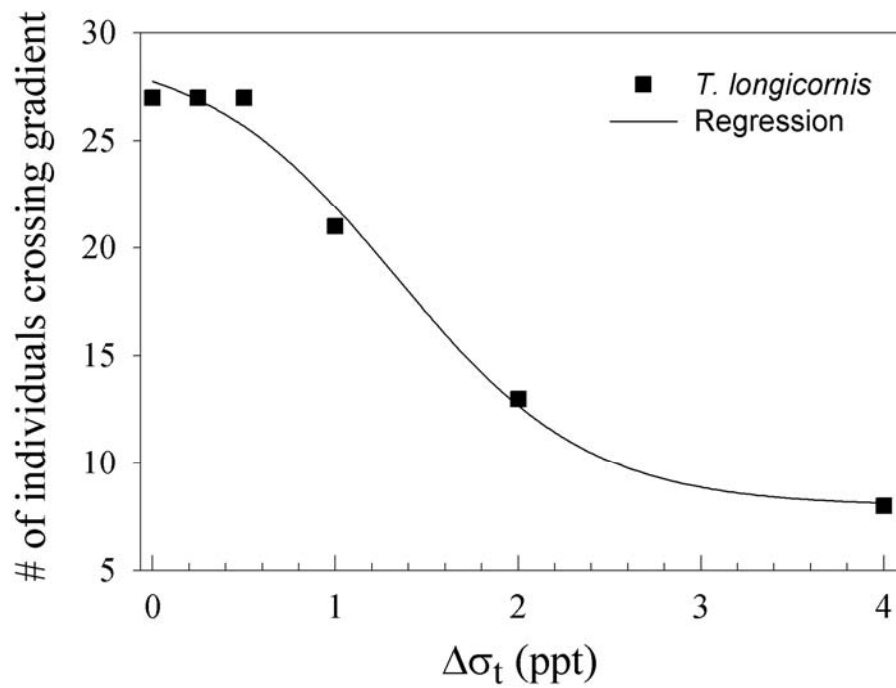


Figure 4.27 Behavioral response of *T. longicornis* to density gradient layer treatment is represented by the number of individuals that cross the gradient layer (sigmoidal curve fit; $R^2 = 0.996$, $p = 0.011$). Sample sizes are the same for all gradient levels ($n = 40$).

(Runs test, $u_{0.20(2),6} = 2$, $u = 1$). Thus, sigmoidal regression was used in order to estimate the lower response threshold. Regression of the number of individuals crossing versus density jump strength revealed a lower threshold boundary of $\Delta\sigma_i = 0.5$ (Curve begins to decrease near this value). The response to the density gradient asymptotically approaches approximately 75% of the population not crossing the gradient by $\Delta\sigma_i = 2.0$.

4.3.3 Responses to the chemical/biological gradient layer

Chemical exudate and food layer experiments with *Tetraselmis* spp. showed significant increases in proportional residence time over controls at $200 \mu\text{g C L}^{-1}$ (Fig. 4.21 and Table 4.4). As with *Acartia tonsa*, this result was attributed to different behavioral responses in the respective layers. In the food layer, *T. longicornis* individuals contacted the layer and began feeding behavior. Comparisons of swimming speed pre-contact and post-contact with the food layer support feeding observations, and the behavior was similar to that reported for *Acartia tonsa* by Tiselius (1992). *T. longicornis* individuals did not significantly increase turn frequency ($df = 58$; $F = 3.09$; $p = 0.08$). In the chemical layer (no food present), individuals significantly increased swimming speed (Table 4.5; $df = 70$, $F = 12.01$, $p < 0.001$) and turn frequency (Table 4.6; $df = 48$, $F = 4.13$, $p = 0.047$), indicating an excited area-restricted search behavior.

T. longicornis responded in a graded fashion to varying concentration of phytoplankton chemical exudates (Fig. 4.28). Single factor ANOVA revealed significant differences in the proportional residence times between concentration levels for both

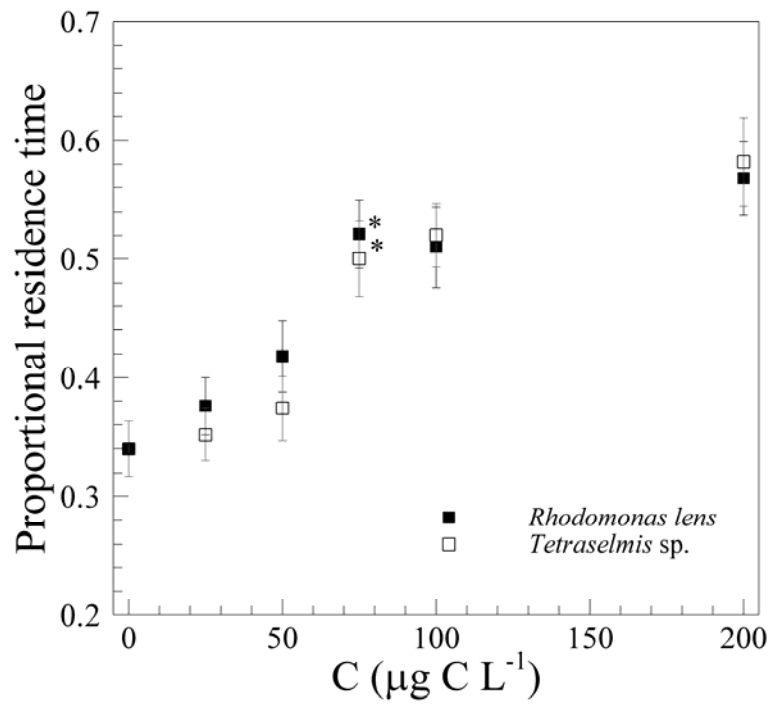


Figure 4.28 Proportional residence time of *T. longicornis* in the presence of a chemical exudate layer of either *Tetraselmis* spp. or *Rhodomonas lens*. Concentration of exudate is calculated as the equivalent biomass concentration ($\mu\text{g C L}^{-1}$). * indicates significant difference ($p < 0.05$) of treatment value versus preceding value via S-N-K post-hoc test.

plankton species (*R. lens*, $F_{5,299} = 10.03$, $p < 0.001$; *Tetraselmis* spp., $F_{5,299} = 13.08$, $p < 0.001$). Post-hoc S-N-K tests revealed that proportional residence time did not significantly increase until chemical exudate concentration reached equivalent biomass values greater than $50 \mu\text{g C L}^{-1}$. *T. longicornis* began to respond to *R. lens* (difference = 0.092, $MSD_{0.05,294,1} = 0.080$) and to *Tetraselmis* spp. (difference = 0.126, $MSD_{0.05,294,1} = 0.080$) at a concentration around $75 \mu\text{g C L}^{-1}$. Saturation of the response to both phytoplankton species occurred beyond $100 \mu\text{g C L}^{-1}$.

4.3.4 Responses to combined layers

Observing responses of *T. longicornis* to combined gradients allows for the determination of the relative importance of different cues associated with oceanic structure. Experiments were conducted for all combinations (velocity-density; velocity-chemical; density-chemical; and velocity-density-chemical). Proportional residence times for all combinations of gradients were similar (Fig. 4.21). No statistical differences were seen between the different combinations; however, all combinations resulted in higher residence times than those reported for single, isolated gradients. *T. longicornis* showed significant interactions between physical and chemical gradients suggesting that responses to either physical factor were different depending on the presence of chemical exudates. In fact, in any combination layer with chemical exudate, proportional residence time appears to be solely reliant on the presence of the chemical cue, suggesting that a hierarchy of cues is present in foraging behavior.

Another experiment was run to determine the importance of the interaction between the velocity and chemical factors. A velocity treatment with $200 \mu\text{g C L}^{-1}$ chemical exudate concentration throughout the system showed no increase in proportional residence time in the model layer ($T_R = 0.361$). Swimming speed and turn frequency also did not change (Tables 4.5 and 4.6), but both were elevated at levels similar to other experiments suggesting that copepods were conducting area-restricted searches throughout the test section. This result suggests that chemical exudates are a more important cue than velocity gradients.

In the velocity-density treatment, *T. longicornis* displayed a combination of the two behaviors observed in previous, isolated cue experiments (excited area-restricted search behavior; Tables 4.5 and 4.6; and a propensity not to cross the halocline, Fig. 4.27) resulting in a significant increase in proportional residence time compared to both velocity and density treatments (Fig. 4.21 and Table 4.4). Similar to behaviors cued by the velocity gradient layer, copepods after contacting the velocity-density layer increased relative swimming speed and turn frequency over controls and compared to pre-contact values (Tables 4.5 and 4.6). Responses to the velocity-chemical layer corresponded to the area-restricted search behavior observed in both individual cue treatments. Similar results were observed in the density-chemical and in the velocity-density-chemical treatments. Individuals in the density-chemical treatment typically exhibited area-restricted search behavior in response to chemical exudates, and again, a behavioral aversion to crossing the density gradient resulting in significantly higher proportional residence times than for the isolated density gradient layer treatment, but not for the

isolated chemical layer treatment. Significant differences in proportional residence time can be attributed to treatment effects (Table 4.4) because no significance is seen at the replicate level. Interactions between velocity and density are not significant, likely due to the velocity response being the same with or without a density gradient. However, velocity-chemical interactions are significant suggesting that a combination of these cues may influence aggregation in the field. *T. longicornis* does not respond to velocity gradients in the presence of a chemical exudate layer. Similar results were seen for the density-chemical interactions, but not for the full combined interaction.

Congruent with area-restricted search behavior, copepods increased swimming speed (Table 4.5) and turn frequency (Table 4.6) after contact with each combined layer compared to pre-contact with the gradient layer, although not all comparisons resulted in significant change, likely due to high behavioral variability. This result was expected in all combined layer experiments due to the presence of at least one isolated cue responsible for this behavior.

T. longicornis did not alter threshold responses to the velocity gradient in the presence of other oceanographic features (Fig. 4.29). Although significant interactions occurred between velocity and chemical exudates, the threshold range did not shift, likely due to copepods contacting the boundary of the wider shear strain rate layer prior to the chemical layer (see Section 4.1.4 and Fig. 4.9).

4.3.5 Significance of responses and variability

All swimming speed measurements in the trials were within previously observed cruise speed ranges for *T. longicornis* (2-12 mm s⁻¹). Because paths containing escape responses were removed (less than 5 per 50 recorded paths) increases in mean swimming speed are a result of a large portion of an experimental population increasing swimming speed or turn frequency by 1-2 mm s⁻¹ or 0.1-0.2 turns ind⁻¹ s⁻¹ respectively.

In this study, individual swimming paths were presented for demonstration purposes, and ensemble-averages of animals prior to and subsequent to contact with the layer were used to show aggregate behavioral changes in the population. For example, ensemble-averaged swimming speed for *T. longicornis* in this study increased by 1.4 mm s⁻¹, a result of 34 individuals (out of 46) increasing swimming speed after contact with the velocity layer. All responsive individuals increased swimming speed between 1 and 2 mm s⁻¹. This type of analysis is important when looking at population level responses such as aggregation because individual behavior influences aggregation. For instance, although it is individuals who respond to different cues in a wide variety of fashions, aggregations can only form when a significant proportion of the population exhibits a similar behavior.

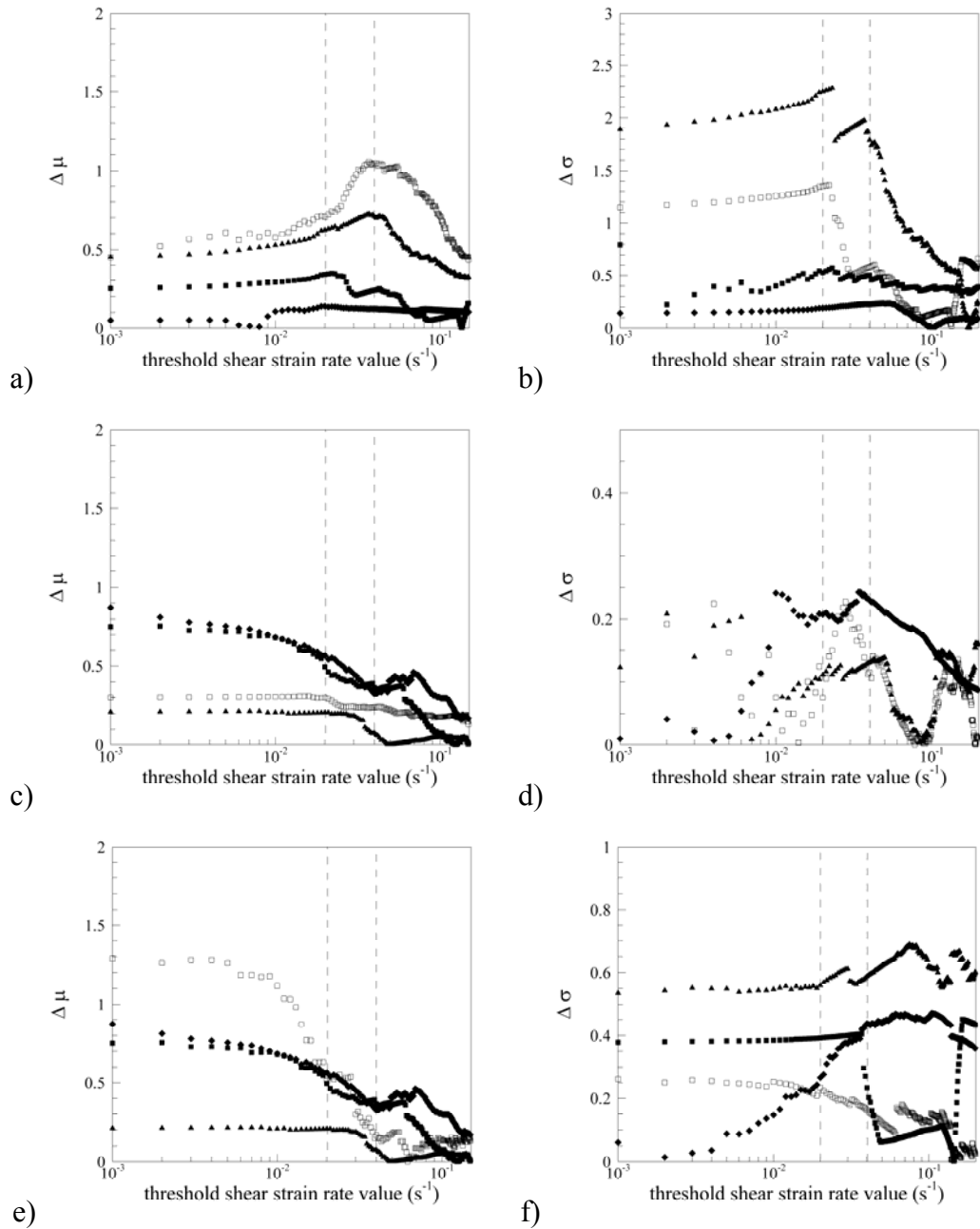


Figure 4.29 Threshold shear strain rate values for *T. longicornis* in combined layers with a velocity gradient: velocity-density (a,b), velocity-chemical (c,d), and velocity-chemical-density (e,f). Data from four sample paths are shown in each figure. (a,c,e) $\Delta\mu$ is the difference between the mean swim speed values calculated for data above and below a threshold. (b,d,f) $\Delta\sigma$ is the difference between the standard deviations for swim speed data above and below a threshold value. An abrupt change in $\Delta\mu$ or $\Delta\sigma$ indicates a behavior transition, and hence suggests the threshold value for behavioral response.

4.4 *Calanus* sp., biogeographic and stage comparisons

Calanus spp. from different geographic regions were tested with isolated layer treatments: *C. finmarchicus* from the Gulf of Maine and *C. pacificus* from Monterrey Bay, CA. Additionally, nauplii (NIII-NIV) of the species *C. finmarchicus* were tested to see if observed responses were present throughout the life cycle, or if they developed in late copepodid or adult stages.

4.4.1 Responses to the velocity gradient layer

Both *Calanus* spp. responded in a positive fashion to the velocity gradient layer. Proportional residence times for all species increased significantly via single-factor ANOVA (Figs. 4-30 and 4-31; *C. finmarchicus*, $df = 99$, $F = 23.07$, $p < 0.001$; *C. pacificus*, $df = 99$, $F = 10.20$; $p < 0.001$) and an S-N-K test (Fig. 4.30, *C. finmarchicus*, difference = 0.296, $MSD_{0.05,99,5} = 0.127$; Fig. 4.31, *C. pacificus*, difference = 0.258, $MSD_{0.05,99,5} = 0.133$). Both *Calanus* spp. increased swimming speed and turn frequency (Table 4.7). *C. finmarchicus* increased swimming speed significantly. However, *C. pacificus* showed a strong trend towards an increase in swimming speed.

Table 4.7 Species comparison of behavioral responses (swimming speed and turn frequency) to the velocity gradient layer treatment. * denotes significant differences ($p < 0.05$) between pre-contact and post-contact values by single-factor ANOVA.

Species	<i>n</i>	Swimming speed mm s ⁻¹ (std err)		<i>p</i>	<i>n</i>	Turn frequency turns ind ⁻¹ s ⁻¹ (std err)		<i>p</i>
		Pre-contact	Post-contact			Out of layer	In layer	
<i>Acartia tonsa</i>	47	3.08 (0.17)	3.68 (0.19)	0.009 *	40	0.09 (0.02)	0.24 (0.05)	0.018 *
<i>Calanus finmarchicus</i>	16	3.61 (0.51)	5.63 (0.60)	0.020 *	16	0.03 (0.01)	0.10 (0.03)	0.028 *
<i>Calanus finmarchicus</i> (nauplii)	16	5.43 (0.61)	4.97 (0.39)	0.560	14	0.16 (0.05)	0.16 (0.04)	0.979
<i>Calanus pacificus</i>	17	6.65 (0.59)	8.18 (0.52)	0.061	17	0.05 (0.03)	0.17 (0.03)	0.012 *
<i>Candacia ethiopica</i>	41	4.06 (0.26)	7.33 (0.47)	< 0.001 *	45	0.17 (0.04)	0.26 (0.08)	0.298
<i>Eurytemora affinis</i>	39	4.79 (0.40)	4.39 (0.66)	0.579	26	0.12 (0.03)	0.10 (0.03)	0.674
<i>Labidocera madurae</i>	37	5.44 (0.36)	7.50 (0.41)	< 0.001 *	43	0.15 (0.04)	0.25 (0.06)	0.150
<i>Metridia pacifica</i>	18	2.57 (0.57)	4.39 (0.43)	0.017 *	13	0.09 (0.04)	0.25 (0.06)	0.038 *
<i>Neocalanus plumchrus</i>	17	2.61 (0.41)	4.11 (0.47)	0.032 *	15	0.03 (0.02)	0.12 (0.03)	0.039 *
<i>Temora longicornis</i>	46	5.40 (0.41)	6.84 (0.52)	0.025 *	40	0.10 (0.02)	0.24 (0.06)	0.046 *

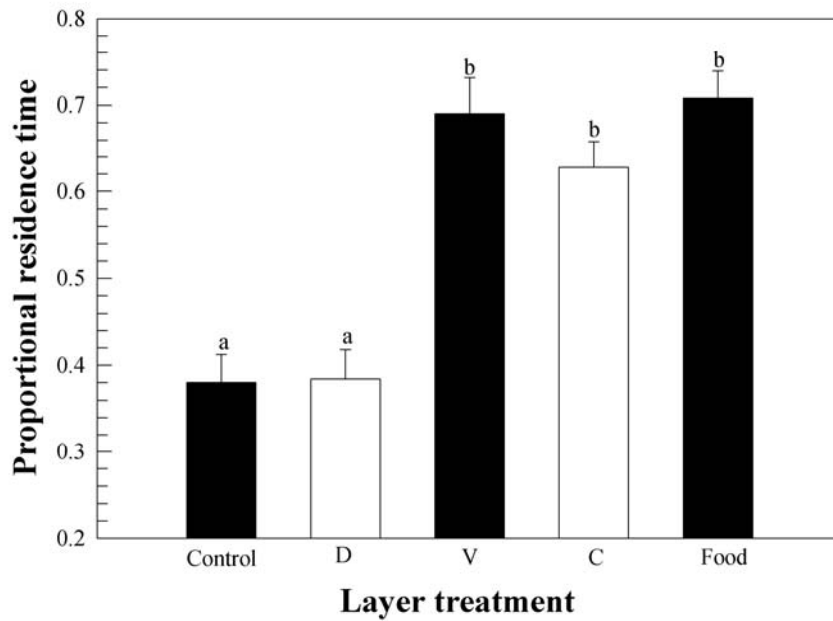


Figure 4.30 Proportional residence time in presence of individual cue layers for *Calanus finmarchicus*. Layer constituents are density (D), velocity (V), chemical exudates (C), and food. Different letters indicate significant differences between treatments via a post-hoc S-N-K test ($p < 0.05$).

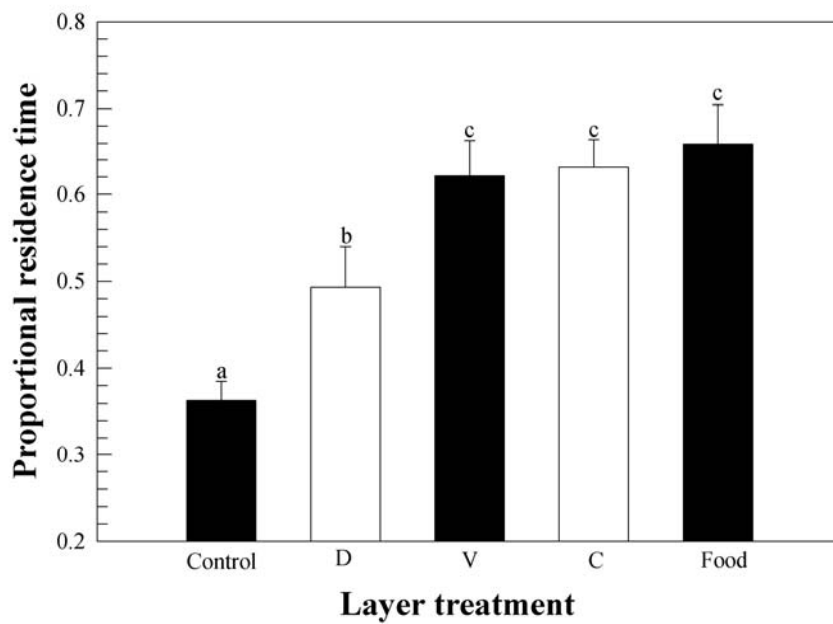


Figure 4.31 Proportional residence time in presence of individual cue layers for *Calanus pacificus*. Layer constituents are density (D), velocity (V), and chemical exudates (C), and food. Different letters indicate significant differences between treatments via a post-hoc S-N-K test ($p < 0.05$).

Threshold responses of the two *Calanus* spp. tested to shear strain rate ranged between 0.01 and 0.04 s⁻¹ based on Figure 4.32. However, *Calanus* spp. are large (>1 mm) and the antennal array much larger. Threshold responses in Fig. 4.32 are based on the centroid location of the organism. To estimate the threshold values corresponding to the antennal location, the mean size of the species was used to extrapolate along the body axis. The thresholds calculated in this manner were in a range between 0.02 and 0.06 s⁻¹. The threshold response for *C. finmarchicus* was the lower of the two species tested (between 0.02 and 0.03 s⁻¹). The behavioral threshold for *C. pacificus* was between 0.03 and 0.06 s⁻¹.

4.4.2 Responses to the density gradient layer

Responses to the density gradient layer varied for the two *Calanus* spp. *C. finmarchicus* show no change in proportional residence time to the density gradient layer (Fig. 4.30, difference = 0.004, $MSD_{0.05,99,5} = 0.096$). *C. pacificus*, however, did show a significant increase in proportional residence time compared to the control (Fig. 4.31, difference = 0.130, $MSD_{0.05,99,5} = 0.110$), and the result is statistically less than the response to the velocity gradient layer treatment (Fig. 4.31, difference = 0.128, $MSD_{0.05,99,5} = 0.110$).

Calanus finmarchicus did not increase swimming speed and turn frequency in response to the density gradient layer (Table 4.8). *C. pacificus* also did not show a significant increase in turn frequency in response to the density gradient layer. However,

Table 4.8 Species comparison of behavioral responses (swimming speed and turn frequency) to the density gradient layer treatment. * denotes significant differences ($p < 0.05$) between pre-contact and post-contact values by single-factor ANOVA.

Species	<i>n</i>	Swimming speed mm s ⁻¹ (std err)		<i>p</i>	<i>n</i>	Turn frequency turns ind ⁻¹ s ⁻¹ (std err)		<i>p</i>
		Pre-contact	Post-contact			Out of layer	In layer	
		<i>Acartia tonsa</i>	48			1.82 (0.07)	1.71 (0.06)	
<i>Calanus finmarchicus</i>	16	5.85 (0.45)	5.77 (0.48)	0.896	16	0.04 (0.02)	0.10 (0.03)	0.118
<i>Calanus finmarchicus</i> (nauplii)	18	4.60 (0.39)	4.66 (0.43)	0.560	18	0.12 (0.03)	0.15 (0.04)	0.496
<i>Calanus pacificus</i>	13	5.29 (0.51)	6.62 (0.66)	0.131	13	0.06 (0.02)	0.08 (0.03)	0.643
<i>Eurytemora affinis</i>	30	2.81 (0.20)	3.52 (0.21)	0.019 *	27	0.05 (0.01)	0.14 (0.04)	0.072
<i>Metridia pacifica</i>	20	4.70 (0.81)	4.76 (0.88)	0.960	15	0.14 (0.05)	0.13 (0.05)	0.856
<i>Neocalanus plumchrus</i>	16	2.77 (0.28)	2.91 (0.22)	0.699	17	0.06 (0.02)	0.08 (0.03)	0.723
<i>Temora longicornis</i>	48	5.37 (0.24)	5.36 (0.19)	0.990	40	0.14 (0.03)	0.13 (0.04)	0.817

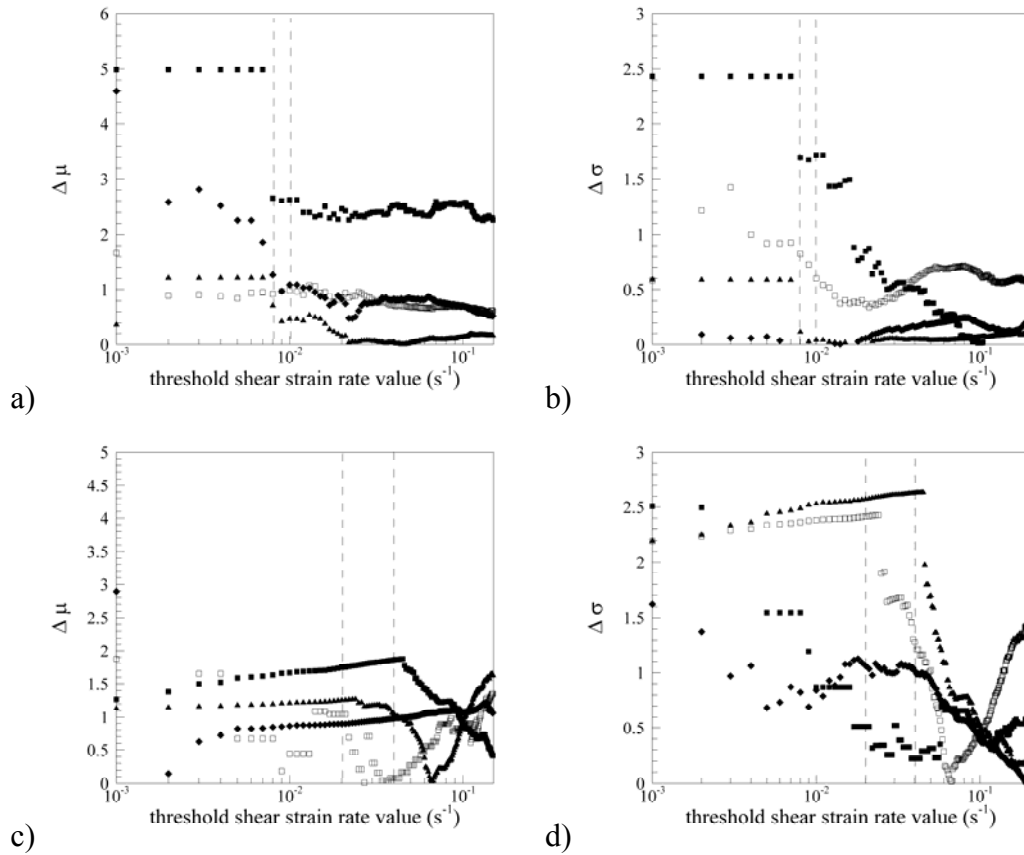


Figure 4.32 Threshold shear strain rate values for *Calanus* spp. in the velocity gradient layer treatment: (a,b) *C. finmarchicus*, (c,d) *C. pacificus*. Data from four sample paths are shown in each figure. (a,c) $\Delta\mu$ is the difference between the mean swim speed values calculated for data above and below a threshold. (b,d) $\Delta\sigma$ is the difference between the standard deviations for swim speed data above and below a threshold value. An abrupt change in $\Delta\mu$ or $\Delta\sigma$ indicates a behavior transition, and hence suggests the threshold value for behavioral response.

C. pacificus showed a strong trend towards an increase in swimming speed pre- and post-contact with the density layer (Table 4.8). Both species showed significant aversion to crossing the density gradient (Table 4.9).

4.4.3 Responses to the chemical/biological layers

Both species of *Calanus* significantly increased proportional residence time in the food layer (Fig. 4.30; *C. finmarchicus*, difference = 0.248, $MSD_{0.05,99,5} = 0.116$; Fig.4.30, *C. pacificus*, difference = 0.296, $MSD_{0.05,99,5} = 0.155$). Responses to the chemical exudates layer resulted in similar observations for both *Calanus* spp. as well (Fig.4.30, *C. finmarchicus*, difference = 0.248, $MSD_{0.05,99,5} = 0.127$; Fig.4.31, *C. pacificus*, difference = 0.269, $MSD_{0.05,99,5} = 0.145$). The isolated food, chemical exudates and velocity gradient layers yielded statistically similar proportional residence times for all species (Fig. 4.30, *C. finmarchicus*, max difference = 0.080, $MSD_{0.05,99,5} = 0.096$; Fig.4.31, *C. pacificus*, max difference = 0.038, $MSD_{0.05,99,5} = 0.096$).

In response to chemical exudates layers, both species significantly increased swimming speed and turn frequency (Table 4.10). Feeding responses during experiments with the food layer resulted in lower average swimming speed and slightly increased turn frequency after contact with the layer for both species (Table 4.11), congruent with observations of other species.

Table 4.9 Species comparison of behavioral responses (individuals crossing the gradient layer) to the density gradient layer treatment. * denotes significant differences ($p < 0.05$; two-tailed) between pre-contact and post-contact values by Fisher's exact test.

Species	<i>n</i>	Control (without density gradient)		Treatment (with density gradient)		<i>p</i>
		Cross	Do not cross	Cross	Do not cross	
<i>Acartia tonsa</i>	30	20	10	7	23	0.002 *
<i>Calanus finmarchicus</i>	20	14	6	6	14	0.026 *
<i>Calanus finmarchicus</i> (nauplii)	20	14	6	8	12	0.111
<i>Calanus pacificus</i>	20	11	9	4	16	0.048 *
<i>Eurytemora affinis</i>	40	22	18	20	20	0.823
<i>Metridia pacifica</i>	20	13	7	6	14	0.026 *
<i>Neocalanus plumchrus</i>	20	14	6	7	13	0.056
<i>Temora longicornis</i>	40	27	13	15	25	0.013 *

Table 4.10 Species comparison of behavioral responses (swimming speed and turn frequency) to the chemical exudate layer treatment at 200 $\mu\text{g C L}^{-1}$. * denotes significant differences ($p < 0.05$) between pre-contact and post-contact values by single-factor ANOVA.

Species	<i>n</i>	Swimming speed mm s^{-1} (std err)		<i>p</i>	<i>n</i>	Turn frequency $\text{turns ind}^{-1} \text{s}^{-1}$ (std err)		<i>p</i>
		Pre-contact	Post-contact			Out of layer	In layer	
<i>Acartia tonsa</i>	40	1.91 (0.18)	2.57 (0.14)	0.005 *	40	0.02 (0.02)	0.20 (0.04)	0.016 *
<i>Calanus finmarchicus</i>	16	2.58 (0.39)	4.19 (0.54)	0.024 *	13	0.02 (0.01)	0.09 (0.03)	0.039 *
<i>Calanus pacificus</i>	16	4.71 (0.61)	6.68 (0.76)	0.049 *	15	0.06 (0.02)	0.16 (0.03)	0.044 *
<i>Eurytemora affinis</i>	33	4.87 (0.20)	5.56 (0.33)	0.079	28	0.05 (0.02)	0.16 (0.04)	0.004 *
<i>Metridia pacifica</i>	15	2.25 (0.66)	4.40 (0.76)	0.046 *	15	0.06 (0.02)	0.15 (0.03)	0.028 *
<i>Temora longicornis</i>	40	2.41 (0.15)	3.72 (0.38)	0.001 *	40	0.11 (0.04)	0.23 (0.04)	0.048 *

Table 4.11 Species comparison of behavioral responses (swimming speed and turn frequency) to food layer treatment (e.g. phytoplankton, *Tetraselmis* spp.). * denotes significant differences ($p < 0.05$) between pre-contact and post-contact values by single-factor ANOVA.

Species	<i>n</i>	Swimming speed mm s ⁻¹ (std err)		<i>p</i>	<i>n</i>	Turn frequency turns ind ⁻¹ s ⁻¹ (std err)		<i>p</i>
		Pre-contact	Post-contact			Out of layer	In layer	
<i>Acartia tonsa</i>	42	2.85 (0.19)	1.97 (0.17)	0.001 *	40	0.06 (0.04)	0.10 (0.04)	0.493
<i>Calanus finmarchicus</i>	12	5.60 (0.61)	4.28 (0.57)	0.129	13	0.08 (0.04)	0.16 (0.03)	0.131
<i>Calanus pacificus</i>	15	5.70 (0.49)	4.41 (0.59)	0.112	15	0.05 (0.02)	0.11 (0.03)	0.108
<i>Eurytemora affinis</i>	33	3.89 (0.18)	2.97 (0.26)	0.005 *	24	0.07 (0.02)	0.13 (0.04)	0.206
<i>Temora longicornis</i>	42	3.57 (0.32)	2.71 (0.17)	0.034 *	40	0.11 (0.04)	0.16 (0.03)	0.267

4.4.5 Nauplii of *Calanus finmarchicus*

Calanus finmarchicus nauplii (NIII-NIV) did not actively respond to the physical gradient layers (Fig. 4.33). For both the velocity and density gradients layers, proportional residence time did not increase (single-factor ANOVA). Also swimming speed and turn frequency did not increase when comparing pre-contact and post-contact with the layer (Table 4.7 through 4.9). These results suggest that responses to physical structure in the ocean develop in adult or copepodid stages for *C. finmarchicus*.

4.5 Survey of species responses

A survey of copepod responses to isolated gradients was conducted for additional species. These include *Candacia ethiopica* (from Conch Reef, FL), *Eurytemora affinis* (from Boothbay Harbor, ME), and *Labidocera madurae* (from Conch Reef, FL), *Metridia pacifica* (from the Gulf of Alaska), and *Neocalanus plumchrus* (from the Gulf of Alaska). Results of these experiments are presented below for each isolated layer.

4.5.1 Responses to the velocity gradient layer

Eurytemora affinis showed significant differences in proportional residence time between all treatments via single-factor ANOVA (Fig. 4.34; $df = 249$; $F = 21.23$; $p < 0.001$). However, in contrast to the responses of all other tested copepod species, *E. affinis* did not show increased proportional residence time in response to the velocity gradient layer (difference = 0.034; $MSD_{0.05,60,5} = 0.064$). Hence, *E. affinis* did

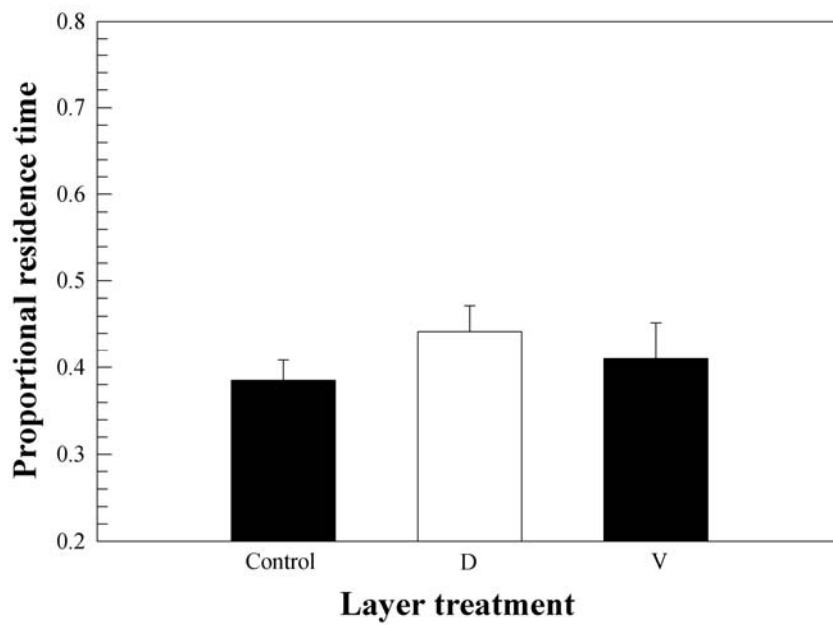


Figure 4.33 Proportional residence time in presence of individual cue layers for *Calanus finmarchicus* nauplii (NIII-NIV). Layer constituents are density (D) and velocity (V). No significant differences occurred between treatments via ANOVA.

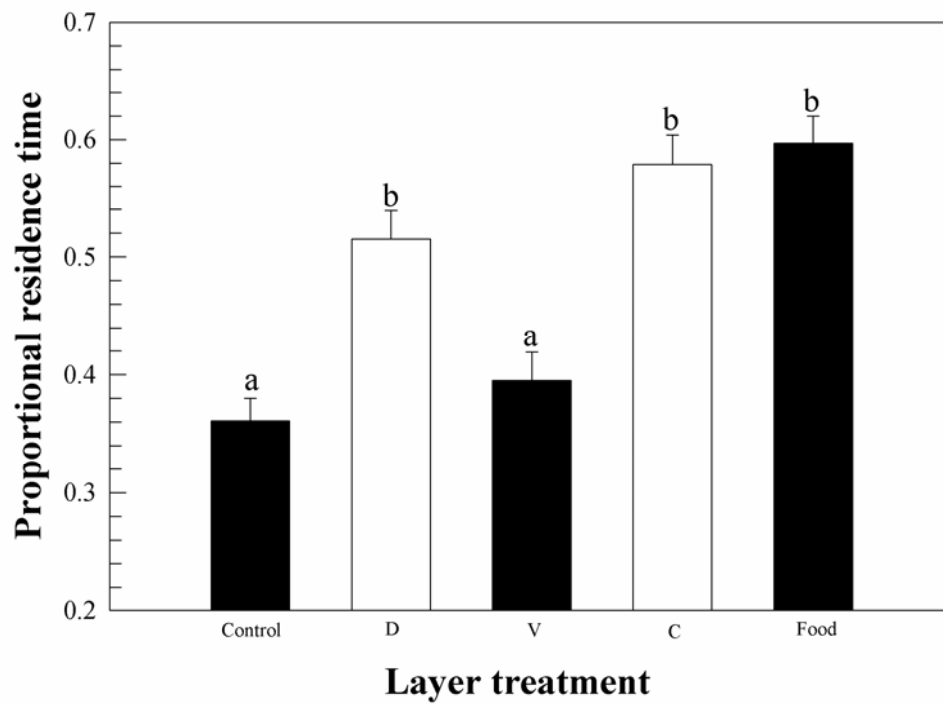


Figure 4.34 Proportional residence time in presence of individual cue layers for *Eurytemora affinis*. Layer constituents are density (D), velocity (V), chemical exudates (C), and food. Different letters indicate significant differences ($p < 0.05$) between treatments via S-N-K post-hoc test.

not appear to respond to the velocity gradient by exhibiting an area-restricted search behavior, since neither swimming speed nor turn frequency increased (Table 4.7).

Metridia pacifica and *Neocalanus plumchrus* responded to the velocity gradient layer in a fashion similar to other species. Proportional residence time in the velocity gradient layer was significantly different than control for both *M. pacifica* and *N. plumchrus* (Fig. 4.35 and 4.36; *M. pacifica*, difference = 0.229; $MSD_{0.05,60,5} = 0.121$; *N. plumchrus*, difference = 0.264; $MSD_{0.05,60,5} = 0.153$). Post-contact swimming speed and turn frequency were significantly increased compared to pre-contact values for both species (Table 4.7). Threshold responses to shear strain rate are similar for both *M. pacifica* and *N. plumchrus* (Fig. 4.37).

The data for responses to hydromechanical stimuli associated with thin layers suggest that these cues are also important in foraging for the larger omnivorous/predatory species, *Candacia ethiopica* and *Labidocera madurae*. Figure 4.38 shows the proportional residence time for *Candacia ethiopica* (live and recently dead specimens), *Eurytemora affinis*, *Labidocera madurae*, *Metridia pacifica*, and *Neocalanus plumchrus* in the velocity gradient layer along with the results for the species presented in previous Sections. All species except *E. affinis* spend more time in the isolated velocity gradient layer when compared to the same region with no strain rate field (*C. ethiopica*, $df = 79$, $F = 4.67$, $p = 0.034$; *L. madurae*, $df = 59$, $F = 22.04$, $p < 0.001$; other statistics reported previously) when compared to the same region with no strain rate field. *C.*

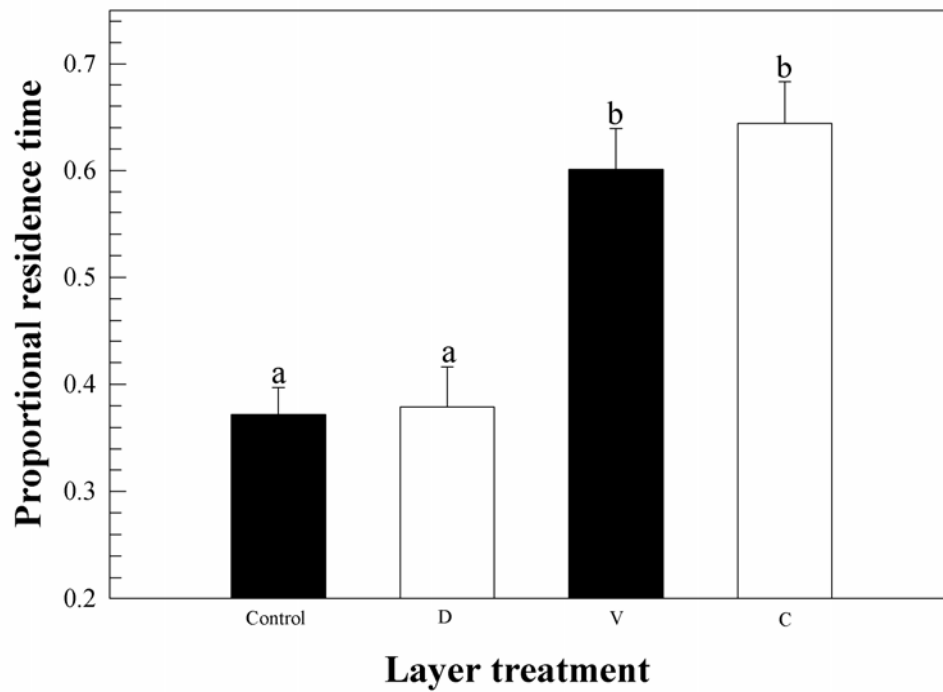


Figure 4.35 Proportional residence time in presence of individual cue layers for *Metridia pacifica*. Layer constituents are density (D), velocity (V), and chemical exudates (C). Different letters indicate significant differences ($p < 0.05$) between treatments via S-N-K post-hoc test.

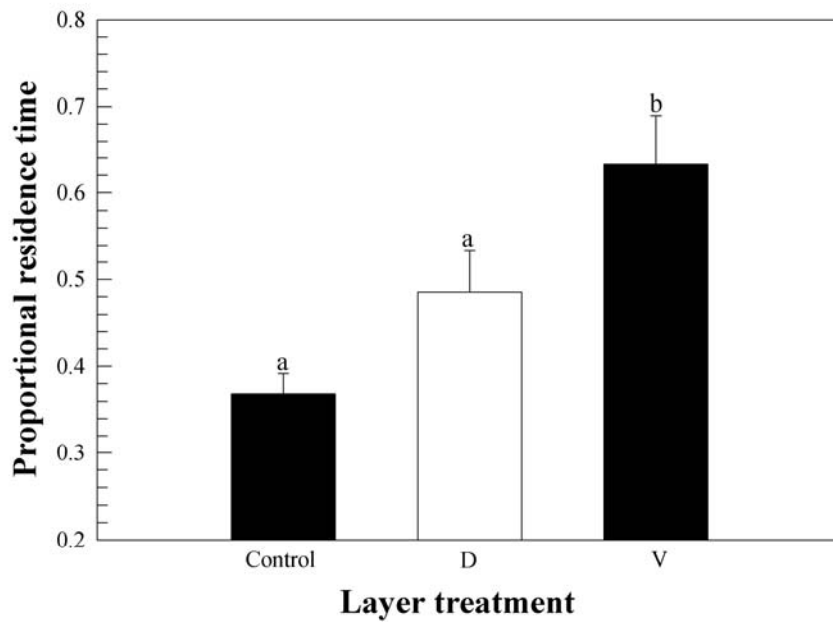


Figure 4.36 Proportional residence time in presence of individual cue layers for *Neocalanus plumchrus*. Layer constituents are density (D) and velocity (V). Different letters indicate significant differences between treatments via a post-hoc S-N-K test ($p < 0.05$).

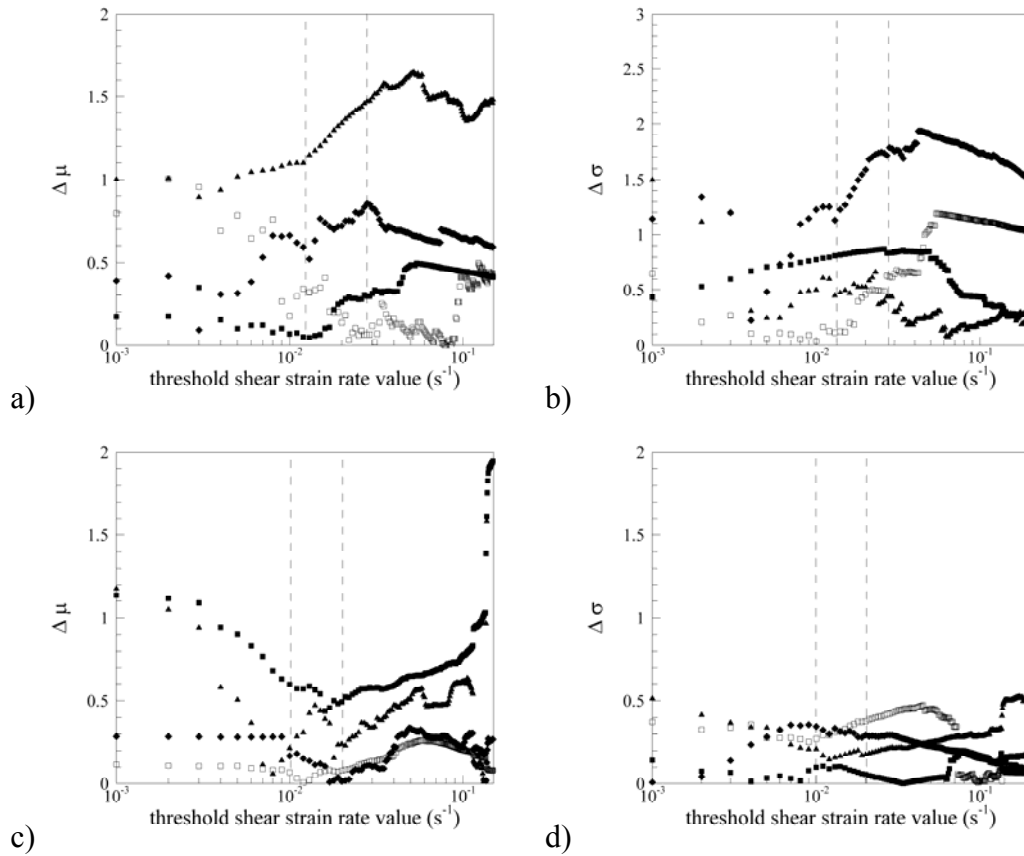


Figure 4.37 Threshold values of shear strain rate for various species in a velocity gradient layer for (a,b) *Metridia pacifica* and (c,d) *Neocalanus plumchrus*. Data from four sample paths are shown in each figure. (a,c) $\Delta\mu$ is the difference between the mean swim speed values calculated for data above and below a threshold. (b,d) $\Delta\sigma$ is the difference between the standard deviations for swim speed data above and below a threshold value. An abrupt change in $\Delta\mu$ or $\Delta\sigma$ indicates a behavior transition, and hence suggests the threshold value for behavioral response.

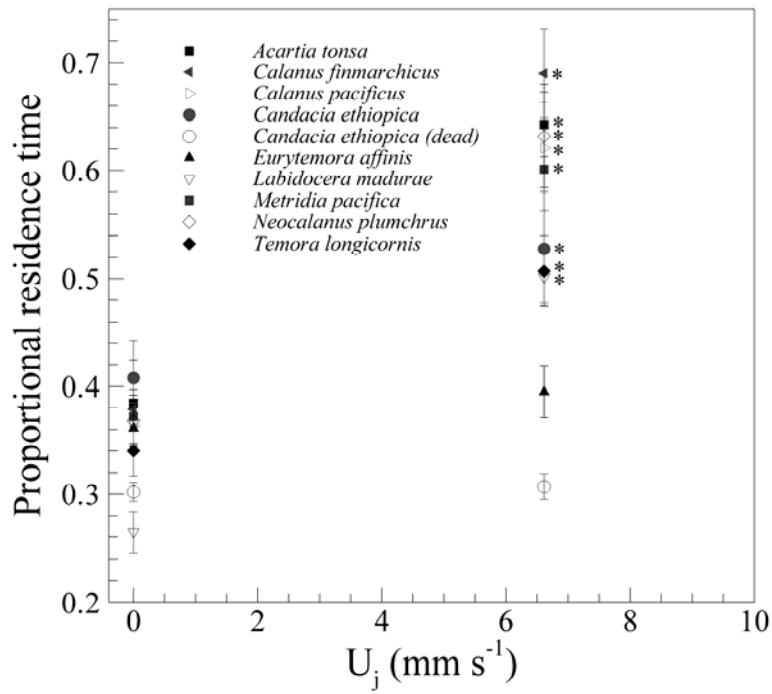


Figure 4.38 Proportional residence time in the velocity gradient treatment ($U_j = 6.7$ mms^{-1}). The controls corresponds to no flow ($U_j = 0$ mms^{-1}). * indicates significant difference between treatment and control ($p < 0.05$).

ethiopica and *L. madurae* also increased swimming speed and turn frequency within the layer (Table 4.7) in the same fashion as other species.

Threshold responses to shear strain rate by *Candacia ethiopica* and *Labidocera madurae* were in a similar range to the thresholds of other species tested (Fig. 4.39). *C. ethiopica* response thresholds were between 0.008 and 0.02 s⁻¹ in Fig. 4.39. However, body size considerations altered this threshold range to 0.02 to 0.04 s⁻¹ to account for the spatial difference between the centroid and the antennae. After body size corrections, the shear strain rate threshold range for *L. madurae* was 0.04 to 0.07 s⁻¹ (compared to 0.02 and 0.05 s⁻¹ shown in Fig. 4.39).

4.5.2 Responses to the density gradient layer

Only *Eurytemora affinis* increased proportional residence time in response to the density gradient layer (Figs. 4.34 and 4.40). The response of other species to the density gradient layer was attributed to an aversion to crossing into a body of water of differing salinity (see previous Sections). For the euryhaline copepod *E. affinis*, however, the response to the density gradient layer was much stronger than the response observed for other species (Fig. 4.34, difference = 0.119; $MSD_{0.05,60,5} = 0.064$). The behaviors exhibited by *E. affinis* in response to the density gradient layer were consistent with excited area-restricted search behavior and included increased swimming speed and turn frequency (Table 4.8). *E. affinis* also did not display an aversion to crossing the density gradient as all other species did (Table 4.9).

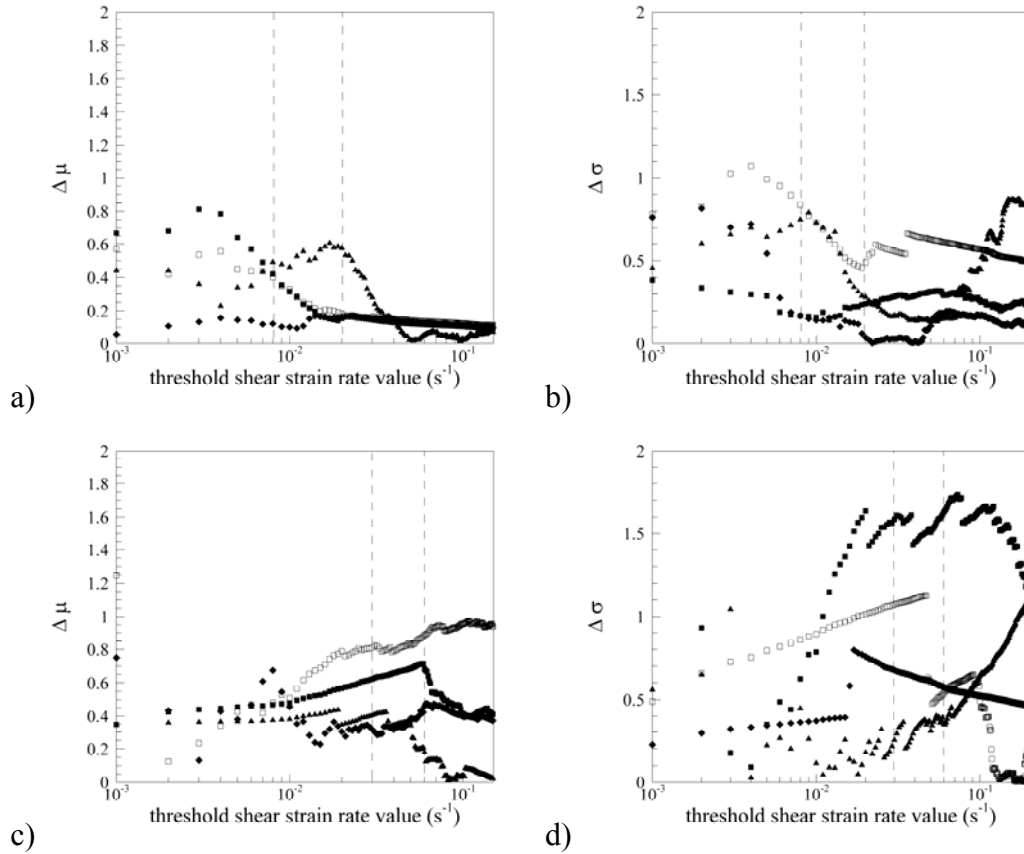


Figure 4.39 Threshold values of shear strain rate for various species in a velocity gradient layer for (a,b) *Candacia ethiopica* and (c,d) *Labidocera madurae*. Data from four sample paths are shown in each figure. (a,c) $\Delta\mu$ is the difference between the mean swim speed values calculated for data above and below a threshold. (b,d) $\Delta\sigma$ is the difference between the standard deviations for swim speed data above and below a threshold value. An abrupt change in $\Delta\mu$ or $\Delta\sigma$ indicates a behavior transition, and hence suggests the threshold value for behavioral response.

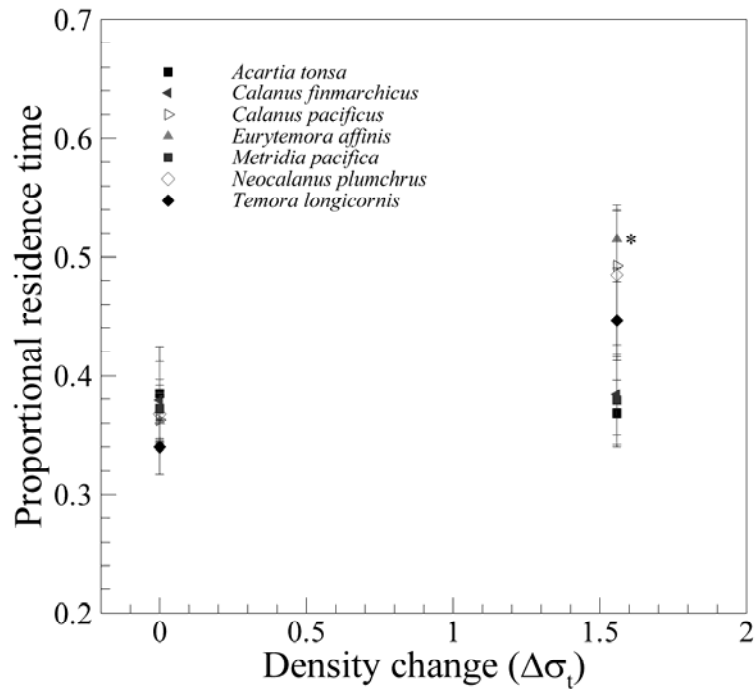


Figure 4.40 Proportional residence time in the density gradient treatment. The control corresponds to constant salinity (32 ppt). Treatments contain a layer consisting of a 2 ppt salinity change ($\Delta\sigma_t = 1.8$). * indicates significant difference between treatment and control ($p < 0.05$).

Metridia pacifica and *Neocalanus plumchrus* did not alter proportional residence time in response to the density gradient layer (Fig. 4.35 and 4.36; *M. pacifica*, difference = 0.008; $MSD_{0.05,60,5} = 0.100$; *N. plumchrus*, difference = 0.127; $MSD_{0.05,60,5} = 0.153$). Swimming speed and turn frequency were not significantly different either (Table 4.8). Both *M. pacifica* and *N. plumchrus* showed statistical aversions to crossing the density gradient (Table 4.9).

4.4.3 Responses to the chemical layer

All species tested exhibited similar responses to the chemical (phytoplankton exudates) layer treatment. Proportional residence times for *E. affinis* and *Metridia pacifica* increased significantly for the chemical exudate layer (Fig. 4.34, *E. affinis*, difference = 0.183 $MSD_{0.05,60,5} = 0.077$; Fig. 4.5, *M. pacifica*, difference = 0.273 $MSD_{0.05,60,5} = 0.133$). Data for other species previously presented and summarized in Fig. 4.41. The responses to the chemical exudate layer included increased swimming speed, and turn frequency (Table 4.10; reported previously for *A. tonsa*, *Calanus* spp., *E. affinis*, and *T. longicornis*), which enabled individuals to remain in the layer. The responses are similar to previous observations for *Acartia clausi*, *Acartia hudsonica*, and *Eurytemora affinis* in the presence of amino acids (Poulet and Marsot 1978; Poulet and Ouellet 1982).

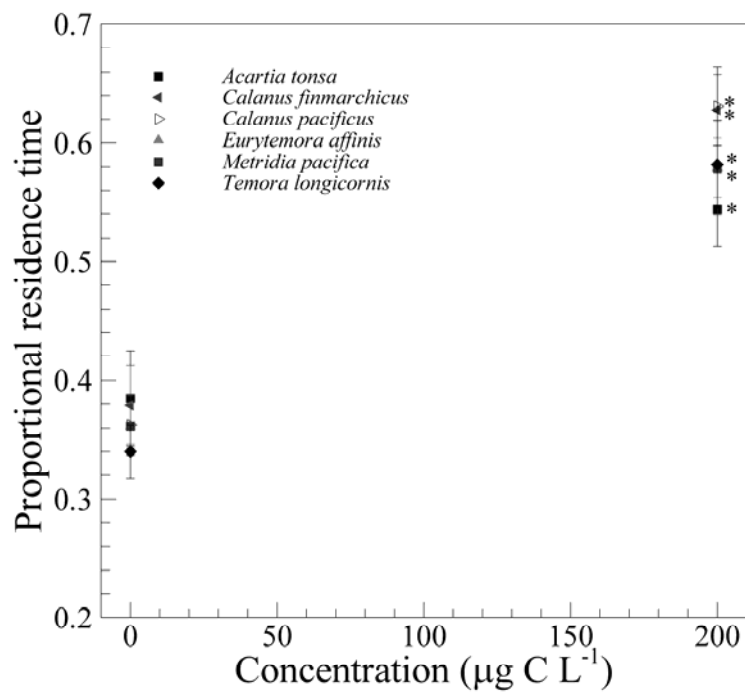


Figure 4.41 Proportional residence time in the phytoplankton chemical exudate (*Tetraselmis* spp.) layer treatment. Concentration is based on equivalent biomass of phytoplankton in $\mu\text{g C L}^{-1}$. The control corresponds to the absence of exudate ($0 \mu\text{g C L}^{-1}$). * indicates significant difference between treatment and control ($p < 0.05$).

4.4.3 Responses to food layers

The combination of food particles and chemical exudates elicited feeding responses in all species tested. The proportional residence time for *E. affinis* increased significantly for the food layer treatment (Fig. 4.34, difference = 0.201, $MSD_{0.05,60,5} = 0.085$). The proportional residence time for all species tested with the food layer are summarized in Fig. 4.42, with a significant increase in each case. The act of feeding leads to reduced overall swimming speed and no change in turn frequency (Table 4.11; reported previously for *A. tonsa*, *Calanus* spp., *E. affinis*, and *T. longicornis*). This feeding behavior is similar to previous observations by Tiselius (1992) and Poulet and Marsot (1978).

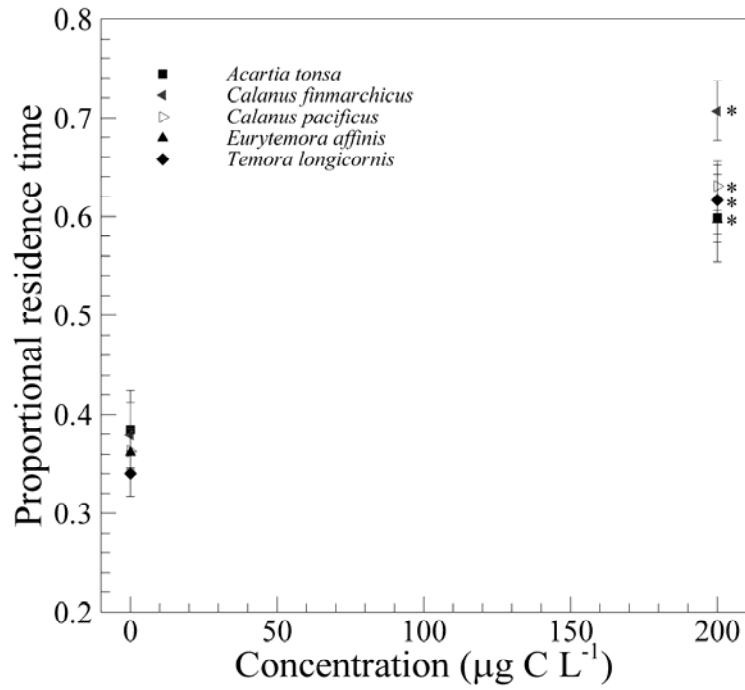


Figure 4.42 Proportional residence time in the food (*Tetraselmis* spp.) layer treatment. The control corresponds to the absence of food (0 µg C L⁻¹). * indicates significant difference between treatment and control ($p < 0.05$).

Chapter 5 Discussion

Copepods are known to aggregate at locations of environmental gradients (e.g., light, flow velocity, fluid density, chemical concentration, biological activity) in the water column (e.g. Emery, 1968; Hamner and Carlton, 1979; Ueda et al., 1983; Alldredge et al., 1984; Wishner et al., 1988; Cowles et al., 1998; Holliday et al., 1998; Deksheniaks et al., 2001), and to maintain position in regions of high food concentration (Tiselius, 1992). In order to alter behavior and maintain position in these regions, copepods must be able to sense and react to the properties associated with these patches. Cowles et al. (1998) and Deksheniaks et al. (2001) reported the important characteristics of oceanic structure as fine-scale gradients in velocity, fluid density, biological activity, and chemical concentration. Gallagher et al. (2004) observed *in situ* copepod aggregations associated with physical structure in the ocean and suggested behavioral mechanisms for these occurrences.

Aggregations of zooplankton near sharp gradients in physical properties, such as flow velocity and density, and biological activity (primary production) are hypothesized to result from interplay between physical forcing and individual behavior (Franks, 1995; Alldredge et al., 2002). Recent evidence suggests that for larger members of the plankton community, individual behavior may play a more important role than previously accepted (Leising and Franks, 2000; Leising, 2001; Gallagher et al., 2004). The exact species composition of these aggregations is not known in many of these studies; however, it is believed that thin layers and similar oceanographic structures are common in many regions. Therefore, if fine-scale patchiness in the plankton is an important feature of

these habitats, some species of zooplankton may have adapted behavioral responses to these features that limit search areas, increase foraging or mating success, and ultimately improve individual fitness.

5.1 Scales, interactions, aggregations

Temporal and spatial scales in the field are often hard to match in the laboratory. In this study, the gradient layer was approximately 4 cm thick, with shear strain rates ranging between zero and 0.5 s^{-1} , density jumps between 0 and $3.7 \sigma_t$ units, and chemical exudate or food concentrations between 0 and 200 mg C m^{-3} (equivalent to $\mu\text{g C L}^{-1}$). The thickness of the layer is below reported minimum thicknesses (10 cm) from the field; however, field estimates are still limited by resolution (Cowles, 2004). Thinner layers, higher shear strain rates, and steeper density gradients than have been reported to date may be present in the ocean. For the current behavioral response study, the important length scale is that of an individual copepod (i.e. roughly 1 mm). The laboratory layer was very large (roughly 4 cm) compared to the copepod, so individuals cannot sense the upper and lower edges of the layer simultaneously. Therefore, from the perspective of the copepod, the fluid deformation (quantified by the shear strain rate) is similar in our model layer to that in an oceanic thin layer. This study observed immediate responses of individuals that could lead to observed aggregations at the population level, and suggests that measurements in the open ocean may need to be performed at a higher-resolution in order to characterize features relevant to actively behaving zooplankton.

The species examined in this study exhibited behaviors congruent with area-restricted search behavior in response to velocity gradients and chemical layers (Buskey, 1984; Turchin, 1991; Mauchline, 1998). Increased swimming speed, variation in speed, and turn frequency within the layer suggest that these animals were excited by the presence of the velocity gradient in a positive fashion and were attempting to remain in the layer. Velocity gradients may act as an initial cue to the presence of a new water body, thus instigating an area-restricted search. Copepods eventually cease local searching and continue 'random-directed' movement if no further cue was present (i.e. food presence or chemical component). If food or chemical stimuli are associated with changes in flow velocity, then velocity gradients would act as a cue to initiate aggregative or swarming behavior in these regions, thus increasing search success by limiting active searching areas. The presence of a resource such as food would negate the area-restricted search response and cue feeding behavior resulting in lower average swimming speed as observed in the current study and by Tiselius (1992).

Responses to the density gradient layer were strikingly different than responses to velocity gradients. *A. tonsa* did not increase proportional residence time in the density gradient layer experiments (0.37 versus 0.39 for the control). Even though *T. longicornis* did significantly increase proportional residence time in the density gradient layer (0.45) compared to that for the control (0.34), other behavioral markers were not significantly different. Evaluation of the paths showed that individuals of both species made contact with the density gradient and then either swam along the gradient layer, or turned and

swam away. This was a significant behavioral change created by the density gradient and similar to a copepod swimming near the water surface or bottom of the tank. Hence, sharp density gradients may act as barriers to vertical migration for copepods thus resulting in aggregations at these boundaries due to a physical restriction or a behavioral change. These observations are consistent with hypotheses and arguments posed by Harder (1968) and more recently Gallagher et al. (2004). In contrast, *Eurytemora affinis* responded to the density gradient layer with an excited area-restricted search response indicated by increased swimming speed and turn frequency (discussed further in Section 5.3).

These results illustrate that gradients in properties of oceanic water bodies, current velocity, fluid density, chemical exudates, and biological activity appear to have differing effects on individual copepods. Physical gradients can act as a positive cue for area-restricted search behavior that can lead to aggregation over larger time scales (Hamner, 1988; Turchin, 1991; Tiselius, 1992; Leising and Franks, 2000) or as barriers to vertical migration, which may also lead to aggregation (Tiselius, 1992; Lougee et al 2002; Bochdanksy and Bollens, 2004; Clay et al., 2004). Chemical exudates act to cue an excited area-restricted search response, while food presence (biological activity) elicits a feeding response. Results herein show that copepods utilize gradients in various oceanographic properties to conduct area-restricted searches for resources. In order for such a strategy to work efficiently, however, another level of organization must be present. In the next section, strategies that enhance foraging at intermediate scales are discussed in the context of the observed responses.

5.2 Cue hierarchy and associations

Responses to combinations of velocity, density, and chemical exudates revealed a relative hierarchy that can lead to improved fitness (Figs. 5.1 and 5.2). Velocity gradients appear to act as an initial cue that a new water body has been entered. Gradients in flow velocity are expected to be coherent, available cues that may heighten behavioral sensitivity to more accurate cues such as chemical exudates from prey or conspecifics. Because gradients in flow velocity are relatively common features in a water column, and often are associated with the motions of different water bodies, these features provide a boundary for area restricted search behavior for copepods or other zooplankton in analogy with the recognition of a meadow or glade in a forest would cue searching by a wolf looking for rabbit prey. This analogy is further supported by a significant difference in proportional residence time between the isolated velocity cue and the combined velocity-chemical exudate layer as well as a significant interaction between the two factors. Similar differences are not seen when comparing the chemical exudate layer to the combined velocity-chemical layer, suggesting that the response in this situation is dominated by the presence of the chemical component. For all combined experiments, density gradients continue to act as a boundary, and thus may indirectly aid the individual in remaining within a region of interest and possibly improving search efficiency.

The utilization of cue hierarchies by many species is a common mechanism for consecutively narrowing search regions, but has not been previously established in the

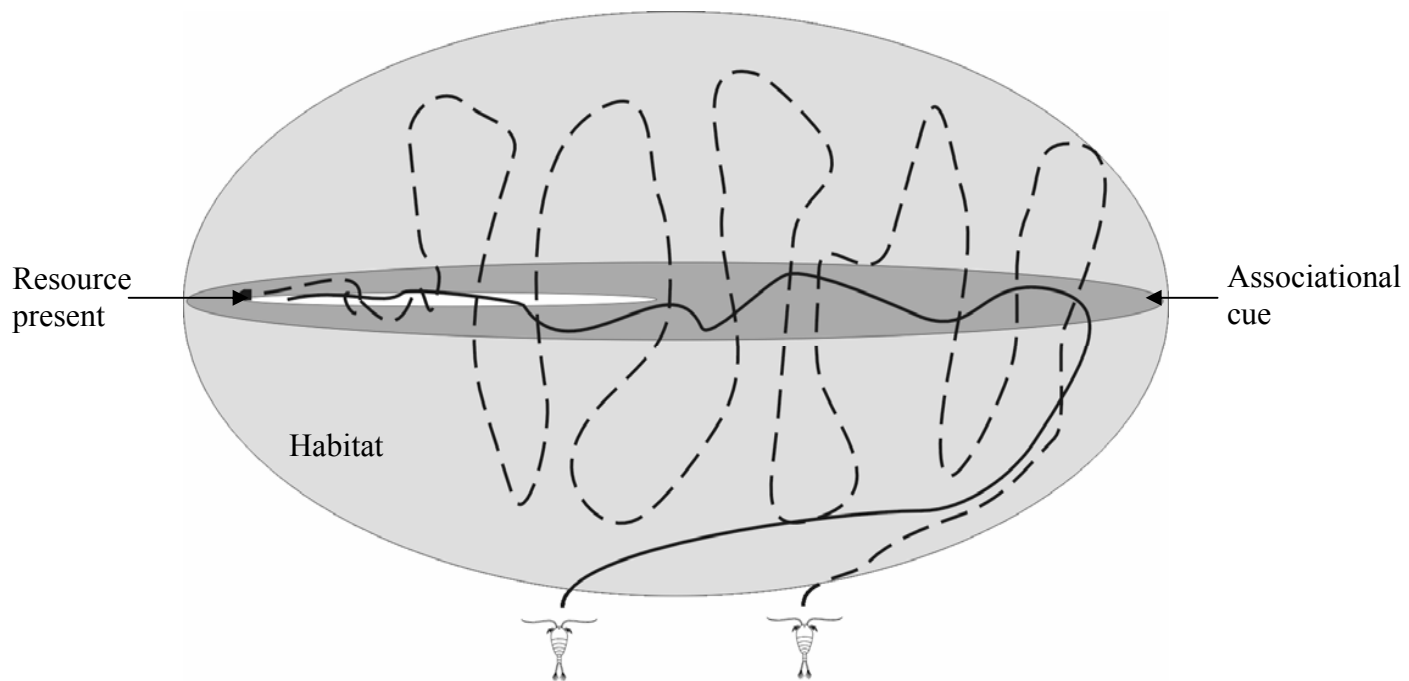


Figure 5.1 Use of associational cues during foraging by copepods. The individual on the left utilizes cue hierarchy to narrow search region, thus finding resources faster and with better success than the individual on the right, who does not use associational cues. The large light gray oval represents a hypothetical habitat region. The darker oval is the portion of the habitat containing an associational cue such as a velocity or a density gradient. The small white oval is the portion of the habitat containing an associated resource (food, mates, etc.).

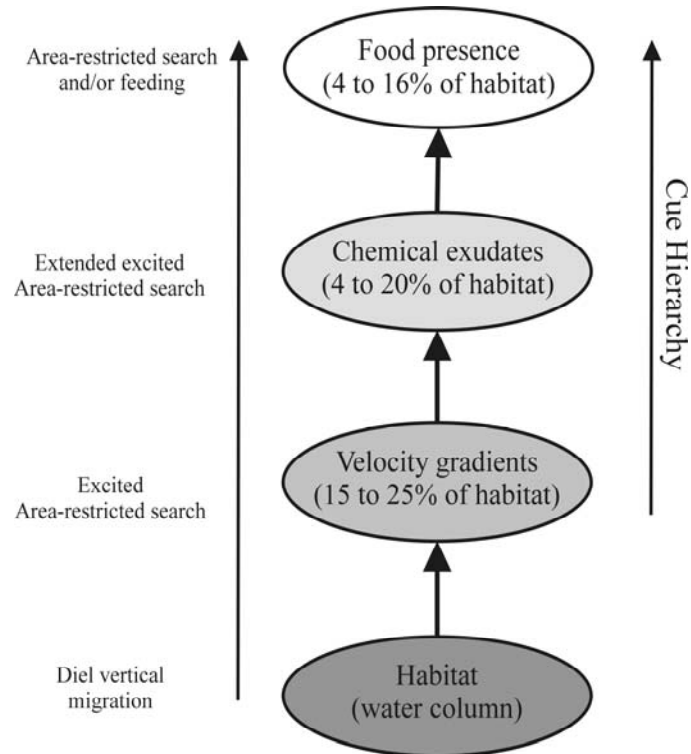


Figure 5.2 Cue hierarchy for copepod foraging based on experimental results. Percentages of the habitat covered by the cues are estimated based on published *in situ* observations (Holliday et al. 1998; Dekshenieks et al. 2001; McManus et al. 2003; Cowles 2004).

Copepoda. Figure 5.1 shows an idealized example of how the use of associational cues improves search success and reduces searching times. As long as a reliable cue (dark grey oval) exists as a smaller portion of the total habitat, some benefit is likely to be gained from narrowing searches to these regions. For example, many insects utilize varying visual, chemical, and physical cues to progressively focus search regions until a host plant or mate is found (Tumlinson et al., 1993). Long range perception being dominated by visual cues, or chemical volatiles from associated plants, followed by scents of fruiting bodies once near to a potential host site, and ultimately dominated by host-specific cues (Vinson et al., 1987; Tumlinson et al., 1993). Recent field observations of thin layers and other fine-scale oceanographic structure suggest that associations between flow velocity gradients, density changes, and biological activity may provide zooplankton with spatial and temporal information that profoundly affect foraging behavior and success. The results of this study support these hypotheses, with a cue hierarchy that begins with gradients in flow velocity and/or density, continuing to waterborne chemical exudates, and culminating in a feeding behavior in response to cell contact or perception of more specific chemical cues. Results of Poulet and Marsot (1978) suggest that for actual feeding to occur, a combination of waterborne or contact chemicals and food particles must be present. These results support these findings and further suggest that a combination of waterborne chemicals and mechanical contact are responsible for feeding behavior, while contact chemicals induce ingestion. These results provide support for optimal foraging theory with respect to both diet and patchiness (MacArthur and Pianka, 1966); however, indirect effects on individuals and populations are still not well understood.

Previous studies concerning fitness of individual copepods in patchy, compared to homogenous environments have not shown significant effects (Tiselius, 1992; Saiz et al., 1993; Bochdanksy and Bollens, 2004). However, the current model (Fig. 5.1) suggests that these experiments may not capture appropriate scales relevant to possible fitness gain. In a hypothetical 25 meter upper ocean water column, >75% of the phytoplankton biomass can be concentrated into one or a few meter thick thin layers (Holliday et al., 1998). Phytoplankton concentration is adequate to support zooplankton populations in approximately 4 to 16% of the habitat (i.e. 1 to 4 meters of a 25 m water column) in regions with thin layers. Discernable velocity gradients occur at up to three to five locations every 10 meters with each covering approximately a half meter (Cowles, 2004). Therefore, the percentage of habitat with a velocity layer is roughly 15 to 25% (1.5 to 2.5 meters over 10 m of the water column). An individual searching for food that narrows search regions using other gradients (velocity or density) raises the percentage of searched area with food by as much as 15 to 70%, and improves foraging efficiency simply by increasing the probability of food encounter. This suggests that experiments that adequately assess the importance of patchiness must be at scales that mimic search regions in the field.

The lack of a foraging/search response to density gradients by most species tested suggests that changes in salinity and temperature may not be as available or detectable as strain rate counterparts. *A. tonsa* and *T. longicornis* appear to employ flow velocity as the primary initial cue for initiating area-restricted search behavior because velocity

gradients and food are often in close proximity in the field. However, in the absence of a velocity gradient, *T. longicornis* still aggregates (Harder, 1968). This, however, appears to be a result of not crossing the gradient, and therefore accumulation occurs. Other species of zooplankton may operate in a functionally different manner, possibly because the flow velocity gradient cannot be sensed due to size limitations, and in that case density gradients may provide better, more reliable information (e.g. rotifers, *Brachionus plicatilis*; Lougee et al., 2002; Ignoffo et al. 2005). Direct individual assessments have not been made, however, and these accumulations may be a result of the behaviors similar to those discussed above for *A. tonsa* and *T. longicornis*.

The resulting threshold curves (Figs. 4.19 and 4.28) indicate that copepods may be utilizing chemical exudates concentration along with cell contact as proxy cues to continue searching for higher resource patches, insuring that an individual does not spend too much time in a single resource patch. This mechanism, originally proposed by Tinbergen et al. (1967), is fundamentally important to the fitness of an organism, especially copepods (Leising and Franks, 2002). By employing a threshold model, copepods, if a resource is located, can quickly determine whether or not to remain in the current resource layer or continue searching for 'better' patches. For *A. tonsa* and *T. longicornis*, this threshold value falls in the range reported for biological peaks (Cowles, 2004), and suggests that these animals do not continue to stay in a layer unless the concentration is near observed biological peaks ($\sim 200 \mu\text{g C L}^{-1}$). The different thresholds observed between species may simply be an artifact of starvation level, but also may

illustrate differences in swimming speed, behavior, or zooplankton-phytoplankton dynamics, all of which have yet to be tested.

Leising and Franks (2002) proposed a classic area-restricted search strategy (Tinbergen et al., 1967) for *Acartia clausi* as a means of dealing with resource patchiness at small spatial and temporal scales (centimeters and minutes). By slowing down, an individual can adequately remain within a patch for time periods sufficient to fill a gut. On larger and longer scales (i.e. meters and days), behaviors, such as diel vertical migration, increase the probability of encountering high resource patches throughout the water column range of the organism. Leising and Franks (2002) suggested that a disparity between these scales exists, and that organisms may utilize a different strategy at intermediate scales. Results of the current study show that at intermediate scales (centimeters and minutes), cue hierarchies allow organisms to focus search regions. Importantly, the behaviors at the intermediate scales are those most aligned with the temporal and spatial scales of fine-scale oceanographic structure (McManus et al., 2003; Cowles, 2004).

5.3 Variability and the ecological niche

Not all organisms tested responded in similar fashions to all gradients. *E. affinis* (Temoriidae) did not exhibit area-restricted search behavior in response to gradients in flow velocity, unlike the sympatric species *T. longicornis* (Temoriidae). The sensory appendages of *E. affinis* and *T. longicornis* are very similar, although *T. longicornis* is

larger and thus has a longer sensory array. Nevertheless, it is not apparent whether the lack of response by *E. affinis* is a result of a physiological limitation, or a behavioral difference. Arguments could be made that physiological strain rate limits in *E. affinis* should be much lower than the strain rates in this study (and *in situ*), suggesting the latter as the reason for observed species differences. Support for a behavioral difference is provided by the fact that the smaller *A. tonsa* actively responds to the velocity gradient layer. Although not in the same genus, *A. tonsa* has a similar mechanosensory array and smaller sensory span. Based on these results, *E. affinis* should be able to sense the gradient, and therefore, the lack or difference in response can be attributed to behavior.

These results suggest one solution to Hutchinson's "Paradox of the Plankton" (1961) as a sensory utilization niche. Differences in responses between species suggest that niche partitioning may be occurring in the plankton and provides a basis for speciation. This is more evident when observing differential behavior between closely related, sympatric (co-occurring, no interbreeding) species such as *Eurytemora affinis* and *Temora longicornis*. Different species of sympatric copepods may have developed due to fine-scale use of different fundamental oceanographic properties. Such a difference might affect the temporal scales at which these organisms forage. However, these differences may simply be due to variations in preferred habitat. For instance, *E. affinis* is an extremely euryhaline copepod, often residing in brackish waters near regions of high freshwater input (Lee, 2000); therefore, velocity gradients in these habitats may not be as associated with resources as observed in outer coastal habitats.

5.4 Modeling and simulation

Aggregations of zooplankton at thin layers are hypothesized to result from individual foraging response to cues such as strain rate, density gradients, or spikes in biological activity (presence of biological and/or chemical constituents). Laboratory results presented in this Thesis show that, for example, the proportional residence time in the velocity gradient layer for *Acartia tonsa* is 0.64 compared to 0.39 with no structure present ($p < 0.001$). However, these data correspond to a layer with a thickness of a few centimeters and a time scale of a couple of hours. The objective of this section is to expand these results to ecologically-relevant scales and hence show that behavioral responses can lead to larger-scale patterns of abundance such as those assumptions of aggregation developed from Hamner (1988) and Leising (2001).

An individual-based model was used to simulate results of small-scale laboratory experiments (cm and hours) and expand the behavior patterns to appropriate temporal and spatial scales. The model was run over larger spatial and temporal scales, which are relevant to open ocean communities (meters and days). For this discussion, only *A. tonsa* and *T. longicornis* responses to the velocity gradient layer are used to link small-scale behavior to large-scale pattern. Although the model does not distinguish the type of cue, responses to other gradients and layers will be qualitatively similar.

5.4.1 Model description and assumptions

The model space is defined by a two-dimensional field of view (Fig. 5.3). The field of view is defined by a Lagrangian 1024-unit coordinate system (i.e. 1024×1024). Model organism positions are defined by an x - and y -value within the constraints of the field of view. Due to the relatively two-dimensional nature of the open ocean habitat this is a reasonable definition of the model space. Initially, model organisms are placed randomly in the field of view to achieve target concentrations based on field estimates. Fig. 5.3 shows an example starting distribution. In order to calculate the organism concentration for the simulation, the model habitat is conceptualized as a cubic volume. Thus, the two-dimensional simulation corresponds to a projection of the three-dimensional position in the cubic space onto a single plane in which the organisms can move vertically and horizontally. A scaling factor allows for the size of the model field of view to be changed to match appropriate spatial scales of the open ocean while employing the same node array size. The location and thickness of the environmental structure or gradient layer also can be adjusted within the field of view.

Individual model organisms are allowed to freely move within the two-dimensional field of view. Movements are defined by both a swimming velocity magnitude and direction for each organism determined separately by a Gaussian random number generator (Mersenne Twister; Matsumoto and Nishimura, 1998). The mean and standard deviation values for swimming speeds are based on published mean and maximum cruising speeds (Mauchline, 1998). Swimming direction is determined in a

similar fashion with a bias towards the direction of previous movement. Individuals do not interact and merely respond to the thin layer structure.

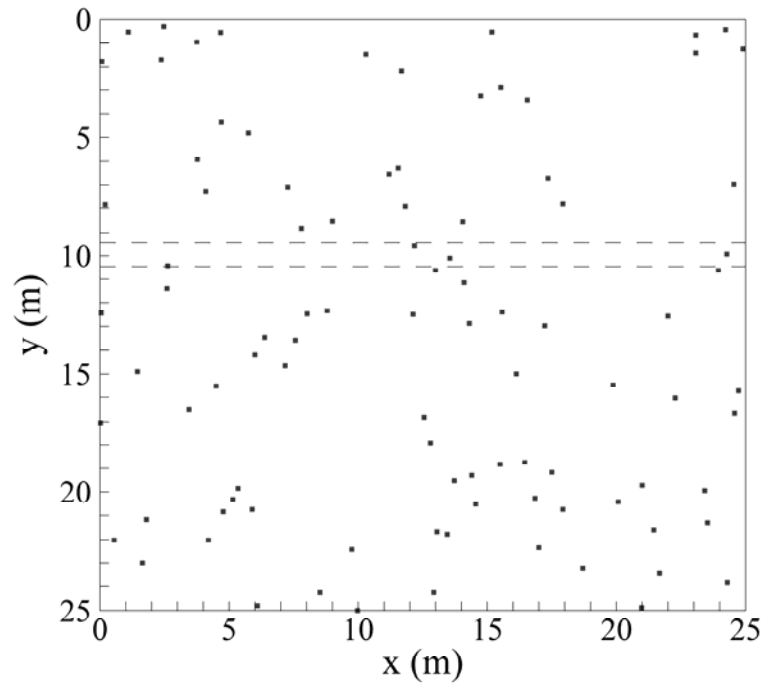


Figure 5.3 Field of view at the beginning of simulation for a model 25 meter water column with 1 meter thick layer located at 10 meters. Each symbol represents an individual model organism.

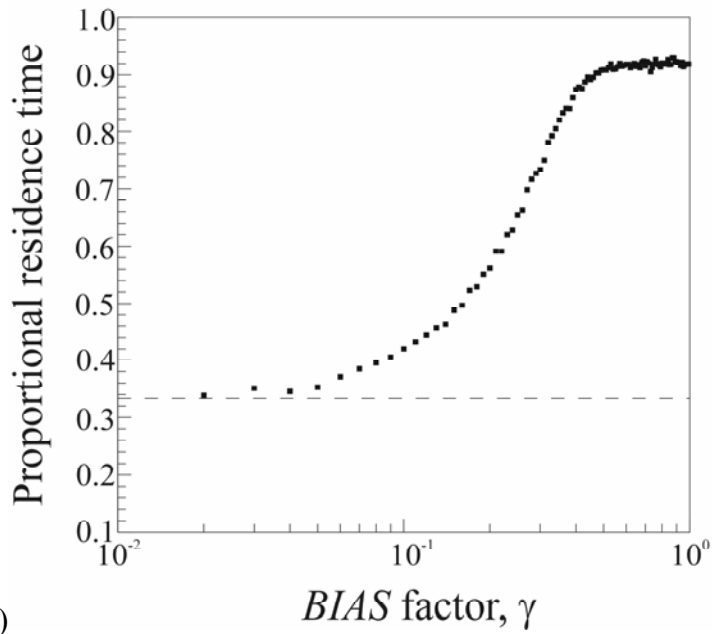
Individual movements were biased toward the layer to simulate the observed area-restricted search behavior in the presence of environmental structure. The *BIAS* factor (γ) ranged from 0 to 1 and defined the propensity of an individual to remain in a region based on the presence of a particular cue. The *BIAS* factor is 0 outside the layer and above zero in the layer. Individual behavior is determined by comparing a randomly generated behavioral indicator between 0 and 1 (Mersenne Twister) to the defined *BIAS* factor. If the behavior value is above the predetermined *BIAS* factor, the animal responds to the layer by increasing swimming speed and turn frequency. At each time step, a new behavior value is generated and compared to the *BIAS* factor to determine if the behavior is continued or ceases.

The concentration of organisms is based the target species (e.g. *A. tonsa* concentrations at roughly 1000 ind m⁻³) and is constant once the simulation starts. Individuals that exit the field of view are replaced by an incoming organism placed randomly at the edge of the viewing window so that the number of organisms in the field of view is constant over the simulation duration. The model provides information about the location of each organism at each time-step, the amount of time spent in the layer by each organism, and the average time spent in the layer by all organisms.

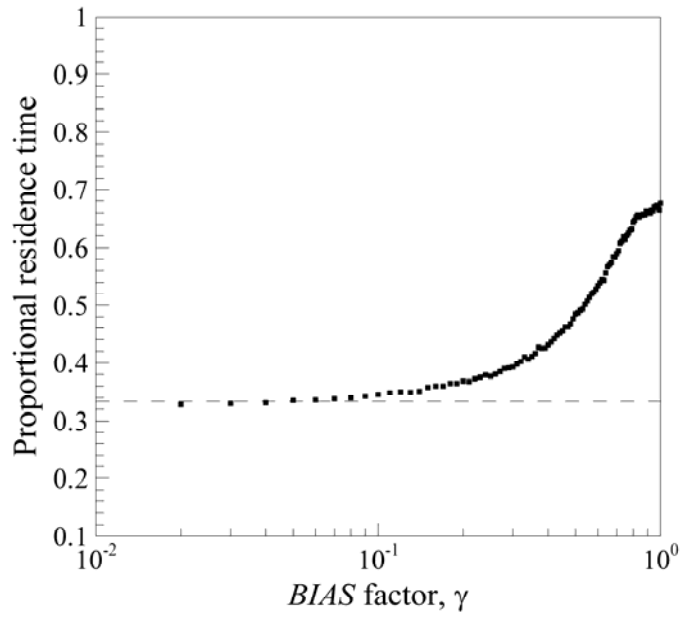
5.4.2 Model calibration

Calibration of the aggregation model is accomplished by running the simulation over temporal and spatial scales that match laboratory experiments (e.g. 10 cm \times 10 cm field of view and 2 hours). Each species must be calibrated and simulated independently because swimming speed significantly influences the BIAS factor. Adjusting the BIAS factor (γ) from 0 to 1 at increments of 0.01, the proportional residence time in the model layer was determined. The BIAS factor is then selected based on the value that best matches the laboratory results.

Figure 5.4a shows the effect of γ on the proportional residence time in the laboratory-scale layer for *Acartia tonsa*. For small values of γ , the proportional residence time basically matches a random distribution (0.33). For a middle range of γ , the proportional residence time increases quickly. At high γ (above about 0.70), the proportional residence time becomes saturated at about 0.90. The conditions in Fig. 5.4a that best match the results of laboratory experiments for *A. tonsa* exposed to an isolated velocity gradient layer ($T_R = 0.64$) correspond to a BIAS factor of 0.26. The model can be calibrated in this fashion for each species based on motility (e.g. for *T. longicornis*; $T_R = 0.51$; $\gamma = 0.55$; 4 mm s⁻¹ average cruising speed; Fig. 5.4b). Once the BIAS factor is selected for a particular species, the value is used for simulations corresponding to larger spatial and temporal scales to assess aggregation.



a)



b)

Figure 5.4 Model calibration curve: BIAS factor (γ) for (a) *A. tonsa* and (b) *T. longicornis*.

5.4.3 Model results

Performing a simulation for time and length scales relevant to field conditions (25 m × 25 m field of view; 24 hour run time, 1 m thick layer) demonstrates that aggregations can occur due to behavioral response to environmental structure (Fig. 5.5). Figure 5.6 shows the increase in the concentration of *A. tonsa* within the thin layer over a 24-hour period. Initially, the concentration of *A. tonsa* is equivalent to a random distribution, The proportion increases such that the total concentration is six times higher within 6 hours ($p < 0.001$ compared to random-walk model Kolmogorov-Smirnov goodness of fit, $D = 0.2714$, $D_{0.001,160} = 0.1067$). Similar results for *T. longicornis* are shown in Figure 5.7. *T. longicornis* shows significant aggregation within 4 hours ($p < 0.001$ compared to random-walk model, Kolmogorov-Smirnov goodness of fit, $D = 0.2608$, $D_{0.001,160} = 0.1067$) and the aggregation concentration continues to increase over the entire simulation. Based on these results it is reasonable to suggest that observed zooplankton aggregations in and near thin layers can be partially explained via individual responses to gradients of velocity. Similar arguments can be made for the response to layers of density (for *Eurytemora affinis*), food and chemical exudates since the observed proportional residence time is greater in those conditions as well.

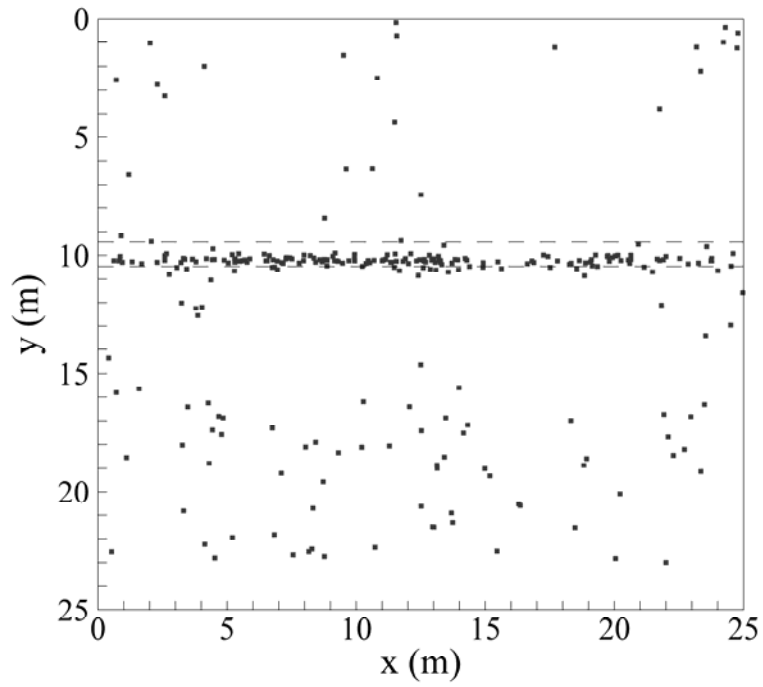


Figure 5.5 Field of view after 24 hours of simulation for *A. tonsa* for a model 25 meter water column with 1 meter thick layer located at 10 meters. Each symbol represents an individual model organism.

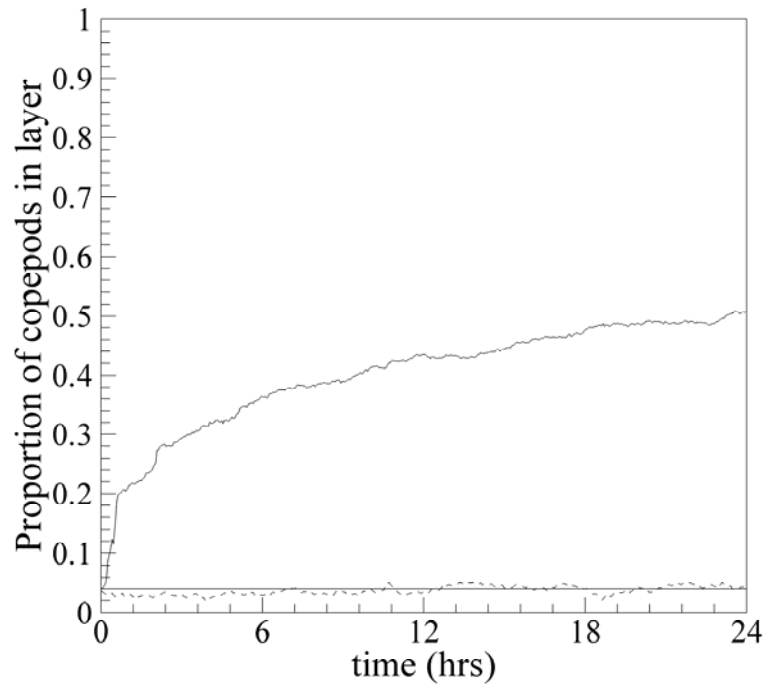


Figure 5.6 Aggregation of *A. tonsa* based on the model simulation. The solid line is the proportion of copepods in the layer with the layer present. The dashed line corresponds to the proportion of copepods in the same region with no layer present (i.e. no behavioral cue).

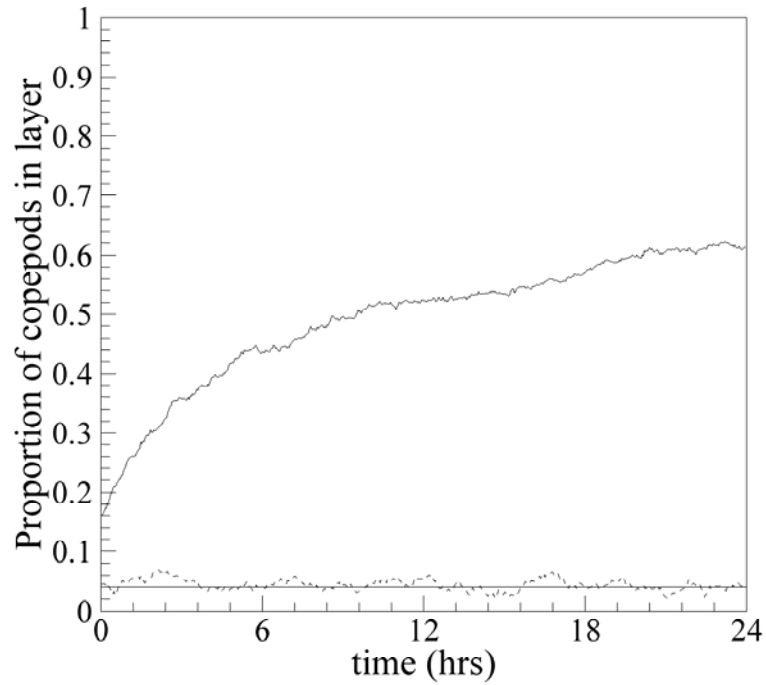


Figure 5.7 Aggregation of *T. longicornis* based on the model simulation. The solid line is the proportion of copepods in the layer with the layer present. The dashed line corresponds to the proportion of copepods in the same region with no layer present (i.e. no behavioral cue). The reference horizontal solid line shows the proportion of the model region covered by the model layer.

Chapter 6 Conclusions and Future Directions

6.1 Summary

This study addressed the ability of eight copepod species, *Acartia tonsa*, *Calanus finmarchicus* (adults and nauplii), *Calanus pacificus*, *Eurytemora affinis*, *Candacia ethiopica*, *Labidocera madurae*, *Neocalanus plumchrus*, and *Temora longicornis*, to react to laboratory mimics of oceanographic structure. Laboratory gradients in flow velocity, density, chemicals, and biological activity corresponding to *in situ* field measurements were modeled in the lab using a unique laminar plane jet apparatus. The apparatus allowed for quantification and calibration of physical and chemical gradients to match those from *in situ* oceanographic observations. All gradient layers were contained entirely within the region defined by the shear strain rate threshold of 0.025 s^{-1} as determined from the velocity gradient layer treatment. Also, the layer was much larger (40 mm on average) than an individual copepod (0.5-5 mm) so that the edges of the layer were not sensed simultaneously in any configuration. Therefore, copepods could completely enter the layer and interact with it.

Behavioral responses of copepods to physical and chemical gradients suggest that these gradients are important components of pelagic habitats, both from a physical and an ecological standpoint. All species tested exhibited an excited area-restricted search response to one of the physical gradients (flow velocity and fluid density), but not both. This response was similar to the response to the chemical exudate (*Tetraselmis* sp.) layer suggesting that the response is linked to foraging and aggregation. Finally, copepods

began feeding after entering food layers above threshold concentrations. These results show that copepods have developed a cue hierarchy foraging strategy (Figs. 5-1 and 5-2) that begins with a physical gradient (area-restricted search) and culminates in food presence (feeding).

6.2 Conclusions

Oceanographic structure plays an immensely important role in defining pattern at all scales. Physical forcing acts at large scales (kilometers and meters); however, copepod behavior is believed to influence patterns at fine scales. The results of this Thesis support the hypothesis that copepod behavior is important at fine to intermediate scales (centimeters to meters) by showing that oceanographic structure is sensed and utilized by several species of copepods in foraging behavior. Behavior changes lead to increased residence time in high resource patches and thus can lead to aggregation of populations over longer time scales. Hence, copepod behavior can define ecological patterns as observed *in situ*.

6.3 Unique contributions and applications

This thesis provided several unique contributions:

- (i) Developed the first laboratory experiments designed to mimic oceanographic structure for fine-scale analysis of zooplankton behavior.
- (ii) Illustrated the importance of fine-scale oceanographic structure to copepod behavior and ecology.

- (iii) Showed that zooplankton behavior can bridge the disparity between scales of physical forcing (kilometers and meters) and observed *in situ* patterns (centimeters) in oceanography.
- (iv) Established threshold levels for responses to velocity, density, chemical exudates layers.
- (v) Discovered the use of a cue hierarchy in copepod foraging behavior.
- (vi) Suggested the possibility of ecological niches once thought to be absent in the plankton associated with sensory and behavioral ecology.

6.4 Implications

The establishment and use of various oceanographic structures and a cue hierarchy by copepods leads to many questions about oceanographic structure with respect to broader ecological arenas. Do other species of copepods use velocity gradients to aggregate? Do other members of the zooplankton community utilize this environmental information in similar fashions? Can differentiated responses to these gradients provide functional niches possibly leading to speciation and thus affecting biodiversity (Hutchinson, 1961)? Do disruptive forces (energy sources), such as winds, which tend to mix water columns and remove oceanographic features impact succession and biodiversity in the plankton (Huston, 1979; Smayda, 1980)? Finally, can predictions be made about the frequency and strength of phytoplankton blooms and zooplankton aggregations from bathymetric and oceanographic data?

The response of *A. tonsa* to a distinct velocity gradient raises questions about the cues used by other *Acartia* spp. to aggregate near coral heads, or other obstructions in flow (Emery, 1968; Hamner and Carleton, 1979; Ueda et al., 1983). Although the primary functional reasons for these aggregations are not fully understood (Ambler, 2002), the physical and behavioral mechanisms that lead to aggregation at these features can be evaluated. Two mechanisms potentially can lead to aggregation in the wake regions of obstructions in flow; passive accumulation and active behavior (Fig. 6.1). Copepods could be passively aggregated in the wake of an obstruction due to lower velocities in the wake region. Individual organisms that are swept past the obstruction collect behind the obstacle, where flow velocities are lower in the recirculation region. However, most *in situ* observations of aggregations near benthic features tend to be monospecific. Aggregation due to passive accumulation would not result in such specificity; rather, the aggregation would appear as a random conglomeration of organisms. Thus, behavioral responses to changes in the environment are a more likely mechanism behind these aggregations. *A. tonsa* responds to shear strain rates (between 0.035-0.06 s⁻¹) in a fashion that can result in aggregation. Increased residence time in the vicinity of a velocity gradient by a particular species could result in species-specific aggregations in the wake regions of coral heads and other obstructions. If other species of *Acartia* or other copepods exhibiting similar aggregative behaviors (Oithonids; Hamner and Carleton, 1979; Ueda et al., 1983; Ambler et al., 1991) respond to velocity gradients in similar fashions, gradients in flow velocity could provide well defined boundaries for aggregation in a wake region. Other hypotheses include migration to a region of lower turbulence, or aggregation in light (Ambler, 2002; Banas et al., 2004).

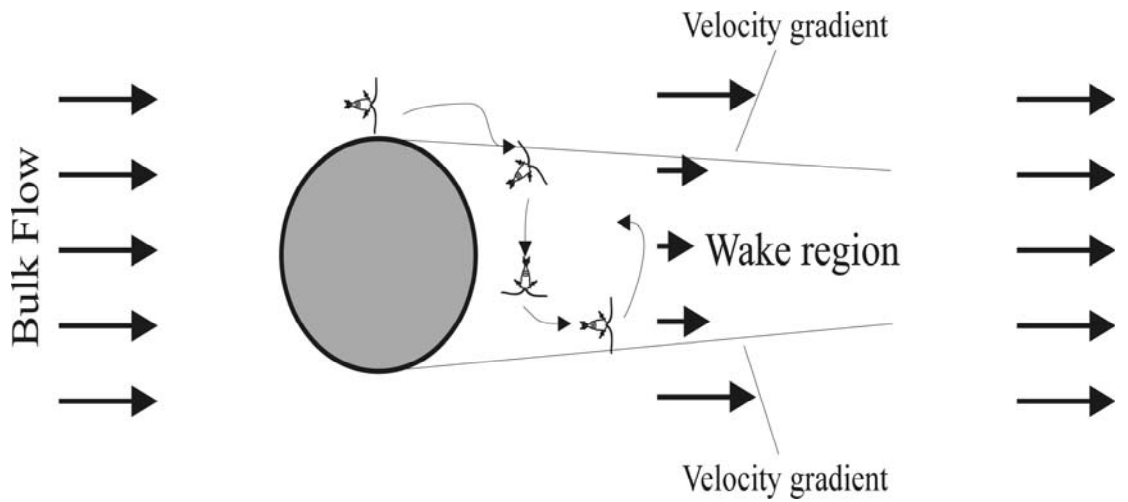


Figure 6.1 Schematic of copepod aggregation behind an obstruction (e.g. a coral head) in flow, for passive aggregation and/or active behavioral aggregation in response to either turbulence, light, or velocity gradients.

Many higher trophic level organisms are known to aggregate in regions of high productivity at large scales (kilometers), however it is generally not known if these larger consumers actively utilize fine-scale oceanographic structure to locate prey. Larvae and juveniles of larger crustaceans and fish species comprise the next level in the trophic web. Fish may be ideal for this type of investigation due to extensive knowledge of the mechanosensory systems such as the lateral line (Coombs and Janssen, 1990). Similarly, much is known about crustacean sensory systems (Weissburg, 1997, 2000). Understanding the scales at which larvae and juveniles aggregate will have significant applications in conservation and fisheries management.

Behavioral adaptations to oceanographic structure should impact an organism's fitness, population dynamics, and community structure. Consequently, the seascape appears much more structured than previously accepted such that differential use of the seascape may create functional niches and therefore promote biodiversity in the plankton (Hutchinson, 1961). Studies aimed at addressing these issues could include mesocosm studies with homogenous and structured treatments. Although the appropriate scales for such experiments may require manipulation experiments and comparison studies *in situ*.

The generation times of many species of the plankton community may provide excellent model systems to assess Huston's (1979) disturbance-diversity hypothesis. Often in terrestrial and benthic systems, assessing disturbance-diversity interactions is difficult because the frequencies of events occur on the order of years (forest fires,

regrowth of trees; Huston, 1979). But in the plankton, disturbance events (strong winds, turbulence) and generation times occur on the order of days. This allows for better experimental manipulation and is possible now that important scales and oceanographic features have been identified.

Strong haloclines are suspected to play important roles in phytoplankton bloom dynamics (Andersen and Nielsen, 2002a,b), and the responses to density changes illustrated in this study suggest that these gradients may also provide a refuge from primary foragers, the implications being widespread, and possibly impacting local fisheries on grand scales (Holligan, 1979; Cloern, 1984; Franks, 2001; Erga et al., 2003). Large-scale field experiments should be designed to target regions with intense density gradients such as locations of large freshwater inputs (Mackas and Loutit, 1988). Strong density gradients may promote harmful algal blooms (HABs) at the edges of the Mississippi River plume in the Gulf of Mexico, thus the high rate of HABs along Florida's west coast (Tester and Steidinger, 1997; Steidinger et al., 1998; Magana et al., 2003) may be directly linked to freshwater input from the Mississippi River.

The extent that gradients in oceanographic properties affect populations and communities is still not understood, but results here suggest that from the perspective of a copepod, the ocean is a structured and patterned habitat at scales much smaller than historically accepted (e.g. Hutchinson, 1961; Yamazaki et al., 2002; Cowles, 2004). The influence of individual behavior on pattern in pelagic habitats warrants further investigation at the fine-to-intermediate scales (mm to m), and emphasis on better

resolution in field measurements, combined with continued laboratory investigations is imperative to developing our understanding of zooplankton behavior and ecology at appropriate scales. A continued drive toward understanding and answering some of these large scale issues will benefit from collaborations between field studies and experimental investigations where specific aspects can be accurately isolated and controlled. As we become more aware of the importance of fine-scale structure in the ocean, it is necessary to begin to test the impact of these features on larger scale ecological processes.

6.5 Future directions

Based on the increase in knowledge and implications of this study, future applications and directions include:

- (i) Evaluation of the impacts of patchiness on copepod ecology at appropriate scales.
- (ii) Targeting sites for thin layer observations in the field based on physical and/or chemical characteristics.
- (iii) Utilizing copepod foraging strategies to evaluate chemosensory behaviors such as the determination or recognition of chemically-defended phytoplankton.
- (iv) Continued evaluation of sympatric species to determine the importance of oceanographic structure as a functional niche in plankton communities.
- (v) Testing higher trophic level organisms and applying to fisheries management and conservation decisions.

REFERENCES

- Abraham, E. R. 1998. The generation of plankton patchiness by turbulent stirring. *Nature* **391**: 577-580.
- Acroumanis, C., J.J. McGuirk, and J.M.L.M. Palma. 1990. On the use of fluorescent dyes for concentration measurements in water flows. *Exp. Fluids* **10**: 177-180.
- Allredge, A. L., B. H. Robinson, A. Fleminger, J. J. Torres, J. M. King, and W. M. Hamner. 1984. Direct sampling and in situ observation of a persistent copepod aggregation in the mesopelagic zone of the Santa Barbara basin. *Mar. Biol.* **80**: 75-81.
- Allredge, A. L., T. J. Cowles, S. MacIntyre, J. E. B. Rines, P. L. Donaghay, C. F. Greenlaw, D. V. Holliday, M. M. Deksheniaks, J. M. Sullivan, and J. R. V. Zaneveld. 2002. Occurrence and mechanisms of formation of a dramatic thin layer of marine snow in a shallow Pacific fjord. *Mar. Ecol. Prog. Ser.* **233**: 1-12.
- Ambler, J. W. 2002. Zooplankton swarms: Characteristics, proximal cues, and proposed advantages. *Hydrobiol.* **480**: 155-164.
- Ambler, J. W., F. D. Ferrari, and J. A. Fornshell. 1991. Population structure and swarm formation of the cyclopoid copepod *Dioithona oculata* near mangrove cays. *J. Plankton Res.* **13**: 1257-1272.
- Andersen, C. M., and T. G. Nielsen. 2002a. The effect of a sharp pycnocline on plankton dynamics in a freshwater influenced Norwegian fjord. *Ophelia* **56**: 135-160.
- Andersen, C. M., and T. G. Nielsen. 2002b. Plankton community structure and production along a freshwater influenced Norwegian fjord system. *Mar. Biol.* **141**: 707-724.
- Andrade, E. N. C. 1939. The velocity distribution in a liquid into liquid jet. Part 2. The plane jet. *Proceedings of the Physical Society* **51**: 784-793.
- Banas, N. S., D. P. Wang, and J. Yen. 2004. Experimental validation of an individual-based model for zooplankton swarming. *In Handbook of Scaling methods in Aquatic Ecology: Measurements, Analysis, and Modeling.* L. Seuront and P.G. Sutton (eds.). CRC Press, Boca Raton, FL. pp. 161-180.
- Barth, F. G., U. Wastl, J. A. C. Humphrey, and R. Devarakonda. 1993. Dynamics of arthropod filiform hairs. II. Mechanical properties of spider trichobothria (*Cupiennius salei* Keys). *Phil. Trans. Roy. Soc. Lon. B* **340**: 445-461.

- Barth, F. G., J. A. C. Humphrey, U. Wastl, J. Halbritter, and W. Brittinger. 1995. Dynamics of arthropod filiform hairs. III. Flow patterns related to air movement detection in a spider (*Cupiennius salei* Keys). *Phil. Trans. Roy. Soc. Lon. B* **347**: 397-412.
- Bashir, J., and M. S. Uberoi. 1975. Experiments on turbulent structure and heat-transfer in a two-dimensional jet. *Phys. Fluids* **18**: 405-410.
- Bickley, W. G. 1937. The plane jet. *Philosophical Magazine Series 7* **23**: 727-731.
- Bigelow, H. B. 1926. Plankton of the offshore waters of the Gulf of Maine. *Bulletin of the Bureau of Fisheries* **40**: 287-293.
- Bjornsen, P. K., and T. G. Nielsen. 1991. Decimeter scale heterogeneity in the plankton during a pycnocline bloom of *Gyrodinium aureolum*. *Mar. Ecol. Prog. Ser.* **73**: 263-267.
- Bleckmann, H., and J. S. Rovner. 1984. Sensory ecology of a semi-aquatic spider (*Dolomedes triton*) I. Roles of vegetation and wind-generated waves in site selection. *Behavioral Ecology and Sociobiology* **14**: 297-301.
- Bochdansky, A. B. and S. M. Bollens. 2004. Relevant scales in zooplankton ecology: Distribution, feeding, and reproduction of the copepod *Acartia hudsonica* in response to thin layers of the diatom *Skeletonema costatum*. *Limnol. Oceanogr.* **49**: 625-636.
- Bode, A., M. T. Alvarez-Ossorio, S. Barquero, J. Lorenzo, A. Louro, M. Varela. 2003. Seasonal variations in upwelling and in the grazing impact of copepods on phytoplankton off A Coruna (Galicia, NW Spain). *J. Exp. Mar. Biol. Ecol.* **297**: 85-105.
- Bollens, S. M., B. W. Frost, and J. R. Cordell. 1994. Chemical, mechanical and visual cues in the vertical migration behavior of the marine planktonic copepod *Acartia hudsonica*. *J. Plankton Res.* **16**: 555-564.
- Bradshaw, P. 1977. Effect of external disturbances on spreading rate of a plane turbulent jet. *J. Fluid Mech.* **80**: 795-797.
- Brown, G. L., and A. Roshko. 1974. Density effects and large structure in turbulent mixing layers. *J. Fluid Mech.* **64**: 775-816.
- Bucklin, A., and C.A. Manning. 2005. Multivariate analysis of the copepod community of near-shore waters in the western Gulf of Maine. *Mar. Ecol. Prog. Ser.* **292**: 233-249.

- Buskey, E. J. 1984. Swimming pattern as an indicator of the roles of copepod sensory systems in the recognition of food. *Marine Biology* **79**: 165-175.
- Chu, V. H., and R. E. Baddour. 1984. Turbulent gravity-stratified shear flows. *J. Fluid Mech.* **138**: 353-378.
- Clay, T. W., S. M. Bollens, A. B. Bochdansky, and T. R. Ignoffo. 2004. The effects of thin layers on the vertical distribution of larval Pacific herring, *Clupea pallasii*. *J. Exp. Mar. Biol. Ecol.* **305**: 171-189.
- Cloern, J. E. 1984. Temporal dynamics and ecological significance of salinity stratification in an estuary (South San Francisco Bay, USA). *Oceanol. Acta* **7**: 137-141.
- Comte-Bellot, G., and S. Corrsin. 1966. The use of a contraction to improve the isotropy of grid turbulence. *J. Fluid Mech.* **25**: 657-682.
- Coombs, S., and J. Janssen. 1990. Water flow detection by the mechanosensory lateral line. *In Comparative Perception - Volume II: Complex signals*. W. C. Stebbins and M. A. Berkley (eds.). John Wiley and Sons, New York.
- Cowles, T. J. 2004. Planktonic layers: physical and biological interactions on the small scale. *In Handbook of Scaling Methods in Aquatic Ecology: Measurements, Analysis, Simulation*. L. Seuront and P. G. Sutton (eds.). CRC Press, Boca Raton, FL. pp. 31-49.
- Cowles, T. J., and R. A. Desiderio. 1993. Resolution of biological microstructure through in situ fluorescence emission spectra. *Oceanography* **6**: 105-111.
- Cowles, T. J., R. A. Desiderio, and M. E. Carr. 1998. Small-scale planktonic structure: Persistence and trophic consequences. *Oceanography* **11**: 4-9.
- Cowles, T. J., R. A. Desiderio, and S. Neuer. 1993. In situ characterization of phytoplankton from vertical profiles of fluorescence emission spectra. *Mar. Biol.* **115**: 217-222.
- Crow, S. C., and F. H. Champagne. 1971. Orderly structure in jet turbulence. *J. Fluid Mech.* **48**: 547-591.
- Dagg, M. J., and J. T. Turner. 1982. The impact of copepod grazing on the phytoplankton of Georges Bank and the New York Bight. *Can. J. Fish. Aq. Sci.* **39**: 979-990.
- Dam, H. G., and W. T. Peterson. 1993. Seasonal contrasts in the diel vertical distribution, feeding behavior, and grazing impact of the copepod, *Temora longicornis*, in Long Island Sound. *J. Mar. Res.* **51**: 561-594.

- Daro, M. H. 1988. Migratory and grazing behavior of copepods and vertical distributions of phytoplankton. *Bull. Mar. Sci.* **43**: 710-729.
- Dasi, L. P. 2004. The small-scale structure of passive scalar mixing in turbulent boundary layers. Ph.D. Thesis Georgia Institute of Technology, Atlanta, GA.
- da Silva, C. B., and O. Metais. 2002. On the influence of coherent structures upon interscale interactions in turbulent plane jets. *J. Fluid Mech.* **473**: 103-145.
- Davies, A. E., J. F. Keffer, and W. D. Baines. 1975. Spread of a heated plane turbulent jet. *Phys. Fluids* **18**: 770-775.
- Davis, C. S., S. M. Gallager, and A. R. Solow. 1992. Microaggregations of oceanic plankton observed by towed video microscopy. *Science* **257**: 230-232.
- De Meester, L., P. Dawidowicz, E. Van Gool, and C.J. Loose. 1999. Ecology and evolution of predator-induced behavior of zooplankton: Depth selection behavior and diel vertical migration. *In* The Ecology and Evolution of Inducible Defenses. R. Tollrian and C.D. Harvell (eds.) Princeton University Press, Princeton, New Jersey. pp. 160-176.
- DeMott, W. R., and F. Moxter. 1991. Foraging on cyanobacteria by copepods - Responses to chemical defenses and resource abundance. *Ecology* **72**: 1820-1834.
- Dehnhardt, G., B. Mauck, W. Hanke, and H. Bleckmann. 2001. Hydrodynamic trail-following in harbor seals (*Phoca vitulina*). *Science* **293**: 102-104.
- Dekshenieks, M. M., P. L. Donaghay, J. M. Sullivan, J. E. B. Rines, T. R. Osborn, and M. S. Twardowski. 2001. Temporal and spatial occurrence of thin phytoplankton layers in relation to physical processes. *Mar. Ecol. Prog. Ser.* **223**: 61-71.
- Dimotakis, P. E. 1991. Turbulent free shear layer mixing and combustion. *In* High-speed Flight Propulsion Systems. A. R. Seebass, S. N. B. Murthy, and E. T. Curran (eds.). American Institute of Aeronautics and Astronautics, Washington, D.C.
- Doall, M. H., S. P. Colin, J. R. Strickler, and J. Yen. 1998. Locating a mate in 3D: The case of *Temora longicornis*. *Phil. Trans. Roy. Soc. Lon. B* **353**: 681-689.
- Dodson, S. I., R. Tollrian, and W. Lampert. 1997. Daphnia swimming behavior during vertical migration. *J. Plankton Res.* **19**: 969-978.
- Donaghay, P. L., and D. V. Holliday. 2005. Temporal and spatial variation in the shear ambit of a plankter in the ocean. Abstract Aquatic Sciences Meeting, American Society Limnology Oceanography.

- Dusenbery, D.B. 1992. Sensory Ecology: How Organisms Acquire and Respond to Information. W. H. Freeman and Company, New York.
- Emery, A. R. 1968. Preliminary observations on coral reef plankton. *Limnol. Oceanogr.* **13**: 293-303.
- Erga, S. R., M. Dybwad, Ø. Frette, J. K. Lotsberg, and K. Aursland. 2003. New aspects of migratory behavior of phytoplankton in stratified waters: Effects of halocline strength and light on *Tetraselmis* sp. (Prasinophyceae) in an artificial water column. *Limnol. Oceanogr.* **48**: 1202-1213.
- Fernandez, D., and J. L. Acuna. 2003. Enhancement of marine phytoplankton blooms by appendicularian grazers. *Limnol. Oceanogr.* **48**: 587-593.
- Fields, D. M., D. S. Shaeffer, and M. J. Weissburg. 2002. Mechanical and neural responses from the mechanosensory hairs on the antennule of *Gaussia princeps*. *Mar. Ecol. Prog. Ser.* **227**: 173-186.
- Fields, D. M., and J. Yen. 1996. The escape behavior of *Pleuromamma xiphias* in response to a quantifiable fluid mechanical disturbance. *In Zooplankton: Sensory Ecology and Physiology*. Vol. 1. P. H. Lenz, D. K. Hartline, T. E. Purcell, and D. L. Maximillian (eds.). Gordon and Breach Publishers, Amsterdam. pp. 323-340.
- Fields, D. M., and J. Yen. 1997a. The escape behavior of marine copepods in response to a quantifiable fluid mechanical disturbance. *J. Plankton Res.* **19**: 1289-1304.
- Fields, D. M., and J. Yen. 1997b. Implications of the feeding current structure of *Euchaeta rimana*, a carnivorous pelagic copepod, on the spatial orientation of their prey. *J. Plankton Res.* **19**: 79-95.
- Fields, D.M., and J. Yen. 1996. The escape behavior of *Pleuromamma xiphias* in response to a quantifiable fluid mechanical disturbance. *In Zooplankton: Sensory Ecology and Physiology*. Vol. 1. Lenz, P.H., Hartline, D.K., Purcell, T.E., and Maximillian, D.L. (eds.). Gordon and Breach Publishers Amsterdam. pp. 323-340.
- Fischer, H. B., E. J. List, R. C. Y. Koh, J. Imberger, and N. H. Brooks. 1979. Mixing in Inland and Coastal Waters. Academic Press, San Diego, CA.
- Forthmann, E. 1936. Turbulent jet expansion. Technical Memorandum. National Advisory Committee for Aeronautics, Washington, D.C.
- Franks, P. J. S. 1995. Thin layers of phytoplankton: A model of formation by near-inertial wave shear. *Deep Sea Res. I* **42**: 5-91.

- Franks, P. J. S. 2001. Phytoplankton blooms in a fluctuating environment: The roles of plankton response time scales and grazing. *J. Plankton Res.* **23**: 1433-1441.
- Gallager, S. M., H. Yamazaki, and C. S. Davis. 2004. Contribution of fine-scale vertical structure and swimming behavior to formation of plankton layers on Georges Bank. *Mar. Ecol. Prog. Ser.* **267**: 27-43.
- Genin, A., J. S. Jaffe, R. Reef, C. Richter, and P. J. S. Franks. 2005. Swimming against the flow: A mechanism of zooplankton aggregation. *Science* **308**: 860-862.
- Gerritsen, J., and J. R. Strickler. 1977. Encounter probabilities and community structure in zooplankton: A mathematical model. *J. Fish. Res. Board Can.* **34**: 73-82.
- Gutmark, E., and I. Wygnanski. 1976. Planar turbulent jet. *J. Fluid Mech.* **73**: 465-495.
- Hamner, W.M. 1988. Behavior of plankton and patch formation in pelagic ecosystems. *Bull. Mar. Sci.* **43**: 752-757.
- Hamner, P.P., and W. M. Hamner. 1977. Chemosensory tracking of scent trails by the planktonic shrimp *Acetes sibogae australis*. *Science* **195**: 886-888.
- Hamner, W. M., and J. H. Carleton. 1979. Copepod swarms: attributes and role in coral reef systems. *Limnol. Oceanogr.* **24**: 1-14.
- Hamner, W. M., P. P. Hamner, S. W. Strand, and R. W. Gilmer. 1983. Behavior of Antarctic krill, *Euphausia superba*: Chemoreception, feeding, schooling, and molting. *Science* **220**: 433-435.
- Hanson, A. K., and P. L. Donaghay. 1998. Micro- to fine-scale chemical gradients and layers in stratified coastal waters. *Oceanography* **11**: 10-17.
- Harder, W. 1968. Reactions of plankton organisms to water stratification. *Limnol. Oceanogr.* **13**: 156-168.
- Haury, L. R. 1976. Small-scale pattern of a California Current zooplankton assemblage. *Mar. Biol.* **37**: 137-157.
- Hay, M. E. and Kubanek, J. 2002. Community and ecosystem level consequences of chemical signaling in the plankton. *J. Chem. Ecol.* **28**: 2001-2016.
- Hazel, P. 1972. Numerical studies of the stability of inviscid stratified shear flows. *J. Fluid Mech.* **51**: 39-61.
- Ho, C. M., and P. Huerre. 1984. Perturbed free shear layers. *Ann. Rev. Fluid Mech.* **16**: 365-424.

- Holliday, D. V., R. E. Pieper, C. F. Greenlaw, and J. K. Dawson. 1998. Acoustical sensing of small-scale vertical structures in zooplankton assemblages. *Limnol. Oceanogr.* **11**: 18-23.
- Holliday, D. V., P. L. Donaghay, C. F. Greenlaw, D. E. McGehee, M. M. McManus, J. M. Sullivan, and J. L. Miksis. 2003. Advances in defining fine- and micro-scale pattern in marine plankton. *Aq. Liv. Res.* **16**: 131-136.
- Holligan, P.M. 1979. Dinoflagellate blooms associated with tidal fronts around the British Isles. *In Toxic dinoflagellate blooms*. D. L. Taylor and H. H. Seliger (eds.). Elsevier, North Holland. pp. 249-256.
- Hsiao, F. B., and J. M. Huang. 1990. On the evolution of instabilities in the near-field of a plane jet. *Phys. Fluids* **2**: 400-412.
- Hussein, H. J. 1994. Evidence of local axisymmetry in the small scales of a turbulent planar jet. *Phys. Fluids* **6**: 2058-2070.
- Hussain, A. K. M. F., and A. R. Clark. 1977. Upstream influence on the near field of a plane turbulent jet. *Phys. Fluids* **20**: 1416-1426.
- Huston, M. 1979. A general hypothesis of species diversity. *Am. Nat.* **113**: 81-101.
- Hutchinson, G. E. 1961. The paradox of the plankton. *Am. Nat.* **95**: 137-145.
- Ignoffo, T. R., S. M. Bollens, and A. B. Bochdansky. 2005. The effects of thin layers on the vertical distribution of the rotifer, *Brachionus plicatilis*. *J. Exp. Mar. Biol. Ecol.* **316**: 167-181.
- Ikeda, M. 1977. Finite disturbances and growing vortices in a two-dimensional jet. *J. Fluid. Mech.* **80**: 401-421.
- Incze, L. S., D. Herbert, N. Wolff, N. Oakey, and D. Dye. 2001. Changes in copepod distributions associated with increased turbulence from wind stress. *Mar. Ecol. Prog. Ser.* **213**: 229-240.
- Jaffe, J. S., P. J. S. Franks, and A. W. Leising. 1998. Simultaneous imaging of phytoplankton and zooplankton distributions. *Oceanography* **11**: 24-29.
- Janssen, J. 2003. Lateral line sensory ecology. *In Senses of Fishes: Adaptations for the Reception of Natural Stimuli*. G. V. D. Emde, J. Mogdans, and B. G. Kapoor (eds.). Narosa Publishing, New Delhi.
- Janssen, J., and J. Corcoran. 1993. Lateral line stimuli can override vision to determine sunfish strike trajectory. *J. Exp. Biol.* **176**: 299-305.

- Jenkins, P. E., and V. W. Goldschmidt. 1976. Conditional (point averaged) temperature and velocities in a heated turbulent plane jet. *Phys. Fluids* **19**: 613-617.
- Jiang, H., T. R. Osborn, and C. Meneveau. 2002. Chemoreception and the deformation of the active space in freely swimming copepods: A numerical study. *J. Plankton Res.* **24**: 495-510.
- Kjørboe, T., and E. Saiz. 1995. Planktivorous feeding in calm and turbulent environments with emphasis on copepods. *Mar. Ecol. Prog. Ser.* **122**: 135-145.
- Kjørboe, T., E. Saiz, and A. Visser. 1999. Hydrodynamic signal perception in the copepod *Acartia tonsa*. *Mar. Ecol. Prog. Ser.* **179**: 97-111.
- Kjørboe, T., and A. W. Visser. 1999. Predator and prey perception in copepods due to hydromechanical signals. *Mar. Ecol. Prog. Ser.* **179**: 81-95.
- Kotsovinos, N. E. 1976. Note on spreading rate and virtual origin of a plane turbulent jet. *J. Fluid Mech.* **77**: 305-311.
- Kundu, P. K. 1990. *Fluid Mechanics*. Academic Press, New York.
- Lee, C. E. 2000. Global phylogeography of a cryptic copepod species complex and reproductive isolation between genetically proximate "populations." *Evolution* **54**: 2014-2027.
- Leising, A. W. 2001. Copepod foraging in patchy habitats and thin layers using a 2-D individual-based model. *Mar. Ecol. Prog. Ser.* **216**: 167-179.
- Leising, A. W., and P. J. S. Franks. 2000. Copepod vertical distribution within a spatially variable food source: A simple foraging-strategy model. *J. Plankton Res.* **22**: 999-1024.
- Leising, A. W., and P. J. S. Franks. 2002. Does *Acartia clausi* (Copepoda: Calanoida) use an area-restricted search foraging strategy to find food? *Hydrobiologia* **480**: 193-207.
- Lenz, P. H., and J. Yen. 1993. Distal setal mechanoreceptors of the first antennae of marine copepods. *Bull. Mar. Sci.* **53**: 170-179.
- Lougee, L.A., S. M. Bollens, and S. R. Avent. 2002. The effects of haloclines on the vertical distribution and migration of zooplankton. *J. Exp. Mar. Biol. Ecol.* **278**: 111-134.
- MacArthur, R. H., and E. R. Pianka. 1966. On the optimal use of a patchy environment. *Am. Nat.* **100**: 603-609.

- Mackas, D. L., and G. C. Louttit. 1988. Aggregation of the copepod, *Neocalanus plumchrus* at the margin of the Fraser River plume in the Strait of Georgia. *Bull. Mar. Sci.* **43**: 810-824.
- Mackas, D. L., H. Sefton, C. B. Miller, and A. Raich. 1993. Vertical habitat partitioning by large calanoid copepods in the oceanic sub-Arctic Pacific during spring. *Prog. Oceanogr.* **32**: 259-294.
- Magana, H. A., C. Contreras, and T. A. Villareal. 2003. A historical assessment of *Karenia brevis* in the western Gulf of Mexico. *Harmful Algae* **2**: 163-171.
- Manning, C. A., and A. Bucklin. 2005. Multivariate analysis of the copepod community of near-shore waters in the western Gulf of Maine. *Mar. Ecol. Prog. Ser.* **292**: 233-249.
- Matsumoto, M., and T. Nishimura. 1998. Mersenne twister: A 623-dimensionally equidistributed uniform pseudo-random number generator. *ACM Trans. Model. Comp. Simul. (TOMACS)*. **8**: 3-30.
- Mauchline, J. 1998. *The Biology of Calanoid Copepods*. Elsevier Academic Press. San Diego, CA.
- McManus, M. A., A. L. Alldredge, A. H. Barnard, E. Boss, J. F. Case, T. J. Cowles, P. L. Donaghay, L. B. Eisner, D. J. Gifford, C. F. Greenlaw, C. M. Herren, D. V. Holliday, D. Johnson, S. MacIntyre, D. M. McGehee, T. R. Osborn, M. J. Perry, R. E. Pieper, J. E. B. Rines, D. C. Smith, J. M. Sullivan, M. K. Talbot, M. S. Twardowski, A. Weidemann, and J. R. Zaneveld. 2003. Characteristics, distribution, and persistence of thin layers over a 48 hour period. *Mar. Ecol. Prog. Ser.* **261**: 1-19.
- Mehta, R. D., and P. Bradshaw. 1979. Design rules for small low speed wind tunnels. *Aeronautical Journal* **83**: 443-449.
- Miller, C. A., D. L. Penry, and P. M. Glibert. 1995. The impact of trophic interactions on rates of nitrogen regeneration and grazing in Chesapeake Bay. *Limnol. Oceanogr.* **40**: 1005-1011.
- Mitchell, J. G., A. Okubo, and J. A. Fuhrman. 1989. The contribution of phytoplankton to ocean density gradients. *Deep Sea Res.* **36**: 1277-1282.
- Moore, P. A., D. M. Fields, and J. Yen. 1999. Physical constraints of chemoreception in foraging copepods. *Limnol. Oceanogr.* **44**: 166-177.
- Mullin, M. M., and E. R. Brooks. 1976. Some consequences of distributional heterogeneity of phytoplankton and zooplankton. *Limnol. Oceanogr.* **21**: 784-796.

- Nevitt, G. A. 2000. Olfactory foraging by Antarctic procellariiform seabirds: Life at high Reynolds numbers. *Biol. Bull.* **198**: 245-253.
- Nielsen, T. G., T. Kiørboe, and P. K. Bjornsen. 1990. Effects of a *Chrysochromulina polylepis* subsurface bloom on the planktonic community. *Mar. Ecol. Prog. Ser.* **62**: 21-35.
- Okubo, A. 1972. A note on small organism diffusion around an attractive center: A mathematical model. *J. Oceanogr. Soc. Japan* **28**: 1-7.
- Okubo, A. 1986. Dynamical aspects of animal grouping: swarms, schools, flocks, and herds. *Adv. Biophysics* **22**: 1-94.
- Okubo, A., and J. J. Anderson. 1984. Mathematical models for zooplankton swarms: their formation and maintenance. *EOS* **65**: 731-732.
- Osborn, T. 1998. Finestructure, microstructure, and thin layers. *Oceanography* **11**: 36-43.
- Paffenhofer, G. A. 1998. On the relation of structure, perception and activity in marine planktonic copepods. *J. Mar. Sys.* **15**: 457-473.
- Pai, S. I. 1951. On the stability of two-dimensional laminar jet flow of gas. *J. Aero. Sci.* **18**: 731-742.
- Platt, T. 1972. Local phytoplankton abundance and turbulence. *Deep Sea Res.* **19**: 183-187.
- Pohlmann, K., F. W. Grasso, and T. Breithaupt. 2001. Tracking wakes: The nocturnal predatory strategy of piscivorous catfish. *Proc. Nat. Acad. Sci. U.S.A.* **98**: 7371-7374.
- Poulet, S. A., and P. Marsot. 1978. Chemosensory grazing by marine calanoid copepods (Arthropoda Crustacea). *Science* **200**: 1403-1405.
- Poulet, S. A., and G. Ouellet. 1982. The role of amino acids in the chemosensory swarming and feeding of marine copepods. *J. Plankton Res.* **4**: 341-361.
- Powell, T. M., and A. Okubo. 1994. Turbulence, diffusion and patchiness in the sea. *Phil. Trans. Roy. Soc. Lon. B* **343**: 11-18.
- Prezioso, J. and J. Kane. 2001. Seasonal abundance of *Temora longicornis* on the Northeast Continental Shelf of the United States based on 24 years of ecosystem monitoring data. NEFSC. <http://www.nefsc.noaa.gov/nefsc/publications/crd/crd0117/symposium/prezioso-kane-presentation/presentation.pdf>
- Raffel, M., C Wilbert, and J. Kompenhans. 1998. Particle Image Velocimetry: A Practical Guide. Springer, Berlin.

- Rajagopalan, S., and N. W. M. Ko. 1996. Velocity and spanwise vorticity measurements in an excited mixing layer of a plane jet. *Exp. Fluids* **20**: 346-357.
- Ramaprian, B. R., and M. S. Chandrasekhara. 1985. LDA measurements in plane turbulent jets. *J. Fluids Eng. Trans. ASME*. **107**: 264-271.
- Rengefors, K., and C. Legrand. 2001. Toxicity in *Peridinium aciculiferum*: An adaptive strategy to outcompete other winter phytoplankton? *Limnol. Oceanogr.* **46**:1990-1997.
- Revuelta, A., A. L. Sanchez, and A. Linan. 2002. The virtual origin as a first-order correction for the far-field description of laminar jets. *Phys. Fluids* **14**: 1821-1824.
- Rines, J. E. B., P. L. Donaghay, M. M. Deksheniaks, J. M. Sullivan, and M. S. Twardowski. 2002. Thin layers and camouflage: hidden *Pseudonitzschia* spp. (Bacillariophyceae) populations in a fjord in the San Juan Islands, Washington, USA. *Mar. Ecol. Prog. Ser.* **225**: 123-137.
- Roberts, P. J. W., and P.R. Mathews. 1984. Dynamics of jets in two-layer stratified fluids. *J. Hydr. Eng.* **110**: 1201-1217.
- Roberts, P. J. W., and P.R. Mathews. 1987. Behavior of low buoyancy jets in a linearly stratified fluid. *J. Hydr. Res.* **25**: 503-519.
- Roberts, P. J. W., K. Maile, and G. Daviero. 2001. Mixing in stratified jets. *J. Hydr. Eng.* **197**: 194-200.
- Rose, M. D., and G. A. Polis. 1998. The distribution and abundance of coyotes: the effects of allochthonous food subsidies from the sea. *Ecology* **79**: 998-1007.
- Saiz, E., and M. Alcaraz. 1992. Free-swimming behavior of *Acartia clausi* (Copepoda, Calanoida) under turbulent water movement. *Mar. Ecol. Prog. Ser.* **80**: 229-236.
- Saiz, E., M. Alcaraz, and G.A. Paffenhofer. 1992. Effects of small-scale turbulence on feeding rate and gross-growth efficiency of three *Acartia* species (Copepoda, Calanoida). *J. Plankton Res.* **14**: 1085-1097.
- Saiz, E., P. Tiselius, P. R. Jonsson, P. Verity, and G. A. Paffenhofer. 1993. Experimental records of the effects of food patchiness and predation on egg production of *Acartia tonsa*. *Limnol. Oceanogr.* **38**: 280-289.
- Sato, H., and F. Sakao. 1964. An experimental investigation of the instability of a two-dimensional jet at low Reynolds numbers. *J. Fluid Mech.* **20**: 337-352.

- Seuront, L., and Y. Lagadeuc. 2001. Multiscale patchiness of the calanoid copepod *Temora longicornis* in a turbulent coastal sea. *J. Plankton Res.* **23**: 1137-1145.
- Smayda, T. 1980. Phytoplankton species succession. *In* The Physiological Ecology of Phytoplankton. Studies in Ecology 7. L. Morris (ed.). Univ. of California Press, Berkeley, CA . pp. 493-570.
- Steidinger, K. A., G. V. Vargo, ; P. A. Tester; and C. R. Tomas. 1998. Bloom dynamics and physiology of *Gymnodinium breve* with emphasis on the Gulf of Mexico. *In* Physiological Ecology of Harmful Algal Blooms. D. M. Anderson, A. D. Cembella, and G. M. Hallegrawff (eds.). Springer, New York.
- Strickler, J. R. 1977. Observations of swimming performances of planktonic copepods. *Limnol. Oceanogr.* **22**: 165-169.
- Strickler, J. R. 1998. Observing free-swimming copepods mating. *Phil. Trans. Roy. Soc. Lon. B* **353**: 671-680.
- Svensen, C., and T. Kiørboe. 2000. Remote prey detection in *Oithona similis*: hydromechanical versus chemical cues. *J. Plankton Res.* **22**: 1155-1166.
- Tatsumi, T., and T. Kakutani. 1958. The stability of a two-dimensional laminar jet. *J. Fluid Mech.* **4**: 261-275.
- Tennekes, H. and Lumley, J. L. 1972. A First Course in Turbulence. The MIT Press Cambridge, MA.
- Tester, P. A., and K. A. Steidinger. 1997. *Gymnodinium breve* red tide blooms: Initiation, transport, and consequences of surface circulation. *Limnol. Oceanogr.* **42**: 1039-1051.
- Thunell, R., C. Pride, P. Ziveri, F. Mullen-Karger, C. Sancetta, and D. Murray. 1996. Plankton response to physical forcing in the Gulf of California. *J. Plankton Res.* **18**: 2017-2026.
- Tinbergen, N., M. Impeken, and D. Franck. 1967. An experiment on spacing-out as a defense against predation. *Behaviour* **28**: 307-321.
- Tiselius, P. 1992. Behavior of *Acartia tonsa* in patchy food environments. *Limnol. Oceanogr.* **37**: 1640-1651.
- Tiselius, P. 1998. An *in situ* video camera for plankton studies: design and preliminary observations. *Mar. Ecol. Prog. Ser.* **164**: 293-299.
- Tiselius, P., G. Nielsen, and T. G. Nielsen. 1994. Microscale patchiness of plankton within a sharp pycnocline. *J. Plankton Res.* **16**: 543-554.

- Titelman, J. 2001. Swimming and escape behavior of copepod nauplii: implications for predator-prey interactions among copepods. *Mar. Ecol. Prog. Ser.* **213**: 203-213.
- Titelman, J., and T. Kiørboe. 2003a. Motility of copepod nauplii and implications for food encounter. *Mar. Ecol. Prog. Ser.* **247**: 123-135.
- Titelman, J., and T. Kiørboe. 2003b. Predator avoidance by nauplii. *Mar. Ecol. Prog. Ser.* **247**: 137-149.
- Tumlinson, J. H., W. J. Lewis, and L. E. M. Vet. 1993. How parasitic wasps find their hosts. *Sci. Am.* **268**: 100-106.
- Turchin, P. 1991. Translating foraging movements in heterogeneous environments into spatial distribution of foragers. *Ecology* **72**: 1253-1266.
- Turner, J. S. 1991. Convection and mixing in the oceans and the earth. *Phys. Fluids A* **3**: 1218-1232.
- Turner, J. T. 2004. The importance of small planktonic copepods and their roles in pelagic marine food webs. *Zool. Stud.* **43**: 255-266.
- Ueda, H., A. Kuwahara, M. Tanaka, and M. Azeta. 1983. Underwater observations on copepod swarms in temperate and subtropical waters. *Mar. Ecol. Prog. Ser.* **11**: 165-171.
- Vet, L. E. M. 1999. From chemical to population ecology: Infochemical use in an evolutionary context. *J. Chem. Ecol.* **25**: 31-49.
- Videler, J. J., E.J. Stamhuis, U. K. Müller, and L. A. van Duren. 2002. The scaling and structure of aquatic animal wakes. *Integr. Comp. Biol.* **42**: 988-996.
- Vinson, S. B., G. W. Elzen, , and H. J. Williams. 1987. The influence of volatile plant allelochemicals on the third trophic level (parasitoids) and their herbivorous hosts. *In* *Insects Plants*. V. Labeyrie, G. Fabres, and D. Lachaise (eds.). W. Junk Publishers, Dordrecht.
- Viitasalo, M., T. Kiørboe, J. Flinkman, L. W. Pedersen, and A. W. Visser. 1998. Predation vulnerability of planktonic copepods: consequences of predator foraging strategies and prey sensory abilities. *Mar. Ecol. Prog. Ser.* **175**: 129-142.
- Visser, A. W., H. Saito, E. Saiz, and T. Kiørboe. 2001. Observations of copepod feeding and vertical distribution under natural turbulent conditions in the North Sea. *Mar. Biol.* **138**: 1011-1019.

- Webster, D. R., P.J.W. Roberts, and L. Ra'ad. 2001. Simultaneous DPTV/PLIF Measurements of a Turbulent Jet. *Exp. Fluids* **30**: 65-72.
- Webster, D.R., S. Rahman, and L. P. Dasi 2003. Laser-induced fluorescence measurements of a turbulent plume. *J. Eng. Mech.* **129**: 1130-1137.
- Weissburg, M. J. 1997. Chemo- and mechanosensory orientation by crustaceans in laminar and turbulent flows: From odor trails to vortex streets. *In* Orientation and Communication in Arthropods. M. Lehrer (ed.). Birkhauser Verlag Basel, Switzerland. pp. 215-246.
- Weissburg, M. J. 2000. The fluid dynamical context of chemosensory behavior. *Biol. Bull.* **198**: 188-202.
- Weissburg, M. J., M. C. Ferner, D. P. Pisut, and D. L. Smee. 2002. Ecological consequences of chemically mediated prey perception. *J. Chem. Ecol.* **28**: 1953-1970.
- Weissburg, M. J., and R. K. Zimmer-faust. 1993. Life and death in moving fluids: Hydrodynamic effects on chemosensory-mediated predation. *Ecology* **74**: 1428-1443.
- Wishner, K., E. Durbin, A. Durbin, M. MacCaulay, H. Winn, and R. Kenney. 1988. Copepod patches and Right Whales in the Great South Channel off New England. *Bull. Mar. Sci.* **43**: 825-844.
- Yamazaki, H. 1993. Lagrangian study of planktonic organisms: Perspectives. *Bull. Mar. Sci.* **53**: 265-278.
- Yamazaki, H., and L.R. Haury. 1993. A new Lagrangian model to study animal aggregation. *Ecol. Model.* **69**: 99-111.
- Yamazaki, H., and A. Okubo. 1995. A simulation of grouping: An aggregating random-walk. *Ecol. Model.* **79**: 159-165.
- Yamazaki, H., and T. Osborn. 1988. Review of oceanic turbulence: Implications for biodynamics. *In* Toward a Theory on Biological-Physical Interactions in the World Ocean. B. J. Rothschild (ed.). Kluwer Academic, Dordrecht.
- Yamazaki, H., D. L. Mackas, and K. L. Denman. 2002. Coupling small-scale physical processes with biology. *In* The Sea. Vol. 12. J. J. McCarthy and B. J. Rothschild (eds.). John Wiley and Sons, New York. pp. 51-112.
- Yen, J. 2000. Life in transition: Balancing inertial and viscous forces by planktonic copepods. *Biol. Bull.* **198**: 213-224.

- Yen, J., and D. M. Fields. 1992. Escape responses of *Acartia hudsonica* (Copepoda) nauplii from the flow field of *Temora longicornis* (Copepoda). *Archive Hydrobiol. Beih.* **36**: 123-134.
- Yen, J., and J. R. Strickler. 1996. Advertisement and concealment in the plankton: What makes a copepod hydrodynamically conspicuous? *Invert. Biol.* **115**: 191-205.
- Yen, J., P. H. Lenz, D. V. Gassie, and D. K. Hartline. 1992. Mechanoreception in marine copepods: Electrophysiological studies on the first antennae. *J. Plankton Res.* **14**: 495-512.
- Yen, J., M. J. Weissburg, and M. H. Doall. 1998. The fluid physics of signal perception by mate-tracking copepods. *Phil. Trans. Roy. Soc. Lon. B* **353**: 787-804.
- Yen, J., A. C. Prusak, M. Caun, M. Doall, J. Brown, and J. R. Strickler. 2004. Signaling during mating in the pelagic copepod, *Temora longicornis*,. *In Handbook of Scaling Methods in Aquatic Ecology: Measurements, Analysis, Simulation.* L. Seuront and P. G. Strutton (eds.). CRC Press, Boca Raton, FL. pp. 149-159.
- Zaman, K. B. M. Q., and A. K. M. F. Hussain. 1980. Vortex pairing in a circular jet under controlled excitation. I. General jet response. *J. Fluid Mech.* **101**: 449-491.
- Zar, J.H. 1999. *Biostatistical Analysis* 4th Edition. Prentice Hall. Upper Saddle River, NJ.
- Zimmer, R. K., and C. A. Butman. 2000. Chemical signaling processes in the marine environment. *Biol. Bull.* **198**: 168-187.